Colloids at Liquid Crystal Interfaces

Anne Claire Pawsey

Doctor of Philosophy
The University of Edinburgh
2014

Abstract

This thesis presents a study of colloidal particles dispersed in thermotropic liquid crystals. It has a specific focus on colloids in the presence of an interface between the liquid crystal and an isotropic fluid. Three systems are studied: colloids trapped at a planar interface between a cholesteric liquid crystal (CLC) and an isotropic oil, nematic emulsions with interfacial colloids and the influence of colloids on the phase transition kinetics of the cholesteric blue phase.

Experiments are carried out using polarising optical and confocal microscopy. By combining these techniques, the director field of the liquid crystals could be imaged in combination with precise observation of the colloid locations. Custom image analysis algorithms are developed to extract the information.

In the first system, we create an interface between a cholesteric liquid crystal and an isotropic liquid. Homeotropic anchoring leads to a well aligned cholesteric layer and the formation of the fingerprint texture. Fluorescent colloidal particles with planar surface anchoring are dispersed in the CLC. A majority of these particles decorate the interface. The final distribution of particles perpendicular to the interface has a clear dependence on the particle size. In the plane of the interface, surface defects form a template for the colloids.

The second system is a particle dispersion within a short pitch CLC which exhibits a blue phase. The colloidal particles and associated defects act as nucleation sites for the blue phase in the cholesteric to blue phase transition. Colloidal particles cause localised melting from the blue phase to the isotropic phase and lead to a larger temperature range for coexistence between isotropic and blue phases. Furthermore, the isotropic regions can be faceted, their shape and size is controlled by the blue phase elasticity.

In the final system, a nematic emulsion is created. Droplets of nematic LC are dispersed in water. Colloidal particles initially mixed into the liquid crystal decorate the interface between the two fluids. The addition of a surfactant switches the liquid crystal alignment at the fluid-fluid interface from planar to homeotropic. This forces a change in defect structure, from two boojums at the poles to a hedgehog defect in the droplet centre. The presence of colloids affects the switching dynamics and alters the final liquid crystal alignment preventing the droplets from forming a central radial defect.

There is a symbiotic relationship between the particle properties — size and anchoring at the surface — and the elastic properties of the liquid crystal in the bulk and in the presence of an interface with an isotropic fluid. How the systems respond when the balance of these factors is altered is explored throughout the thesis.

Lay Summary

This thesis describes experiments on materials which are mixtures of liquid crystals and colloids (micron-sized particles). Liquid crystals are a phase of matter between a liquid and a solid; they flow like liquids but have a partial degree of order. This results in striking textures and unique properties for use in applications such as flat panel displays (LCDs) and sensors. The key feature of liquid crystals is that they are sensitive to external influences such as temperature and electric fields.

Adding colloids to liquid crystals disturbs the latters order and produces asymmetric interactions between the colloids, leading them to assemble into structures which do not occur in simple liquids.

There are three liquid crystal - colloid systems explored in this thesis. Each system possesses an interface between the liquid crystal and an isotropic (normal) fluid. In the first system a flat interface between a liquid crystal and an isotropic liquid is created. The liquid crystal creates a periodic pattern at the interface and colloids are found preferentially in certain locations. The position of the particles perpendicular to the interface depends on their size and the periodicity of the liquid crystal. In the second system, colloids are found to influence how a liquid crystal melts. In the third system, a study was made of how small liquid crystal droplets alter in appearance to a chemical added to the water in which they are suspended. The final state is shown to be dependent on the number of colloids present in the liquid crystal droplet.

Declaration

I declare that this thesis was composed by myself, that the work contained herein is my own except where explicitly stated otherwise in the text, and that this work has not been submitted for any other degree or professional qualification except as specified.

Work which has formed part of jointly-authored publications has been included. The contribution of the candidate and the other authors to this work has been explicitly indicated below. I confirm that appropriate credit has been given within the thesis where reference has been made to the work of others.

Jointly-authored publications form the basis of chapter 4. All the experiments were carried out by the candidate. Simulations were carried out by J.Lintuvuori and others and are included to aid interpretation of the experimental results. The papers have been published as:

Pawsey, A. C., J. S. Lintuvuori, T. A. Wood, J. H. J. Thijssen, D. Marenduzzo and P. S. Clegg, "Colloidal particles at the interface between an isotropic liquid and a chiral liquid crystal." *Soft Matter* (2012), 8422, doi: 10.1039/c2sm25434d

Lintuvuori, J. S., A. C. Pawsey, K. Stratford, M. E. Cates, P. S. Clegg and D. Marenduzzo, "Colloidal Templating at a Cholesteric-Oil Interface: Assembly Guided by an Array of Disclination Lines." *Phys. Rev. Lett.* (2013), **110**, 187801, doi: 10.1103/PhysRevLett.110.187801

(*Anne Claire Pawsey, April 2014*)

Acknowledgements

I owe a huge dept of gratitude to the many people who have supported me during the preparation of this thesis. First, I would like to thank my supervisor Paul Clegg for his scientific insights, humour and encouragement throughout my PhD. Thanks to Juho Lintuvuori for his patience in explaining the simulation results which inspired so much of the work in this thesis. I'm sorry I could not just rotate the sample 90° to get perfect agreement with the boundary conditions.

I would also like to acknowledge Andy Schofield for providing colloidal particles, Job Thijssen and Tiffany Wood for their help with experiments. I've had many extremely helpful discussions with Oliver Henrich and Davide Marrenduzzo throughout the course of this project. I'd like to thank Jenny, Holly, Siobhan, Diarmuid and Kym for proofreading this manuscript. Special mention should go to the residents of the retirement home (past and present) for teaching me to code.

On a personal note, thank you to all my friends here in Edinburgh and further afield for moral support and interesting distractions. Thanks to my parents for their love, support and encouragement. Finally, thank you to Bengt for everything.

Contents

List of Figures

List of Tables

Chapter 1

Introduction

The phase of a material, whether it is a solid, liquid or gas has a profound effect on its material properties as can be seen in figure 1.1. Solids can support their own weight, liquids deform under gravity and flow. The optical properties of the material can also change. The difference between solid and liquid water is familiar as is the process (melting/freezing) which transforms one phase into another.

In some materials, there are phases between these two states which share properties of both liquids and crystalline solids. These are liquid crystals, they flow like a liquid but have some partial order. Liquid crystals are most commonly found imprisoned behind glass in the form of liquid crystal displays (LCDs). In these devices the liquid crystals are prized for their optical properties and sensitivity to external influences such as electric fields.

This sensitivity means that liquid crystals have applications outside displays including as emulsion-based bio-sensors [55], and when combined into a rubber as temperature or light triggered actuators [31]. In these non- display applications, liquid crystals are frequently combined with other materials to add additional functionality.

These materials are part of a class of materials known as soft matter, which also share properties of liquids and solids. Examples of soft matter include emulsions e.g mayonnaise, foams, colloidal dispersions e.g milk, pastes and gels. These systems all have components which are of a size between the atomic $\sim 1\,\mathrm{nm}$ and the bulk $\sim 1\,\mathrm{mm}$. The components with this mesoscopic length scale are the oil droplets in the emulsion, the bilayers in a foam or the particle radius


(a) (b)

Figure 1.1 Water in (a) solid and (b) liquid form (b) (Ice photo courtesy of B.Tegner)

in the dispersion. This intermediate length scale is often similar to the wave length of light allowing materials to be studied using optical microscopy. The materials are also soft and responsive to external fields as the interactions between the components are typically similar in magnitude to thermal fluctuations. Soft materials can be metastable, out-of-equilibrium states. Such materials are exquisitely sensitive to how they are prepared and can often have history dependent behaviour.

In this thesis, systems with two (or more) competing mesoscopic length scales are studied. This competition between the different length scales adds a greater degree of richness to the physics. The behaviour of each of the systems studied is shown to be a delicate balance between competing effects.

The thesis is set out as follows: -

Chapter 2 introduces the physics underlying the materials used in this thesis. The phase behaviour of liquid crystal is explored. The influence of colloidal particles and interfaces on the liquid crystals is discussed with a particular emphasis on the competing length and energy scales of each system.

Chapter 3 details the experimental methods used throughout this thesis.

Chapter 4 contains experiments on colloidal particles at a cholesteric interface. The distributions of the colloidal particles on the interface and perpendicular to it are measured. The competing length scales of the liquid crystal pitch and the colloid radius are found to control the physics.

In **chapter 5** micron-sized particles trapped within the delicate liquid crystal blue phase are studied. The colloidal particles alter the transition temperature and pathway of the phase transitions from the cholesteric to the blue phase and into the isotropic.

In **chapter 6** droplets of nematic are dispersed in water. The response of the droplets to the addition of surfactant is studied. The switching behaviour is altered by the presence of the colloidal particles. The interplay between the colloidal particles and the defects inherent in the system dominates the physics.

Finally, in **chapter 7** the results are summarised and avenues for future work discussed.

Chapter 2

Theoretical Background

2.1 Introduction

This chapter introduces the underlying physics of the three systems explored in this thesis: it describes the relevant liquid crystal (LC) phases. The Oseen-Frank model of liquid crystal elasticity will be introduced and used to discuss the energetics of defects and colloidal inclusions in the liquid crystal phase. The behaviour of liquid crystals at an interface with an isotropic fluid will be described. The importance of the competing energy and length scales within the composites systems is discussed. Specifically, the balance between the liquid crystal elasticity described by the Frank elastic constants (K_{ij}), the anchoring energy of the LC at a surface (W_a), and the radius of any inclusion within the LC or droplet of LC (R).

2.2 Liquid Crystals

Liquid crystals are intermediate, "meso" phases of matter which are found between the isotropic liquid and the solid phase. On cooling from an isotropic liquid, liquid–crystalline phases appear as a milky fluid prior to the fluid freezing. The temperature at which the liquid crystal appears/disappears is known as the clearing point. The liquid crystal mesophases possess properties of both liquids and solids. For example, they flow like a liquid but can transmit torque like a solid.

Liquid crystals are composed of anisotropic mesogens which are typically either rod or disc shaped. Other shapes, including "banana" shaped molecules can also exhibit liquid crystalline behaviour. The phase behaviour of a liquid crystal can be controlled by temperature, in which case the LC is thermotropic or by concentration, in the case of a lyotropic liquid crystal. Mesogens can be molecular, colloidal or surfactant based structures such as micelles.

Friedel [32] classified the liquid crystals into distinct mesophases based on their degree and manner of ordering. The ordering can be orientational, where the mesogens break rotational symmetry and align along a common axis. Additionally there can also be a degree of positional order where the liquid has some periodic structure. The mesophases considered in this thesis are discussed in more detail below.

2.2.1 Nematics

The simplest mesophase is a nematic liquid crystal, where the long axes of the molecules point on average in the same direction characterised by a headless vector known as the director, written $\mathbf{n}$. Their centres of mass remain randomly distributed as shown in figure 2.1(a).

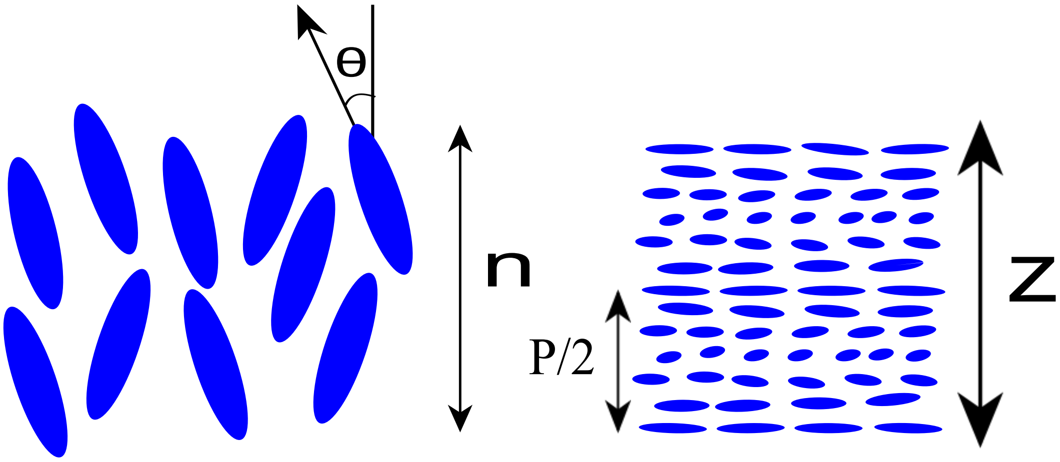

(a) Nematic (b) Cholesteric

Figure 2.1 Schematic of nematic and cholesteric phase. $\mathbf{n}$ is the nematic director. p the pitch length of the cholesteric and z the helical axis direction

2.2.2 Cholesterics

When the mesogens have some degree of chirality or a chiral dopant is added the some of the liquid crystal phases become chiral. The chirality is exhibited on the scale of the bulk liquid crystal in these chiral (cholesteric) phases. The average direction of the mesogens changes through the sample in one of the directions perpendicular to the nematic director $\mathbf{n}$. The director maps out a helix with a characteristic pitch length much larger than the constituent mesogens as shown in figure 2.1(b). The liquid crystal alignment can be described by two vectors: the nematic director $\mathbf{n}$ and the helical axis $\mathbf{z}$. The system is periodic along $\mathbf{z}$. The length scale associated with this periodicity is known as the pitch length p, the distance over which the director rotates by 2π. This periodicity means that cholesterics can be considered mathematically as periodic quasi-lamellar media.

2.2.3 Phase Transitions

The temperature at which a liquid crystal changes from an isotropic liquid into a nematic phase is known as the clearing point. At this temperature the disordered isotropic phase starts to become ordered. The long axis of the mesogens align along a common axis. One can define an order parameter; an average property of the system which is zero in the disordered phase and takes a finite value in the ordered phase. The order parameter has the same symmetry as the ordered phase. In a nematic the order parameter S can be defined as

$$S = \frac{1}{2}\left(3\langle cos^2\theta\rangle - 1\right), \tag{2.1}$$

where θ is the angle between an individual molecule and the director $\mathbf{n}$ (figure 2.1(a)). The average $\langle cos^2\theta\rangle$ is taken over all the mesogens. In the solid phase (perfect alignment) $\langle cos^2\theta\rangle = 1$ and hence $S = 1$. In the isotropic phase $\langle cos^2\theta\rangle = \frac{1}{3}$, $S = 0$. In the nematic phase S is finite and typically ~ 0.6 [35].

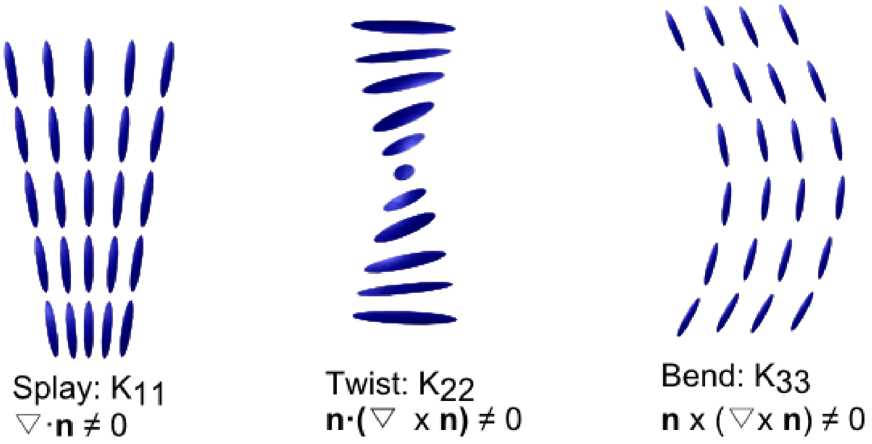

Figure 2.2 Schematic of elastic deformations

2.2.4 Elastic Deformations

A liquid crystal can be deformed elastically from its uniform alignment with an associated energy cost. The general elastic energy density can be written:

$$f_{el} = \frac{1}{2} K_{ijkl} \nabla_i n_j \nabla_k n_l, \tag{2.2}$$

This must be integrated over the sample volume to calculate the elastic energy. K_{ijkl} is a tensor containing the elastic constants. Equation (2.2) simplifies significantly, given that the free energy must be invariant under rotation of the whole sample and under the symmetry operations associated with the nematic $\mathbf{n} \rightarrow$ -$\mathbf{n}$ and $\mathbf{x} \rightarrow$ -$\mathbf{x}$. As $\mathbf{n}$ is unitary $n_i \nabla_j N_i = 0$. This leaves three allowed deformations, shown in figure 2.2, known as splay $\nabla \cdot \mathbf{n} \neq 0$, twist $\mathbf{n} \cdot (\nabla \times \mathbf{n}) \neq 0$ and bend $\mathbf{n} \times (\nabla \times \mathbf{n}) \neq 0$ and they have associated Frank elastic constants K_1, K_2, K_3.

The Frank elastic free energy density can therefore be expressed as:

$$f_{\mathrm{el}} = \frac{1}{2} \left[K_1 (\nabla \cdot \mathbf{n})^2 + K_2 (\mathbf{n} \cdot (\nabla \times \mathbf{n}))^2 + K_3 (\mathbf{n} \times (\nabla \times \mathbf{n}))^2 \right], \tag{2.3}$$

For cholesterics there is an additional term q_0 which reflects the chirality of the liquid crystal, giving;

$$f_{\mathrm{el}} = \frac{1}{2} K_1 (\nabla \cdot \mathbf{n})^2 + \frac{1}{2} K_2 (\mathbf{n} \cdot \nabla \times \mathbf{n} - q_0)^2 + K_3 (\mathbf{n} \times (\nabla \times \mathbf{n}))^2, \tag{2.4}$$

where q_0, the chirality of the liquid crystal is defined as $\frac{2\pi}{p}$ and p is the cholesteric pitch length.

There are also deformations which do not enter into the standard free energy calculations as they take the form of a divergence. In the case of a defect free bulk sample these terms can be integrated out via the divergence theorem. However, they become significant in the presence of surfaces and defects. These deformations, originally described by Nehring and Saupe [73] are known as the divergence terms.

$$f_{13} + f_{24} = K_{13}\left[\nabla \cdot \left(\mathbf{n}\left(\nabla \cdot \mathbf{n}\right)\right)\right] - K_{24}\left[\nabla \cdot \left(\mathbf{n}(\nabla \cdot \mathbf{n}) + \mathbf{n} \times (\nabla \times \mathbf{n})\right)\right], \qquad (2.5)$$

K_{24} is the saddle splay deformation shown in figure 2.2(d). It plays an important role in the stability of blue phases as discussed in section 2.2.6. K_{13} involves 2nd order derivatives of $\mathbf{n}$ and is frequently neglected in analysis. It is useful for analysing the behaviour of liquid crystals in confinement.

2.2.5 Defects

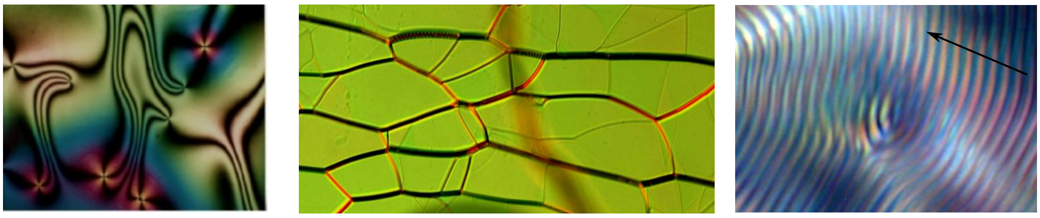

(a) (b) (c)

Figure 2.3 Liquid crystal textures showing defects. (a) Defects in a Nematic LC adapted from [3]. (b) The oily streak network of a cholesteric liquid crystal.Defects are dark streaks against the uniformly aligned yellow/green background. (c) The fingerprint texture of the cholesteric. The arrow shows the direction of the helical axis.

In addition to elastic distortions of the liquid crystal, places exist where there is discontinuity in the director field. These defects are easily visible under the microscope (see figure 2.3). The thread like appearance of disclinations in nematics viewed between crossed polarisers are what led Friedel to name the phase after the Greek for thread “nema” [35]. Cholesterics also have a characteristic defect structure known as oily streaks. Theses are shown in figure 2.3(b). Altering the boundary conditions of a liquid crystal sample can allow defects to be imaged more easily as in the cholesteric fingerprint texture, figure 2.3(c).

The defects are known as disclinations: a location where the orientational order of the LC is disrupted. These are analogous to dislocations in solids, locations where positional order of atoms is disrupted. These defects can take the form of points or lines and are classified via their topology.

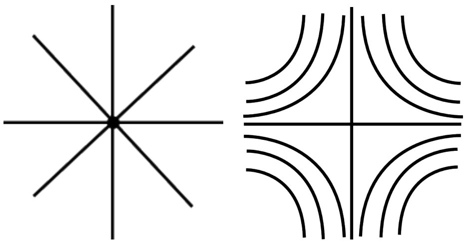

(a) m=1 **(b)** m=-1

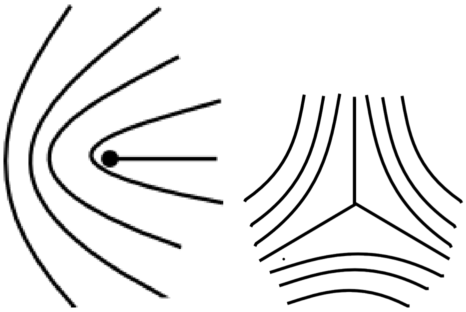

(c) m=1/2 **(d)** m=-1/2

Figure 2.4 Defects of topological charge m

In nematics the classification of defects is relatively simple, one counts the number of rotations the director undergoes when one traverses a circle enclosing the defect. This gives the topological charge m. E.g. If the director rotates clockwise by π as you travel clockwise in a loop around the defect then the charge is $m = +1/2$ (figure 2.4(c)). Examples of various defects can be seen in figure 2.4.

In the cholesteric case there are further restrictions on the types of allowed defects. The restrictions are due to the periodic nature of the cholesteric helix. The overall symmetry of the liquid crystal must be conserved. A method of (mathematically) generating defects in a cholesteric phase is the Volterra process as described in [35]. It proceeds as follows:

1. The cholesteric is ”frozen” into a solid body.
2. This body is cut along a surface S, the boundary of which is a line L,

figure 2.5(a).

3. Displace one of the halves of material by a translation $\mathbf{b}$ and/or a rotation $\mathbf{\Omega}$. After this the material on both sides must still match up with one another. This condition imposes various restrictions on the allowed translations and rotations.

4. Fill up any gaps with in register cholesteric or alternatively remove any excess material, figure 2.5(b).

5. Let the whole system relax, figure 2.5(c),

The restrictions discussed in item 3 lead to the following allowed defects. λ and τ lines are formed by rotating the material about and axis perpendicular to the helix and either perpendicular (for τ lines) or parallel (for λ lines) to the local director. There are also χ lines which are analogous to edge dislocations in lamellar media but can have resulted from translating the two halves of the cut leaving a separation of either a full or a half pitch and inserting an additional cholesteric layer. χ lines frequently decompose into combinations of λ and/or τ defect pairs, figure 2.5(d).

Energetics of Defects

The formation of defects of all forms costs the system energy. The liquid crystal order is destroyed in the centre of a defect and there is an elastic cost from the distortion of the liquid crystal. Following the arguments set out in [78], the elastic cost of a defect line can be calculated as follows. In the single elastic constant approximation ($K_1 = K_2 = K_3 = -2K_{24}$ and $K_{13} = 0$) the elastic free energy can be written as:

$$f_{el} = \frac{1}{2} K \partial_i n_j \partial_i n_j, \tag{2.6}$$

Assuming that the director is confined to a plane normal to the defect then this can be expressed as

$$f_{\mathrm{el}} = \frac{1}{2} K \left(\nabla \varphi \right)^2, \tag{2.7}$$

where $\varphi(x, y)$ is the angle between the director and the x axis (figure 2.6). The energy of the system is minimised when $\Delta\varphi = 0$; written in cylindrical coordinates

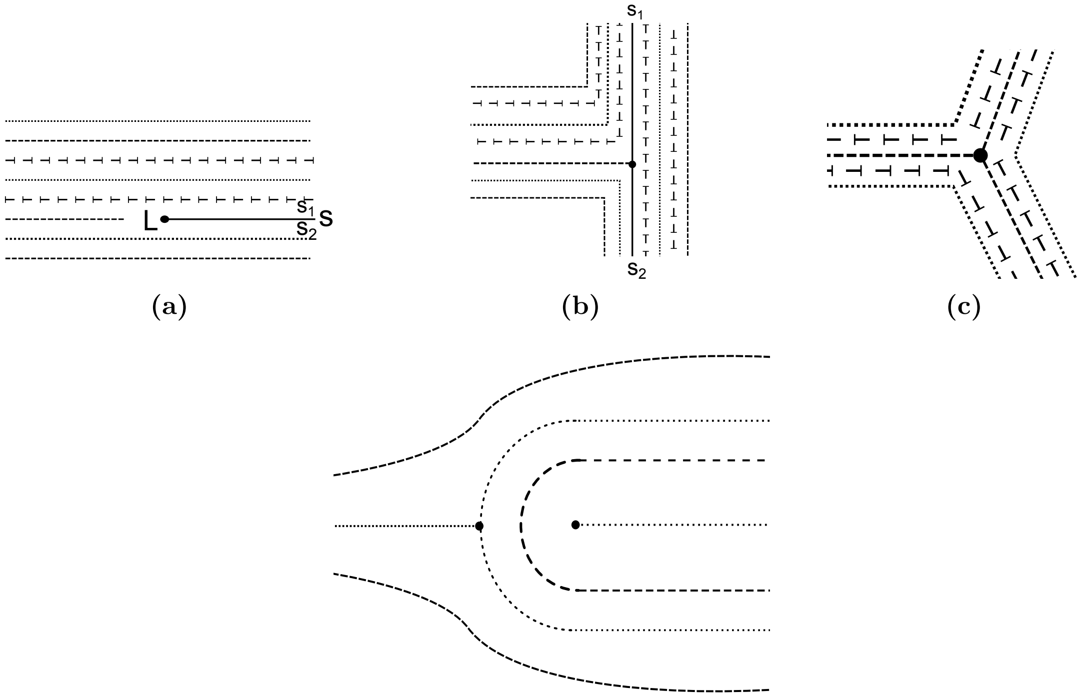

(a) (b) (c)

(d)

Figure 2.5 (a) – (c) Formation of a τ^- defect via the Volterra process. (a) The material is cut along S. (b) the two sides are each rotated by $\pm\pi/2$ about the axis L and additional cholesteric is added on the right hand side. (c) The structure relaxes leaving a singular line (into the page). (d) Shows a χ edge defect decomposed into a $\lambda^+\lambda^-$ pair

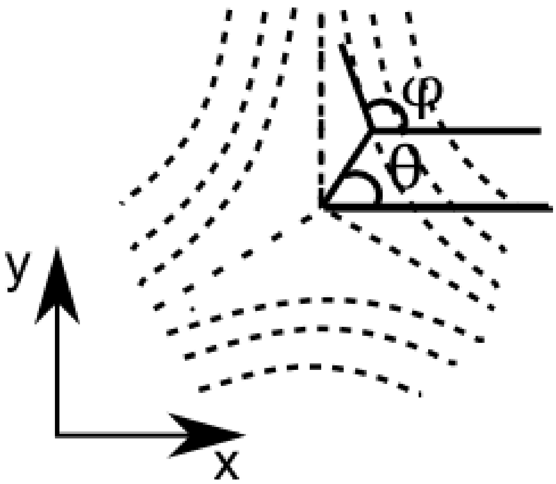

Figure 2.6 Measuring the angle of the nematic director φ at an angle θ

as,

$$\frac{1}{r}\frac{\partial}{\partial r}\left(r\frac{\partial \varphi}{\partial r}\right)+\frac{1}{r^2}\frac{\partial^2 \varphi}{\partial \theta^2}=0, \tag{2.8}$$

one such solution is;

$$\varphi = m\theta + C, \tag{2.9}$$

where m is the topological charge of the defect and C is a constant.

The energy per unit volume from equation (2.7) is

$$f_{el}=\frac{1}{2}K\left(\frac{1}{r}\frac{\partial \varphi}{\partial \theta}\right)^2=\frac{1}{2}K\frac{m^2}{r^2}, \tag{2.10}$$

Per unit length of disclination this is:

$$F_{el}=\int_{r_c}^{R} f_{el}2\pi r dr=\int_{r_c}^{R}\frac{1}{2}K\frac{m^2}{r^2}2\pi r dr=\pi K m^2 \ln\left(\frac{R}{r_c}\right), \tag{2.11}$$

where r_c is a cut off length, known as the core radius, inside which the elastic energy diverges. R denotes the volume of the sample.

There is an energy cost associated with this defect core. The gradients of the director field involved are too large to be treated with the general elasticity theory discussed above. The energy per unit length of the defect therefore contains an additional contribution from the defect core (E_{core}). The full energy per unit length is written as:

$$F=\int_{r_c}^{R} f_{\mathrm{el}}2\pi r dr+E_{\mathrm{core}}=\pi K m^2 \ln\left(\frac{R}{r_{\mathrm{c}}}\right)+E_{\mathrm{core}}, \tag{2.12}$$

The simplest model assumes that the liquid crystal is isotropic in the core. Assuming we have $k_B(T_{\mathrm{NI}}-T)$ in energy per degree of freedom and that the number of degrees of freedom is equivalent to the number of molecules in the core then the core energy per unit length of defect can be expressed as:

$$E_{\mathrm{core}} \sim k_B(T_{\mathrm{NI}}-T)\pi r_c^2\frac{\rho N_A}{M}, \tag{2.13}$$

where ρ is the mass density of the liquid crystal, N_A is Avogadro's number and M is the molecular mass. Substituting this into equation (2.12) and minimising to find r_{c} leads to:

$$r_{\mathrm{c}} \sim m\sqrt{\frac{MK}{\rho N_A k_B(T_{NI}-T)}}, \tag{2.14}$$

And

$$E_c \sim \pi m^2 K, \tag{2.15}$$

The total energy in the presence of a planar defect is therefore:

$$F = \pi K m^2 \ln\left(\frac{R}{r_c}\right) + \pi m^2 K, \tag{2.16}$$

This shows a dependence on the topological charge m. Only low charge defects, $m = \pm 1/2, \pm 1$ are stable. Other defects will decompose into combinations defects with lower topological charge.

2.2.6 Blue Phases

Rather than a representation of a non-ideal system, disclinations are intrinsic to the blue phases. These phases appear in highly chiral liquid crystals in a narrow temperature window between the isotropic and cholesteric phase. A temperature –chirality phase diagram can be seen in figure 2.7(a). The blue phases are typically only stable for a small temperature range of $\sim 1\,\mathrm{K}$ and they only appear in samples with high chirality (short pitch).

There are three distinct blue phases. Blue phase I, figure 2.8(a) and blue phase II, figure 2.8(b) form a cubic network of disclinations. The lattice constant of the network is $\sim 500\,\mathrm{nm}$, so blue phases scatter in the optical region of the spectrum [24, 78]. Different alignments of the blue phase lattice within a sample give rise to the blue phase platelet texture figure 2.7(b)). Blue phase III is amorphous and has a fog like appearance, a possible structure is shown is figure 2.8(c).

Historical Background

Blue phases were first observed experimentally in 1888 [86]. They were not much studied until the 1970's and until then there remained a lingering suspicion that they might not actually exist [24]. In the 1970's theoretical studies showed that blue phases should exist and experiments confirmed this. However, for much of their history blue phases have been considered a mere curiosity; Frank writing in 1983 (quoted in [78]) said that:

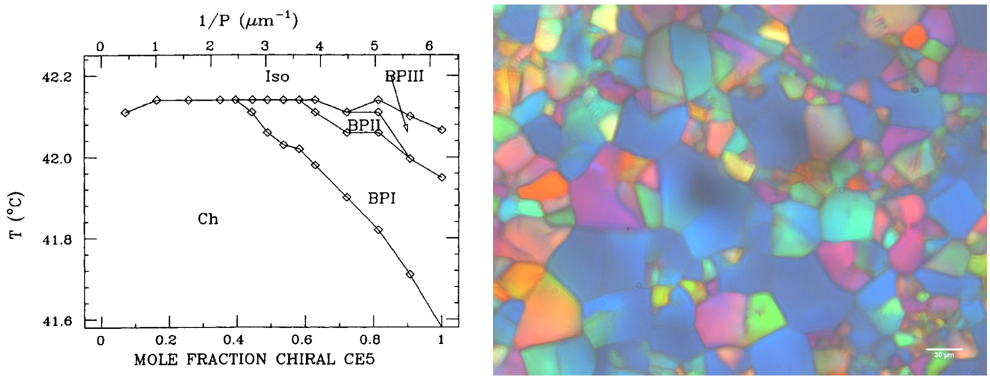

(a) Phase diagram of a cholesteric blue phase from [24]. The x-axis is the chirality of the liquid crystal, linked to quantity of chiral dopant added.

(b) Platelet texture of BPI

Figure 2.7 An example BP phase diagram and the BPI platelet texture.

> "They are totally useless, I think, except for one important intellectual use, that of providing tangible examples of topological oddities, and so helping to bring topology into the public domain of science, from being the private preserve of a few abstract mathematicians and particle theorists."

The most convincing evidence for the existence of blue phases was provided by calorimetry measurements (cited in [24]) which showed unambiguously that there were three distinct, thermodynamically stable phases between the isotropic liquid and the underlying cholesteric phase. Following this discovery, the principle focus of experimental work was elucidating the equilibrium structure and temperature-chirality phase diagram of the blue phases.

Interest in blue phases increased following the creation of BPs with a large temperature range in 2002 by Kikuchi *et al.* [49] and followed in 2005 by Coles *et al.* [19]. The stabilisation mechanisms for these broad range phases are different. Kikuchi *et al.* [49] created a polymer stabilised blue phase with a temperature range of more than 60 K which included room temperature. A mixture of monomers and liquid crystal is cooled from the isotropic into the blue phase and then exposed to UV light. This process is delicate, the blue phase must be maintained until the entire sample has polymerised otherwise the stabilising effect is lost. If the polymerisation takes place in the isotropic or cholesteric phase the blue phase is not stabilised. This suggests that the polymer is concentrated in the cores of the disclinations. The mechanism suggested is that the monomers are more miscible with the isotropic liquid in the defect cores than in the rest of the blue phase and hence are concentrated in the disclination cores where they are polymerised. If the polymer network is formed in the isotropic phase the polymer is too big to diffuse into the core and hence has no stabilising effect. If the monomers are polymerised in the cholesteric phase the oily streak network is stabilised.

Coles *et al.* [19] reported a stable blue phase with a temperature range of 50°C, the mechanism of stabilisation is ascribed to the flexoelectric response of specific bent core mesogens [16]. The bent core nature of the molecules increases the energy saving of the double twist configuration (see below). This system has been further developed with the addition of polymers to create a template for the blue phase which can then be formed from a non chiral LC [15].

Theoretical Background

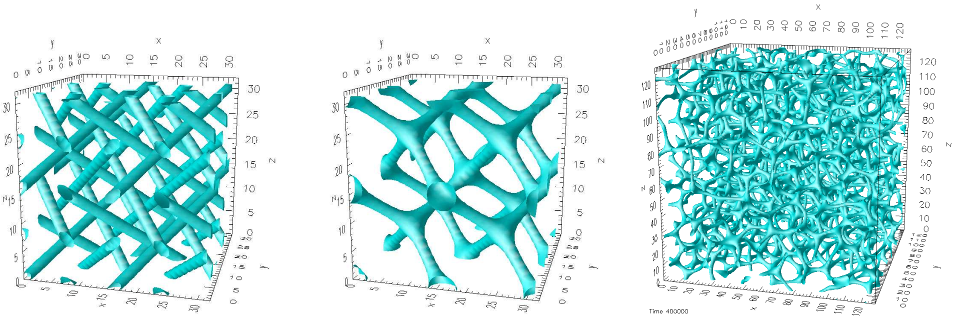

(a) BPI **(b)** BPII **(c)** BPIII

Figure 2.8 Defect structure of the three blue phases [40]

An intuitive understanding of blue phases can be obtained by considering the interactions of the individual chiral molecules. Chiral molecules rotate with respect to one another. Locally it is most favourable for them to twist in any direction perpendicular to the local director. Due to topological constraints it is impossible for this twisting to continue indefinitely without defects appearing. The twist can extend parallel to the helical axis and a short way perpendicular to it creating a structure known as a double twist cylinder, shown in figure 2.9(a). It is impossible for these structures to fill space without the inclusion of $m = -1/2$ disclination lines seen in figure 2.9(b).

The blue phases are only formed if the energy saved by the double twist

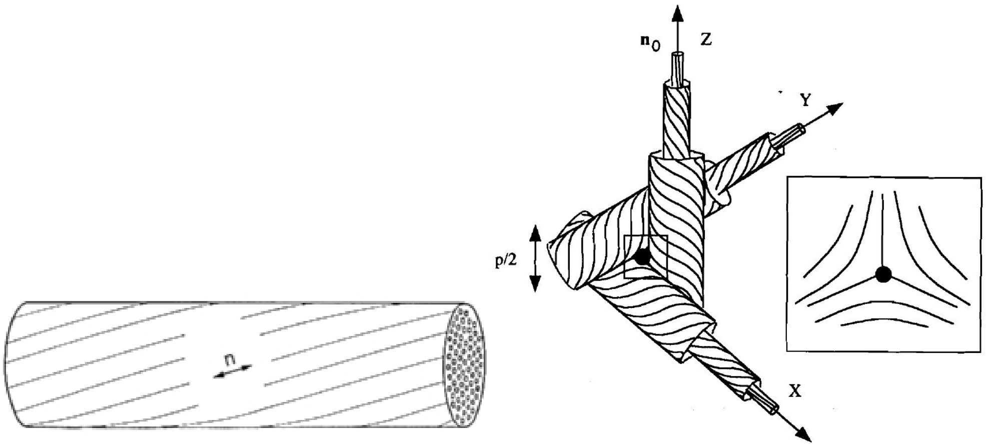

(a) A double twist cylinder (b) Junction between double twist cylinders

Figure 2.9 Double twist cylinders and the m=1/2 defect found at the junction between them [65]

configuration is greater than that required by the creation of the disclinations. A qualitative understanding can be gained by following an argument originally given by Meiboom *et al.* [65]

A general form of the elastic free energy density of the blue phase can be written as:

$$\begin{aligned} f_{\text{elastic}} = \frac{1}{2}K_1\left(\nabla\cdot\mathbf{n}\right)^2 + \frac{1}{2}K_2\left(\mathbf{n}\cdot\nabla\times\mathbf{n}-q_0\right)^2 + \frac{1}{2}K_3\left(\mathbf{n}\times\left(\nabla\times\mathbf{n}\right)\right)^2 \\ +\frac{1}{2}\left(K_2+K_{24}\right)\nabla\cdot\left[\left(\mathbf{n}\cdot\nabla\right)\mathbf{n}-\mathbf{n}\left(\nabla\cdot\mathbf{n}\right)\right], \end{aligned} \tag{2.17}$$

where K_{ij} are the Frank elastic constants associated with elastic deformations of the medium, $\mathbf{n}$ is the director and q_0 is the chirality of the liquid crystal. The first three terms are those in equation (2.4). The final term includes the contribution of the saddle splay deformation (equation (2.5)). In a bulk cholesteric without defects this final term is ignored in free energy calculations as discussed in section 2.2.4. However, in the case of the blue phase this term cannot be ignored as the integration has to take into account the presence of the defects.

First, we consider the energy saving from having the director in the double twist configuaration. The director field can be expressed as,

$$\mathbf{n} = (q_0y, -q_0x, 1), \tag{2.18}$$

where q_0 sets the magnitude of the twist. Substituting into equation (2.17) the free energy of the blue phase in the presence of a double twist can be expressed as;

$$f_{elastic} = \frac{1}{2}k_{22}q_0^2 - (k_{22} + k_{24})q_0^2, \tag{2.19}$$

This is negative, implying that the double twist configuration is locally more stable. However, the double twist arrangement requires that defects are produced. The full free energy must therefore be considered found by integrating the expression in equation (2.17) plus the contributions from the defects:

$$F = \int f_{\mathrm{el}} dV + F_{\mathrm{core}} + F_{\mathrm{interface}} \tag{2.20}$$

f_{el} is the elastic energy density of the liquid crystal. F_{core} is the energy (per unit length) required to have the core of the disclination in the isotropic. $F_{\mathrm{interface}}$ is the cost of having an interface between the isotropic core and the surrounding blue phase.

The elastic free energy can also be split into the standard Frank free energy as per equation (2.3) and the final divergence term. The elastic cost of the $m = -1/2$ can be calculated from equation (2.11) giving:

$$F_{\mathrm{elastic}} = \pi K \frac{1}{4} \ln\left(\frac{R}{r_c}\right), \tag{2.21}$$

As previously there is a contribution from the isotropic core which we approximate using equation (2.13) as

$$F_{\mathrm{core}} \sim a(T^{\mathrm{BP-ISO}} - T)\pi R^2, \tag{2.22}$$

Where $T^{\mathrm{BP-ISO}}$is the blue phase to isotropic phase transition temperature, T is the temperature and R is the core radius, a contains all the material constants present in equation (2.13).

The cost of the interface between the isotropic and liquid crystal phases at the edge of a defect, can be written simply;

$$F_{\mathrm{interface}} = \sigma 2\pi r_c \tag{2.23}$$

where σ is the surface tension between the blue phase and the isotropic — this is very small.

Finally the contribution of the divergence term in the presence of defects can be calculated as:

$$F_{\text{divergence}} \sim -\pi K, \tag{2.24}$$

where K is the elastic constant using the single elastic constant approximation. This is found by integrating the final term in equation (2.17) on the surface of a cylinder surrounding a $m = -1/2$ disclination.

Combining the terms in equations (2.21) to (2.24) the free energy of the blue phase is:

$$F = \pi K \frac{1}{4} \ln\left(\frac{R}{r_c}\right) + a(T^{BP-ISO} - T)\pi r_c^2 + \sigma 2\pi r_c - \pi K, \tag{2.25}$$

The blue phase is stable when this expression is negative.

The above description does not result in a structure for the blue phase, it simply shows that there are circumstances where the double twist is more stable than the alternate cholesteric phase. Possible structures consistent with experimental results were proposed by Meiboom [65], and constructed by interlacing space with sets of double twist cylinders. However, this can feel a little forced and it does not explain the existence of blue phase III.

In order to get a full structure for the blue phase, the full Landau-de Gennes free energy needs to be minimised. This is typically done numerically and gives rise to the structures of BPI and II seen in figure 2.8; for the BPIII structure the hydrodynamics of the system were included via a hybrid-lattice Boltzmann approach [39]. This method of simulation has allowed a huge number of different blue phase systems to be studied in recent years [40, 84, 85, 97] and is also employed to model the behaviour of colloidal particles within cholesteric liquid crystals [56–58] as discussed in chapter 4 of this thesis.

2.3 Colloidal Particles in Liquid Crystals

2.3.1 Colloidal Particles

Colloids are “small” ($< 10\,\mu\mathrm{m}$ particles of solid or droplets of liquid dispersed in liquid medium. In the context of this thesis, these are solid particles dispersed in a liquid/liquid crystalline medium. The typical size of the dispersed particles is between $10\,\mathrm{nm}$ and $10\,\mu\mathrm{m}$ small enough that they undergo Brownian motion but large enough that quantum mechanical properties of the individual particles can be neglected. Colloidal particles in the fluid can collide and stick together on contact, a process known as aggregation. In order to prevent this, colloidal particles are stabilised against agreagtion either by making them charged or by grafting short polymer “hairs” on the particles (steric stabilisation). Both charge stabilised and sterically stabilised colloids are used in this thesis (see section 3.1).

2.3.2 Colloidal Particles in Nematics

Colloidal particles can be dispersed into liquid crystal phases. The surface of a colloidal particle can force the liquid crystal into a given alignment. This means colloidal particles seed defects in the ordered phase. The nature of the defects is dependent on the particle size and the alignment and anchoring strength at the particle surface.

The free energy functional has to be modified to take the colloidal particles into account. In addition to the Frank elastic terms equation (2.3), the F_{24} divergence term equation (2.5), needs to be included and a term taking surface anchoring into account.

$$F = F_{\mathrm{el}} + F_{24} + F_{\mathrm{surface}} \tag{2.26}$$

The surface energy density is usually approximated using the Rapani-Poplar expression [92].

$$f_{\mathrm{surface}} = \frac{W_a}{2}[(1 - \mathbf{n} \cdot \hat{\nu})^2], \tag{2.27}$$

The unit vector $\hat{\nu}$ denotes the preferred orientation at the surface and W_a is the anchoring strength. The full free energy is:

$$
\begin{aligned}
F = \int dV\{\frac{K_1}{2}\left(\nabla\cdot\mathbf{n}\right)^2 + \frac{K_2}{2}\left(\mathbf{n}\cdot\nabla\times\mathbf{n}\right)^2 + \frac{K_3}{2}\left(\mathbf{n}\times\left(\nabla\times\mathbf{n}\right)\right)^2 \\
-\frac{K_{24}}{2}\{\nabla\cdot(\mathbf{n}(\nabla\cdot\mathbf{n}) + \mathbf{n}\times(\nabla\times\mathbf{n}))\} + \int dS\{\frac{W_a}{2}[(1-\mathbf{n}\cdot\hat{\nu})^2]\},
\end{aligned}
\tag{2.28}
$$

The elastic part of the energy is proportional to the particle radius $F_{\text{el}} \sim KR$ and the surface term to the surface area $F_{\text{surface}} \sim WR^2$. The relative contributions of the elastic and surface terms can be expressed as a dimensionless constant WR/K. The magnitude of this quantity governs whether the colloid surface or the bulk LC dominates the physics. Hence, it controls the defect structure associated with the colloidal particle as seen in figure 2.10(b).

For planar anchoring (figure 2.10(d)) at the particle surface the defect structure is always a pair of so called boojum defects situated at the poles of the particles (figure 2.10(a)). The boojum defects are surface defects with a charge of $m = -1/2$. An explanation of boojums and how they acquired their name (outside the context of Lewis Carrol [14]) can be found in the article by Mermin [66].

For radial anchoring (figure 2.10(c)) there are three possible defect structures (figure 2.10(b)). For strong anchoring where $WR/K \gg 1$ a dipolar structure is found with a $m = -1$ hyperbolic hedgehog balancing the $m = +1$ charge from the particle. For weaker anchoring or a smaller particle the structure has quadrupolar symmetry and consists of a $m = -1/2$ ring defect known as a Saturn ring. This surrounds the equator of the particle. For even weaker anchoring the ring defect is found on the particle surface. An extensive review of experiments and theory of colloidal particles in nematic liquid crystals can be found in [92].

Once dispersed in a liquid crystal, colloidal particles tend to aggregate. The defects mediate anisotropic interactions between the colloidal particles. In a nematic chains of colloidal particles form, either parallel or at 30° to the director depending on their surface anchoring [61, 63]. At higher volume fractions, colloidal particles form a self quenched defect glass [102].

2.3.3 Colloidal Particles in Cholesterics

Whilst the behaviour of colloidal particles in nematic liquid crystals is relatively well understood, the situation when the liquid crystal is chiral has only recently

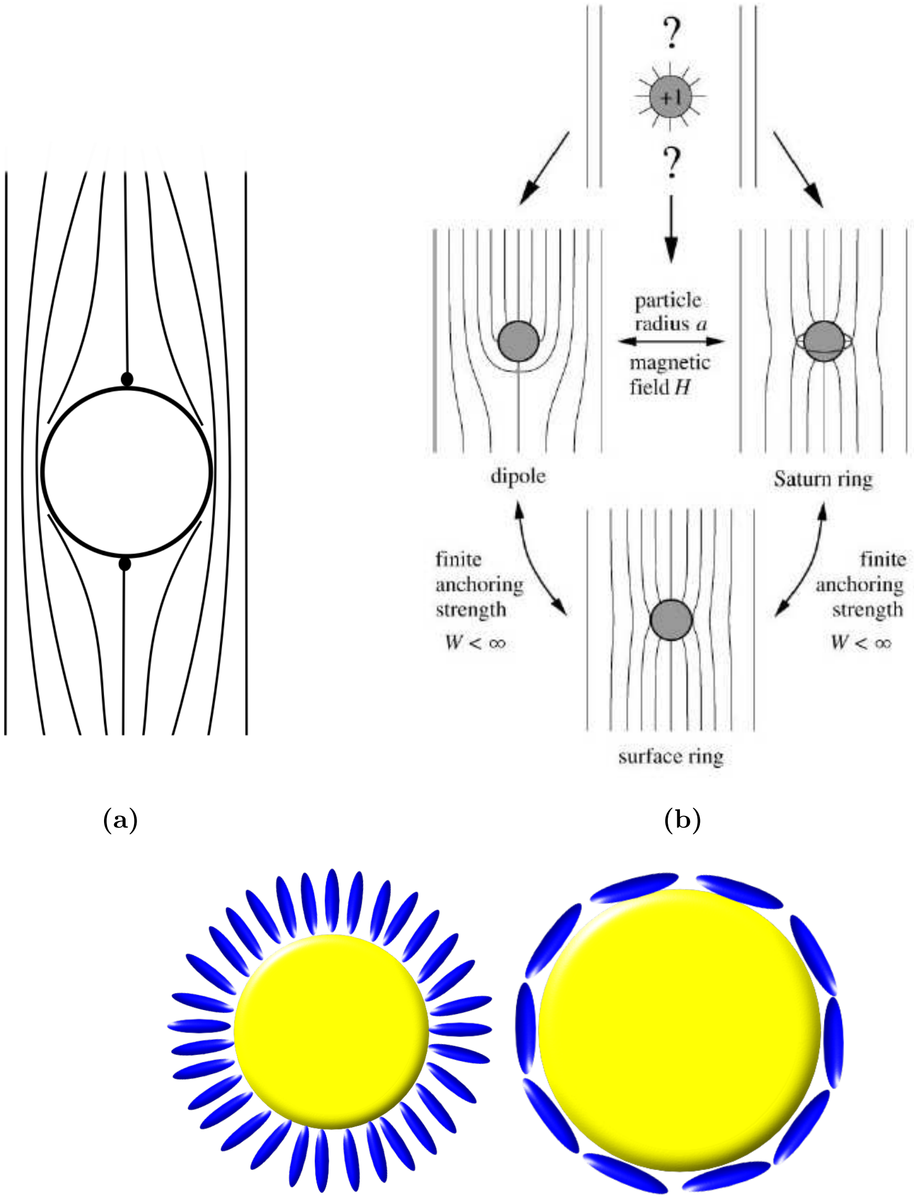

(a) **(b)**

(c) **(d)**

Figure 2.10 (a) Director field around a colloidal particle with planar anchoring. (b)Director field around a colloidal particle with homeotropic anchoring. The anchoring strength and radius determine the defect structure. [92] (c) Schematic of a colloidal particle with homeotropic anchoring. (d) Schematic of a colloidal particle with planar anchoring.

been explored. Simulation studies have suggested that the defect structure at the colloid surface becomes more complex, with the two boojums lengthening into a spiral [57, 59]. The saturn ring structure found with homeotropic colloidal particles also twists into a spiral [57, 59]. This spiral defect has been observed experimentally with a large colloidal particle and a very long pitch cholesteric [46].

In colloidal particle-CLC systems the defect structure and the dynamics of the particles within the CLC is controlled by the ratio between the particle radius and the pitch length of the liquid crystal, R/p. As this ratio increases, the length of the defect surrounding the colloidal particle increases [57, 59]. This alters the dynamics of the colloidal particle within the LC, its behaviour becomes non-Stokesian [59] and colloidal rotors can self assemble [56]. The plate-like aggregates of colloidal particles found in the bulk of chiral LCs become flatter as R/p increases [43].

The addition of even a small degree of twist to a nematic allows complex structures of colloidal particles to be stabilised; colloidal particles can be “knitted” together using a thread of defect lines [100].

Experimental work on bulk dispersions has shown that colloidal particles with homeotropic anchoring are concentrated at the nodes of the cholesteric oily streak network, forming a defect mediated gel [104]. The colloidal particles pin the oily streak network (figure 2.3(b)) in place. Colloidal particles with planar anchoring form flat sheets perpendicular to the helical axis [43]. These sheets become flatter as the pitch is decreased. Given the resolution of the optical microscopes used in these papers it was not possible to resolve the defect structure around the colloidal particles.

If the CLC is sufficiently chiral to form a blue phase, the situation becomes more complicated. Simulations by Ravnik *et al.* [84] suggest that the particles will be incorporated at the junctions of the blue phase disclination lines in BPII forming a 3 dimensional colloidal crystal. The volume of the blue phase unit cell will increase to accommodate the particles. In the simulations the size and anchoring strength of the colloidal particle influences the stability of the structure formed. Experiments by Karatairi et al. [48] use high resolution calorimetry to study blue phase exhibiting liquid crystals doped with cadmium selenide (CdSe) nanoparticles. The particles have a carefully modified surface chemistry to give a very weak interaction with the LC. They report a significant stabilisation of blue phase

III.

They propose that the stabilisation mechanism is similar to that developed by Kikuchi *et al.* [49] to explain polymer stabilised blue phases. As previously discussed, the melted core of the defect lattice which makes up the blue phase costs energy. If a particle is present in the core it can effectively remove an isotropic region reducing the free energy of the core. This can be expressed as:

$$F_{\mathrm{core}} \sim (T^{\mathrm{BP-ISO}} - T)(\pi R^2 h - N_{np} V_{np})/h, \tag{2.29}$$

where h is the length of the disclination N_{np} is the number of nano particles in the disclination and V_{np} is the volume per nano particle. The reduction in core energy extends the temperature stability of the blue phase. A crucial point, elaborated in [21] is that the nano particle must interact weakly with the surrounding liquid crystal. A strong interaction between the liquid crystal and the particle could lead to an additional elastic free energy penalty and potentially have a destabilising effect. An elastic penalty could also lead to the expulsion of the colloidal particles from the liquid crystal; i.e. a bulk phase separation.

A limitation of the nanoparticle studies is that due to their small size the nanoparticles cannot be imaged in situ. Using larger colloidal particles would overcome this problem. A study by Dierking [27] suggests that larger particles increase the temperature range of the BP but to a much lesser degree than smaller particles. This leads to the expectation that with careful temperature control micron sized particles could be imaged within the BP and the influence of the BP defect on the colloidal particles observed directly. This is discussed in chapter 5 of this thesis.

2.3.4 Liquid Crystal Interfaces

The anisotropic nature of a liquid crystal affects the physics of an interface between a liquid crystal and an isotropic fluid. The interface between two immiscible fluids has an energy cost usual expressed as the interfacial tension γ. In liquid crystals the interfacial energy has additional terms due to the anisotropic nature of the LC. The energy of the interface can be split into several parts:

$$\gamma = \gamma_{\mathrm{iso}} + \gamma_{\mathrm{div}} + \gamma_{\mathrm{aniso}} \tag{2.30}$$

The isotropic term γ_{iso} is equivalent to the interfacial tension of an isotropic liquid and does not depend on the liquid crystal alignment. The divergence term γ_{div} is the contribution to the free energy from the divergence terms in the Frank free energy (equation (2.5)) which can no longer be integrated out. The anisotropic term γ_{aniso} is the energy required to distort the nematic director to an angle imposed by the interfacial anchoring. This is equivalent to the surface anchoring energy at a colloidal surface and is described by the Rapini-Poplar approximation as in equation (2.27).

The isotropic part of the surface tension is dominant, γ_{iso} is $\sim 0.03\,\mathrm{J\ m^{-2}}$ which is large compared to the the surface anchoring term $W_a \sim 10 \times 10^{-5}\,\mathrm{J\ m^{-2}}$. γ_{div} is related to the elastic constants which are of the order $10\,\mathrm{pN}$ (example values are taken from [7]).

Liquid crystals can be dispersed in water and other aqueous solutions including glycerol water mixtures to form emulsions [71]. As with normal fluid emulsions droplets can be stabilised using surfactants and particles. In addition elastic and topological effects can play a role in stability.

The alignment of the LC at the LC-aqueous interface can be altered by the addition of surfactants or other molecules to the continuous phase. The alignment of the mesogens is dependent on the concentration of the surfactant. A large number of different substances have been shown to alter the mesogen alignment at the interface. These include surfactants, lipids and proteins [7]. The combination of nanoparticles and surfactants at the interface of a nanodroplet has been shown to exhibit a rich phase behaviour in simulation studies [70]. There is a paucity of experimental work on LC emulsions with colloidal particles. Chapter 6 of this thesis discusses LC emulsion with interfacial particles in more detail and explores the influence of particle on the switching dynamics of the alignment in LC emulsions in the presence of surfactants.

2.4 Particles at Interfaces

Where there is an interface between the liquid crystal and an isotropic phase, colloidal particles, initially mixed into one of the two phases may become trapped at this interface. Once at the interface the colloidal particles reduce the shared area between the two media and reduce the energy cost of the interface (figure 2.11). In cases where the Young equation holds (i.e. simple liquids, no complications due to elastic effects), there is an energy saving

$$\Delta G = -\pi r^2 \gamma (1 \pm \mid \cos\theta \mid)^2 \tag{2.31}$$

where γ is the interfacial tension, θ is the contact angle of the colloidal particle with the interface and r is the particle radius [10]. In contrast to molecular surfactants, the colloidal particles do not alter the interfacial tension between the liquids.

Populations of colloidal particles on fluid-fluid interfaces can self-organize into a variety of patterns. The standard colloidal interactions found in the bulk, such as charge effects, steric repulsion and depletion interactions, are all still applicable. There are also interface specific capillary interactions [76] due to deformations at the interface. colloidal particles can deform the interface due to gravity, shape anisotropy e.g. elongated particles [17, 62], or by pinning on roughness at the particle surface [25]. These deformations create interactions between the particles which can be attractive or repulsive.

The relative importance of gravity can be found by calculating the Bond number, equation (2.32), the ratio between the gravitational forces and the surface tension:

$$Bo = \frac{\Delta\rho g r^2}{\gamma}, \tag{2.32}$$

where $\Delta\rho$ is the difference in density between the solid and the fluid. r is the relevant length scale — in this case the colloidal radius — and γ is the surface tension between the two fluids. In cases where the Bond number is small $Bo \ll 1$ gravitational effects may be discounted. However, even in the case of small Bond number deformations, such as those caused by surface roughness of the particles may still be present.

When one of the media is replaced by a complex fluid, such as a nematic liquid crystal, elastic effects come into play [77], leading to a larger range of colloidal patterns [36, 75, 89]. The type of structure produced depends on the liquid crystal film thickness, the surface anchoring at the interface and at the particles, and the number density of colloidal particles at the interface. The exact nature of the mechanisms involved is unclear. However, the additional interactions appear to be mediated by the liquid crystal elasticity and the formation of defects within the ordered phase. This is supported by the observation that chains of colloidal

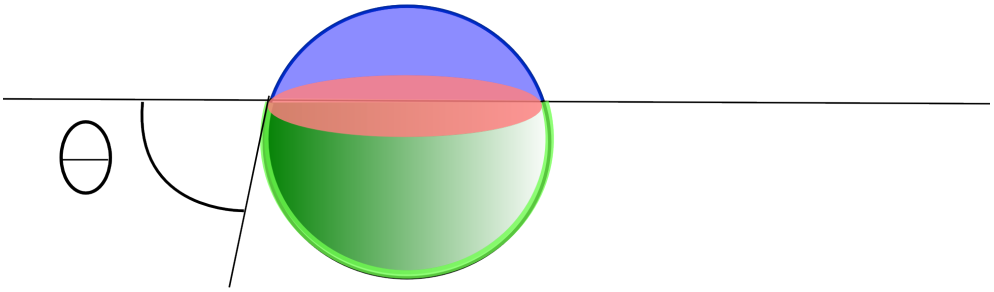

Figure 2.11 Colloidal particle at the interface between two fluids showing the contact angle θ and the removed shared area in red

particles at a water-nematic interface can be triggered to change spacing and then form hexagonal crystals by the addition of a molecular surfactant [52]. The surfactant is believed to modify the boundary conditions at the water-nematic interface which in turn changes the defects in the liquid crystal.

In cholesterics, the medium is spatially heterogeneous due to the periodic helix even before the addition of particles. Particles can occupy well defined locations within a well-ordered phase. Mitov *et al.* [68] find that platinum nano-particles decorate the fingerprint texture of a long pitch cholesteric. This texture can be seen in figure 2.3(c). With hybrid boundary conditions and gold nanoparticles, Bitar *et al.* find a range of structures templated by the cholesteric texture which vary with film thickness [1]. Both these studies use nano particles. In these cases WR/K is small and elastic effects dominate. The case where the particles are micron sized and WR/K is large had not been explored, and forms the basis of chapter 4 of this thesis and the related papers [58, 80].

Chapter 3

Experimental Background

Many of the experimental techniques used in this thesis were applied to all the systems studied. This chapter introduces these techniques. Techniques unique to a specific system will be discussed in the relevant chapter. A majority of the methods used are standard; in these cases the adaptations required in order for them to be used with LC samples is discussed. These techniques include; sample preparation of liquid crystal colloid composites and the construction of sample holders including LC cells with alignment layers. Also discussed in this chapter are polarising optical and confocal microscopy. The image analysis routines used to find the position of the colloidal particles within liquid crystal samples are presented. Finally, the tensiometer set up used to measure the LC surface tension is described.

3.1 Liquid Crystal - Colloid Dispersions

LC colloid composites are prepared by combining commercial liquid crystals with colloidal particles purchased from external sources or synthesised in house. The preparation of each component is described below.

3.1.1 Colloidal Particles

A range of colloidal particles were used in this thesis. Melamine particles with planar surface anchoring were used in the experiments described in chapter 4

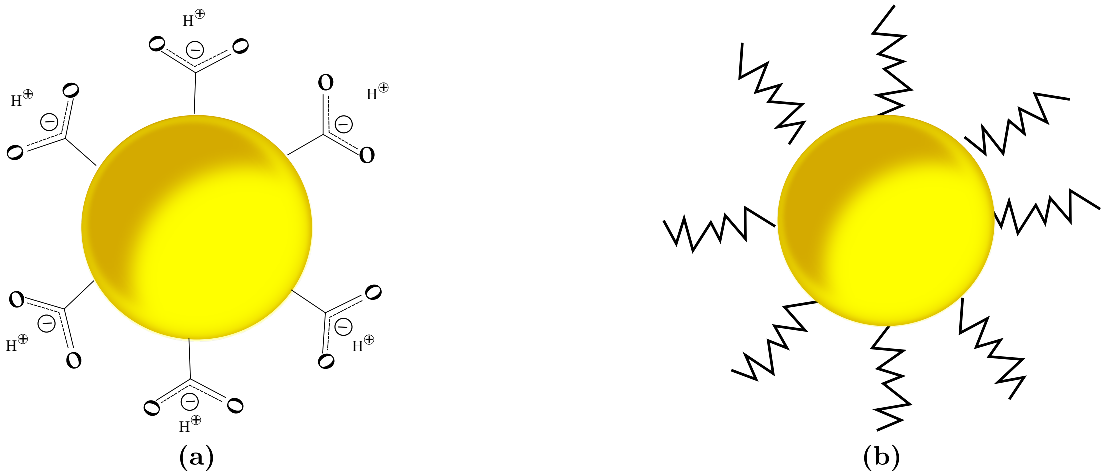

Figure 3.1 Schematics of the colloidal particles used in this thesis. (a) Carboxylate-modified melamine colloidal particles are charged stabilised in water. They are likely to be unstable in oils and LCs. (b) PMMA colloidal particles are sterically stabilised by polymer "hairs" of PHSA. It should be noted that the hairs are not shown to scale here.

and chapter 5. These were fluorescein isothiocyanate (FITC)-labelled melamine with carboxylate-modified surfaces purchased from Fluka. The particles are supplied dispersed in water so were simply dried under vacuum at 40 °C overnight prior to use. Liquid crystals have planar alignment on melamine colloidal particles. As the colloidal particles are charge stabilised with carboxylate groups, dispersions are unlikely to be stable in oils (including LCs). Colloidal particles with radii of $0.5\pm0.05\,\mu\mathrm{m}$, $1.5\pm0.1\,\mu\mathrm{m}$,$3\pm0.075\,\mu\mathrm{m}$, and $5\pm0.15\,\mu\mathrm{m}$ were used in the experiments.

4-Chloro-7-nitrobenzofurazan (NBD)–labelled poly-methyl-methacrylate (PMMA) particles stabilised by poly (12-hydroxystearic acid) (PHSA) hairs were used in the experiments described in chapter 6. These particles have homeotropic anchoring. The PMMA particles were synthesised by Dr. Andrew Schofield and supplied in the form of a dry powder.

3.1.2 Dispersions

Liquid crystal-colloid dispersions were prepared by adding a known mass of colloidal particles to a known volume of liquid crystals. All liquid crystals mixtures were well mixed prior to the addition of the colloidal particles. The colloidal particles were dispersed using stirring, sonication (via an ultrasound bath VWR Ultrasonic Cleaner) and whirly mixing. Care was taken to ensure that the liquid crystal did not enter the isotropic phase. This is especially important during sonication as significant heating of the sample can take place. Cooling from the isotropic in the presence of particles can result in the formation of a cellular solid [6]. Once the samples were uniform (confirmed via visual inspection and microscopy) they were used immediately. If samples were stored then the colloidal particles were re-dispersed prior to use. This dispersion method was chosen over a co-solvent transfer method to avoid the risk of contamination.

3.2 Sample Holders

For microscopy work, samples were sealed in hand-built cells. These are constructed from a microscopy base slide (26 mm × 70 mm). Onto this two 75 µm Mylar spacers are attached using UV curing glue Norland. A 22 mm × 22 mm coverslip is then attached on top using UV curing glue leaving the ends free. An example cell is shown in figure 3.2(a). Samples are loaded via capillary action. The free ends of the cells are sealed using silicone vacuum grease (Dow Corning). These holders can be used with both upright and inverted microscopes. The samples must be sealed in order to avoid flow and to prevent contamination of the sample with immersion oil.

For emulsion samples, bottle cells as shown in figure 3.2(b) were constructed. The bottom of a 2 ml sample vial was removed using a glass cutter. The bottle was then attached to a microscope coverslip 22 mm × 22 mm using UV curing glue. These cells allow bulk samples of emulsions to be imaged.

3.2.1 Aligned and Wedge Cells

Wedge cells with planar alignment were created for experiments in chapter 4 and chapter 5, where varing the sample thickness was important. These cells are shown in figure 3.2(c). They require poly-vinyl alcohol (PVA, 98% hydrolyzed, Mw=13000-23000, Sigma-Aldrich) coated coverslips which are then rubbed to create the uniform planar alignment. There is a multi-step process to create this alignment layer.

1. Coverslips were cleaned by soaking them overnight in a 2.5 M NaOH solution

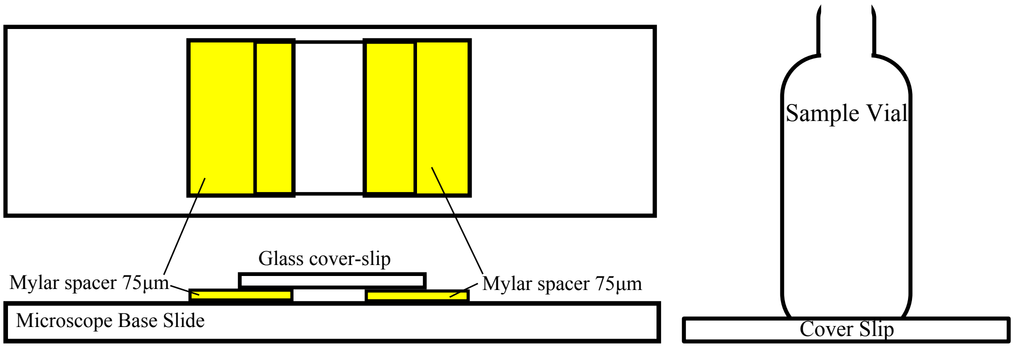

(a) Schematic of a hand built liquid crystal cell (b) Schematic of a bottle cell

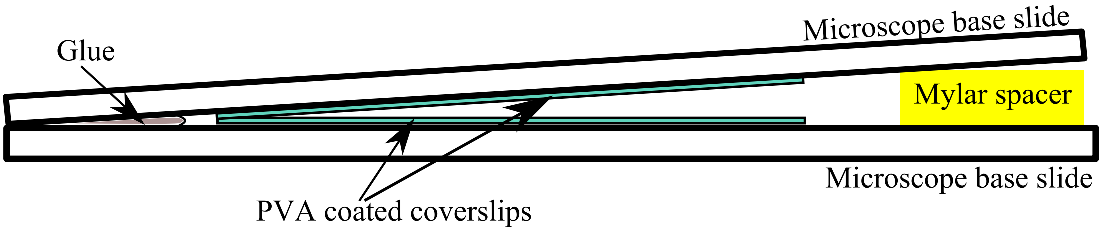

(c) Schematic of a wedge cell

Figure 3.2 Schematics of a hand built liquid crystal cells

made with 60% ethanol and 40% Millipore H_2O. The coverslips are held in Eppendorf tubes so that only their edges were in contact with the walls.

2. The cloverslips were rinsed with distilled H_2O and those that were not used immediately were stored submerged in H_2O in Eppendorfs.
3. Coverslips were mounted wet on a spin-coater (Cammax Pricema) and covered with $\sim$ 2 ml PVA solution (0.25 M). They were then spun at 3000 rpm for 1 min.
4. Coverslips were dried at 120 °C for 30 minutes.
5. Coverslips were attached to microscope base slide using UV curing glue.
6. Once the glue was dry the PVA coated coverslips were rubbed in a single direction using a velvet cloth to obtain uniform alignment.
7. The two base slides were assembled to form a wedge as shown in figure 3.2(c).

Steps 1 to 6 can be used to produce aligned cover slips which can be incorporated into other cell designs.

3.3 Imaging

3.3.1 Polarising Optical Microscopy

Polarising optical microscopy is one of the most widely used techniques for imaging the liquid crystal director field. The liquid crystal sample is placed between crossed polarisers as see in figure 3.4. The anisotropic nature of the mesogens means that the liquid crystal is birefringent with two refractive indices. These are known as the ordinary n_o and extraordinary n_e. Light polarised parallel to the optical axis of the mesogens of the will be refracted with index n_o. That polarised perpendicular to the optical axis will be refracted with index n_e.

When polarised light passes through a liquid crystal sample its polarisation will be altered according to the alignment of the mesogens. The principle consequence is that regions where mesogens which lie in the plane perpendicular to the light path, oriented parallel or perpendicular to the analyser appear dark as in figure 3.3(a). Only one mode propagates through the LC refracted with index n_o (n_e) if the mesogens are parallel (perpendicular) and the polarisation remains unchanged. Mesogens with their long axes parallel to the light beam (vertically) also appear dark as they do not alter the polarisation of the incident light.

Mesogens aligned obliquely (i.e. in none of the above directions) will alter the phases of the ordinary and extraordinary rays. This phase shift is wavelength dependent. If the phase shift leads to a phase difference between the two rays which is an integer multiple of 2π, then extinction occurs and that wavelength of light will not pass through the analyser. This second effect gives rise to the colour variation seen in figure 3.3(b). Finally, the isotropic phase will appear dark, as on average its refractive index is uniform.

The optical microscopy in this thesis was carried out using an upright Nikon E800 microscope fitted with a QImaging Micropublisher 3.3 colour camera. All images were taken in transmission through crossed polarisers. A polariser placed in transmitted light path of the confocal microscope (see next section) also allowed polarising optical microscopy to be carried out in combination with fluorescence microscopy.

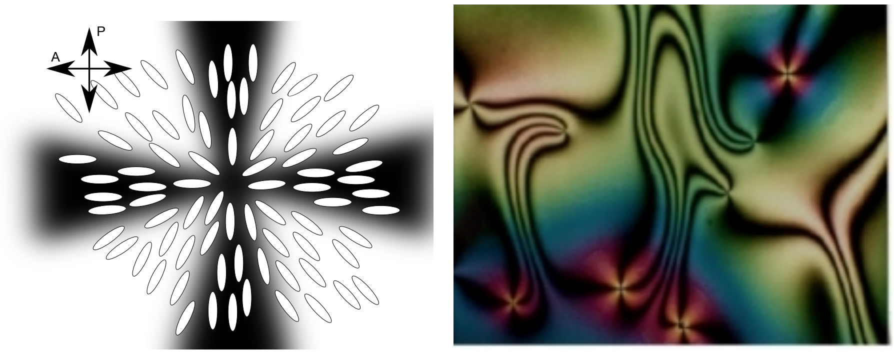

(a) (b)

Figure 3.3 (a) A schematic of mesogen alignment and the resultant dark brushes. (b) An image of a nematic between crossed polarisers showing the dark brushes [3].

3.3.2 Confocal Microscopy

Confocal microscopy is a form of fluorescence microscopy; it has the advantage that it allows resolution in the z direction (parallel to the viewing direction) as well as in the image plane. The ability to create 3 dimensional stacks of images and resolve the colloidal particle positions and liquid crystal alignment in 3d has been essential to this thesis.

A schematic of a confocal microscope is shown in figure 3.6. A laser is used to excite a fluorescent dye within the sample and the fluorescence is collected by a photomultiplier tube (PMT). The emitted light is Stokes shifted to a longer wavelength relative to the incident light. It is separated from the incident light via a dichroic mirror. A pinhole placed in front of the PMT ensures that only fluorescence from the focal point of the laser is collected (the “confocal” light). The laser focus is scanned across the sample and the focus is gradually adjusted to create a 3d image stack. In the setup two separate lasers are used to excite separate dyes in the colloidal particles and the LC. A series of dichroic mirrors are used to separate the fluorescent signals and send them to the relevant PMTs. The transmitted light is collected via a third PMT. A polarising filter aligned perpendicularly to the laser polarisation was placed in the light path for the transmission images. This creates a polarised optical image as discussed in the previous section. The positions of the colloidal particles can be imaged simultaneously with the average liquid crystal director field.

Imaging the colloidal particles is straight forward, the FITC in the colloidal

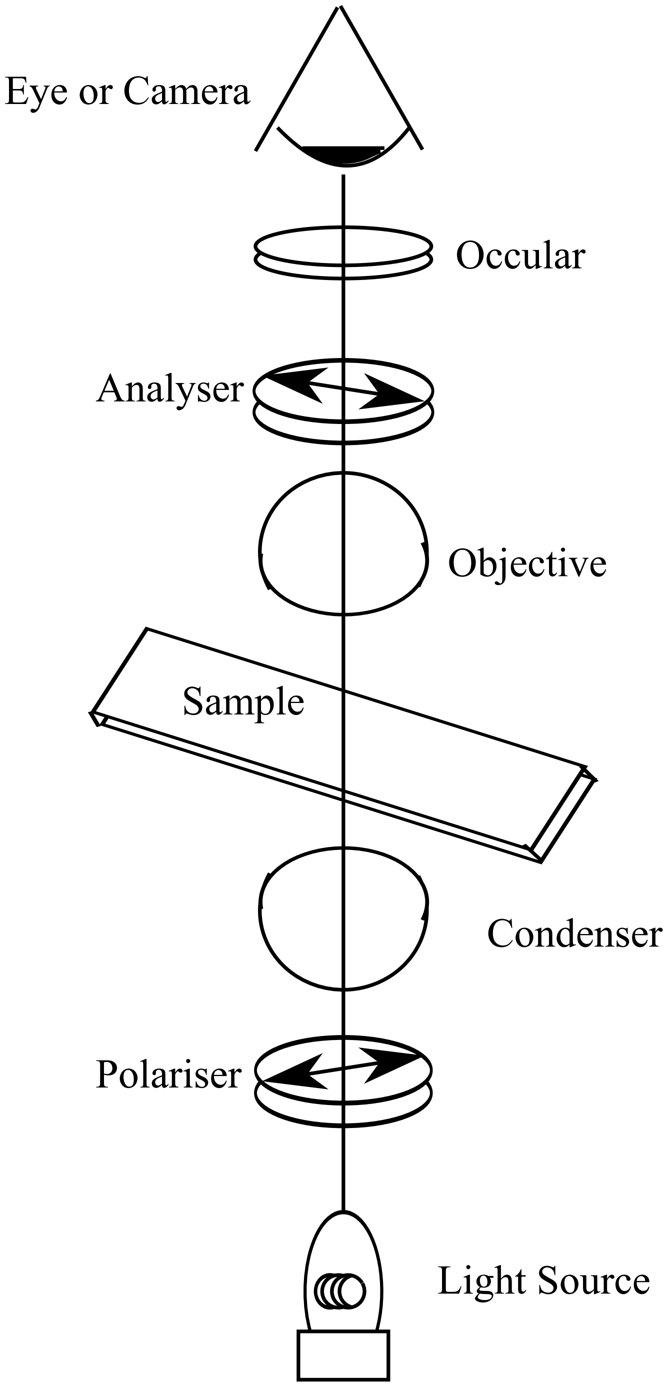

Figure 3.4 Schematic of polarising optical microscope

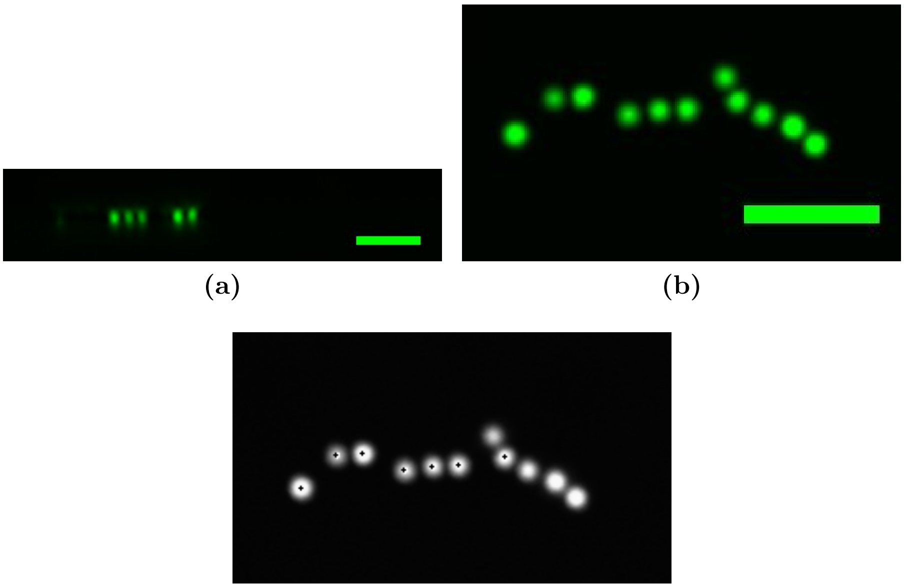

(a) (b)

(c)

Figure 3.5 Confocal images of colloidal particles. (a) shows a vertical slice through the confocal stack. (b) shows a single horizontal slice. (c) shows the centres (black crosses) as found by image analysis routines. The other colloidal particle centres are not in this slice

particles fluoresces and the colloidal particles are sufficiently large to be easily resolved. No significant perturbations due to the anisotropic nature of the liquid crystal solvent are observed. Colloidal particles are circular in the xy plane, figure 3.5(b), and slightly elliptical in z, figure 3.5(a)

The liquid crystal director can be imaged in fluorescence mode by adding a small amount of anisotropic dye (Nile Red). This has the advantage that the director can then be resolved in z. This is in contrast to the transmission mode where any polarisation image is an average of the mesogen alignment through the sample. It is important to keep the dye concentration low to avoid destroying the liquid crystal order.

If an anisotropic dye is used, then the dye molecules align with the liquid crystal molecules. The excitation and emission from anisotropic molecules depend on the orientation of the molecules with respect to the polarisation of the excitation signal. Dye molecules which are aligned parallel to the electric field vector $\vec{E}$ of the excitation are preferentially excited [53].

The emission is also dependent on the orientation of the molecules, the emission will be polarised along the long axis of the molecule. If we define the

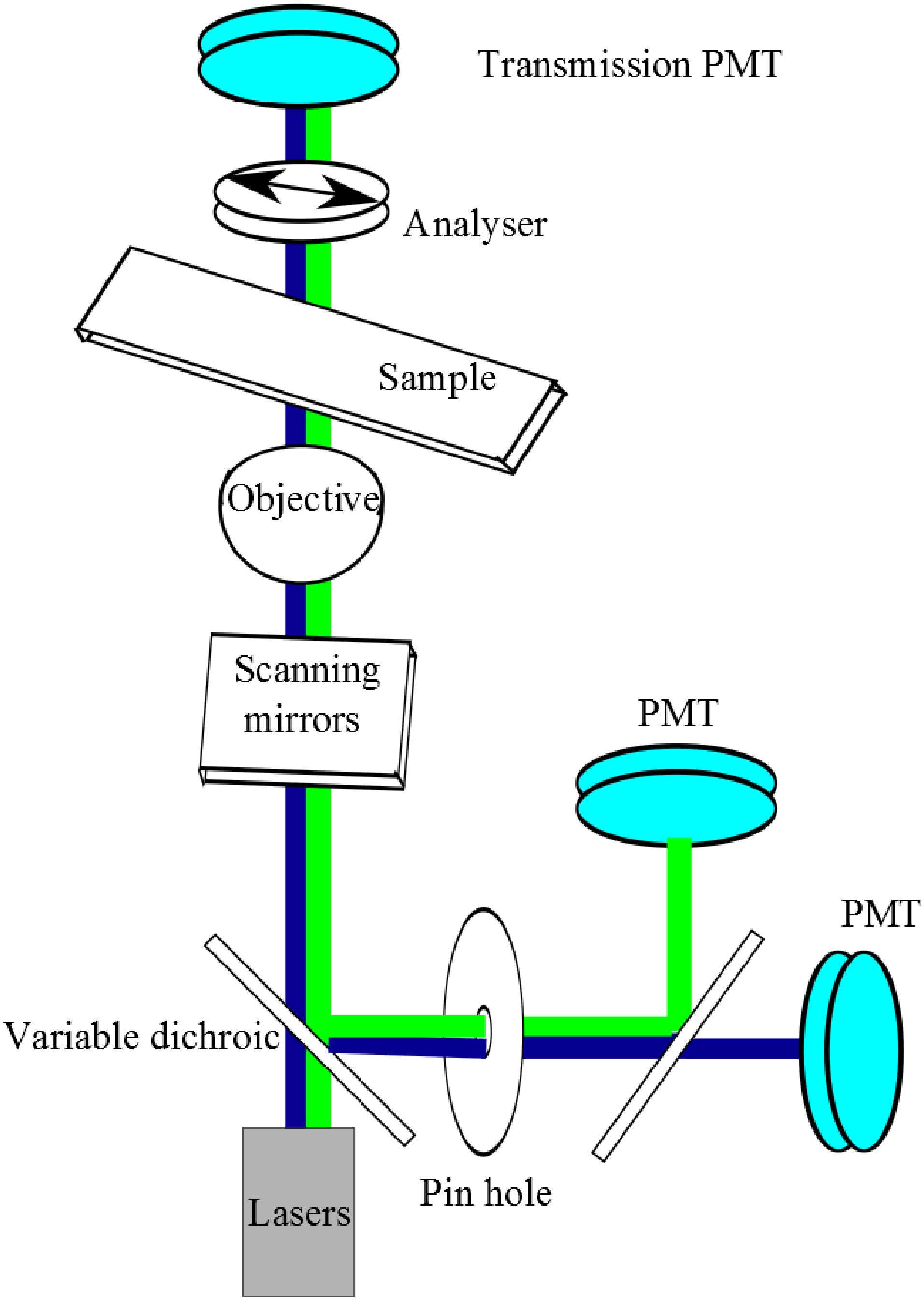

Figure 3.6 Schematic of confocal optical microscope

emission intensity of the dye molecules parallel (perpendicular) to the excitation polarisation as $I_{\parallel}$ ($I_{\perp}$). Dye molecules emit as dipoles with the emission proportional to the square of the vector projected onto the axis of observation as shown in figure 3.7 [53] so,

$$I_{\perp} = \sin^2 \theta \cos^2 \phi, \tag{3.1}$$

$$I_{\parallel} = \sin^2 \theta \sin^2 \phi, \tag{3.2}$$

Where θ and ϕ are defined as shown in figure 3.7. Molecules aligned along $\vec{x}$ will emit light polarised in the $\vec{x}$ direction parallel to the excitation signal $I_{\parallel} = 1$ and $I_{\perp} = 0$. Those along $\vec{y}$ will have minimum intensity $I_{\parallel} = 0$ and $I_{\perp} = 0$ likewise molecules aligned along $\vec{z}$. Hence, the molecules parallel to the polarisation direction emit with maximum intensity, those perpendicular with minimum.

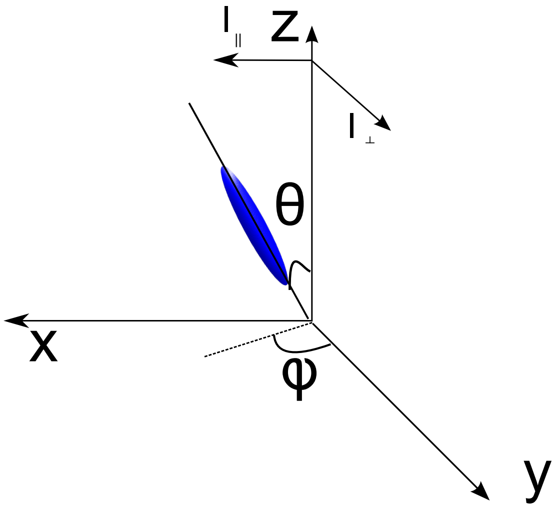

Figure 3.7 Axes used to define molecular orientation and emission directions

The intensity of the fluorescence gives an indication of the alignment of the molecules. Unlike Smalyukh *et al.* [88] there is no polariser inserted in the light path, instead our excitation laser is linearly polarised. The lack of a polarising filter for the emitted light reduces the contrast between the parallel and perpendicular alignments but still permits qualitative analysis of the director field.

All the confocal microscopy experiments were carried out using a Zeiss Observer.Z1 inverted microscope in conjunction with a Zeiss LSM 700 scanning system. The exact combinations of lasers and dyes used in each study are discussed in the relevant chapters.

3.4 Image Analysis

Image analysis routines are used to extract quantitative data from images. Particle tracking algorithms were used to extract the coordinates of the colloidal particles from confocal images. Image analyses were also developed for quantitative analysis of LC textures.

3.4.1 Image Analysis of Colloidal Particles

The positions of colloidal particles within the liquid crystal samples were found using particle tracking routines developed by E. Weeks and others [9, 23] which are freely available online. They were used with a graphical user interface (IAGUI) developed by Dr Tiffany Wood which allowed parameters to be set simply via text boxes.

The algorithms find the centre of mass of the particles in an image (in either 2 or 3 dimensions). The principle idea is that the bright regions of a fluorescent image correspond to the particles. The fluorescent signal from a colloidal particle has a Gaussian profile. By fitting Gaussian profiles to each individual bright region and finding the centre of the distribution the coordinates colloidal particle centre can be found. The process of fitting a Gaussian allows for subpixel accuracy as the maximum does not have to be a whole number of pixels. The steps to extract coordinates are as follows:

- The image is filtered with a band pass filter. This leaves bright Gaussian regions on a black background. The cut off for this filter much be larger than the apparent radius of the colloidal particles in the image.

- Local maxima are then found and refined by fitting a Gaussian. A radius specified by the user excludes maxima within that radius so each maximum is only found once.

- The result often contains “ghost” particles, regions which contain a maxima due to random imaging noise. These can be removed by specifying a minimum “mass” for each particles. This mass is the product of the number of pixels in a region and their brightness.

- Finding the exact values for the bandpass and radial filters is an iterative process. The filters must be set so as not to exclude genuine particles and to avoid any biasing.

- Results are checked by overlaying coordinates on the original image figure 3.5(c) and by checking for pixel bias.

- Once the centres have been found the list of pixel coordinates is converted to real units via the image calibration.

By using this method, the uncertainty in the image plane is typically 1/10 of a pixel [23]. In the z direction, there are fewer pixels per colloidal particle and the uncertainty is 1/2 a confocal slice [9]. The exact value in microns depends on the image resolution. This will be discussed in the relevant chapters.

3.4.2 Image Analysis of Liquid Crystals

Custom image analysis routines were developed to perform quantitative analysis of various liquid crystal textures. Theses are discussed in detail in chapter 4.

3.5 Interfacial Tension Measurements

A bulk measurement of the surface tension of a liquid crystal-oil interface was required in order to perform analysis on the system in chapter 4. The surface tension was measured using a Krüss EasyDrop tensiometer (model 65 FM40Mk2). Droplets of a known volume of LC were dispensed using a computer controlled syringe pump and suspended from the needle in the silicone oil. After the droplet has been allowed to equilibrate digital snapshots are taken. The setup is shown in figure 3.8

The shape of the droplet depends on the balance between the interfacial tension and gravity. This gives rise to the Laplace pressure Δp which is related to the

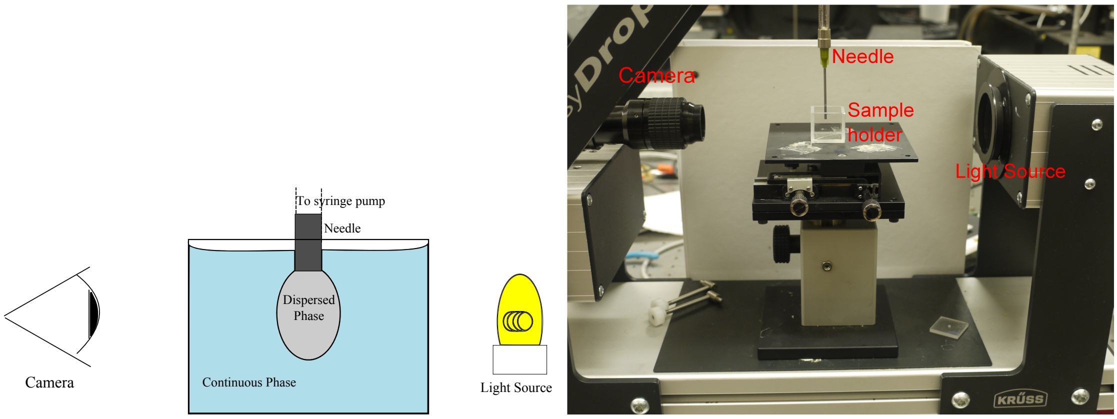

(a) (b)

Figure 3.8 The tensiometer set-up

droplet shape via the Young-Laplace equation

$$\Delta p = \sigma \left(\frac{1}{r_1} + \frac{1}{r_2} \right) \tag{3.3}$$

where σ is the surface tension and r_1 and r_2 are the principle radii of curvature. The edge of the droplet is identified via algorithms built into the commercial software. The Young-Laplace equation 3.3 is used to fit the droplet shape and extract the surface tension. Required input parameters for fitting include: the syringe needle diameter, $1.83 \pm 0.01\,\mathrm{mm}$, for pixel-size calibration and the density difference between the (silicone oil saturated) CLC and the silicone oil $\Delta\rho = 0.038 \pm 0.003\,\mathrm{g\,cm^{-3}}$ (calculated by weighing known volumes of oil and saturated CLC). Caution must be used when interpreting the results of these measurements. The technique has been developed for simple fluids and given the anisotropic nature of the LC surface tension (see section 2.3.4) it is not certain that the Young-Laplace equation holds. However, it is a reasonable technique to use to obtain a value for the isotropic part of the surface tension, which is independent of the LC alignment. The pendent drop technique has been used with some success for nematic liquid crystals [4, 34, 50, 96] and we therefore consider it an apropriate technique to obtain a value for the surface tension of the interface. This can then be used to calculate the magnitude of the trapping energy for colloids at the interface.

For this study CLC droplets of volume $31.3 \pm 0.4\,\mu\mathrm{L}$ were suspended under silicone oil at 23 ± 1°C. After 15 min of equilibration, digital snapshots were recorded. Three measurements on three different droplets were averaged to obtain the value of $\gamma_{CS} = 3.8 \pm 0.4\,\mathrm{mN\ m^{-1}}$. The error was calculated by combining the standard deviation of the three measurements with error estimates for temperature variations, density variations and the partial solubility of silicone oil in the CLC [63]. Given the complex nature of the CLC this measurement gives a bulk value which in practice may depend on the exact geometry of the experiment as discussed in chapter 2.

Chapter 4

Colloidal Particles at a Cholesteric-Isotropic Interface

4.1 Introduction

This chapter presents studies of micron–sized colloidal particleal particles in the presence of a cholesteric-isotropic interface.

Cholesteric liquid crystals possess orientational order but additionally break translational symmetry due to their chiral nature. The average orientation of the molecules, denoted by the local director, $\mathbf{n}$, maps out a helix along an axis, $\vec{h}$. The distance taken for the director to rotate through 2π gives the material an intrinsic length scale, the pitch length, p. This periodic structure can be distorted in order to satisfy boundary conditions at a surface or in response to external fields or inclusions such as colloidal particles. The layers can either be distorted elastically where the layers bend smoothly or via the formation of defects [64, 90].

A clear cholesteric fingerprint texture, figure 4.1(a) is created by using an interface between the cholesteric liquid crystal (CLC) and an isotropic silicone oil. A schematic of the system can be seen in figure 4.3 (a). The distribution of the colloidal particles trapped on the interface and their positions perpendicular to it are studied using confocal and polarising optical microscopy. This is a novel system where elastic and capillary effects could potentially compete.

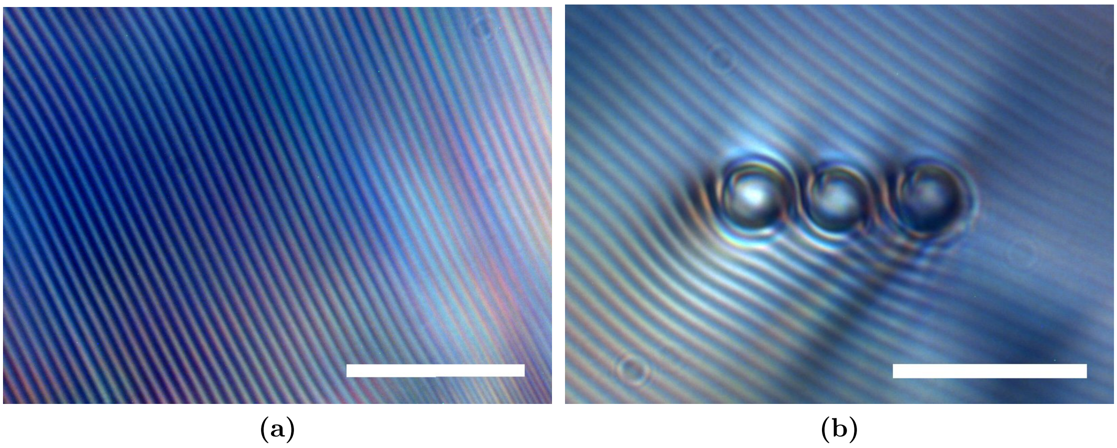

Figure 4.1 A pair of interfaces viewed through the overlying silicone oil. (a) Unadorned fingerprint texture characterized by a reasonably uniform helical axis direction. (b) Polarising optical microscopy image of 3 μm colloidal particles at the interface of a 1.5 μm pitch CLC. Cholesteric layers can be seen between the particles. Scale bars $10\,\mathrm{\mu m}$.

4.1.1 Colloidal Particles in Cholesterics

Adding colloidal particles to liquid crystal meso-phases perturbs the order of the phases and can induce anisotropic interactions between the particles as the elastic energy of the liquid crystal adapts to accommodate the particles. As discussed in chapter 2, the interaction between the colloidal particle and the liquid crystal can be characterised by a dimensionless ratio WR/K where W is the anchoring strength, R is the colloidal particle radius and K is the elastic constant of the liquid crystal. This compares the surface anchoring energy $\sim WR^2$ to the energy of the elastic deformation induced by the presence of the colloidal particle $\sim KR$. In cholesteric liquid crystals, there is an additional dimensionless parameter, R/p the ratio of the colloidal particle radius to the pitch length of the liquid crystal. As this ratio increases, the defects which initially surround the particle twist up into spirals as shown schematically in figure 4.7 and discussed in detail in [59]. This alteration of the defect structure can have a profound effect on the physics of the system, including altering how the colloidal particles move within the cholesteric [59].

4.1.2 Colloidal Particles at Interfaces

Particles trapped on simple fluid-fluid interfaces can self organise into a wide range of different structures including, well ordered two-dimensional crystals [81], which can be extraordinarily sparse [44], and also chains when the particles have rough surfaces [91]. The behaviour of particles trapped at fluid-fluid interfaces is relatively well understood. However, the behaviour when one of the phases is a partially-ordered mesophase has only recently started to be explored. Combining a LC-colloidal particle composite with a fluid-fluid interface adds a greater degree of richness to the interactions. Research to date has principally focused on colloidal particles at the interface of nematic liquid crystals [7, 94].

In this chapter the behaviour of colloidal particles which decorate a cholesteric-isotropic interface is explored. The experiments discussed in this chapter have been published in [80] and [58]. The author of this thesis carried out all of the experiments described in these papers. In what follows, the experimental system and results will be discussed. The results of simulations performed by Lintuvouri and others will be included to aid interpretation.

Liquid crystals can be distorted by the anchoring at the sample boundaries. In cholesterics the competition between the helical twist and surface anchoring of the liquid crystals leads to the appearance of striking textures. Where the anchoring is homeotropic (normal to the interface) at both top and bottom surfaces the helical axis is forced to lie parallel to these surfaces and the fingerprint texture is observed. This texture appears as a periodic array of bright and dark stripes as in figure 4.1(a) when imaged using polarising optical microscopy. The periodicity corresponds to a half of the pitch length of the LC. Using a confocal microscope the periodic nature of the helix can also be seen in a vertical slice through the interface figure 4.3 (c). The fingerprint texture is an example of frustrated orientational order as the constraints of both surface anchoring and helical twist cannot be satisfied simultaneously [35]. The frustration is resolved by the creation of a 2d array of defects (regions of lower nematic order) at the interface, these are sketched in pink in figure 4.3 (a).

The defect array costs the system energy. Colloidal particles trapped at the interface can reduce the energy of the system by removing a portion of the defected region in a similar manner to that discussed in section 2.3.3. Simulations (carried out by J. Lintuvuori) of the colloidal particle-LC system for colloidal

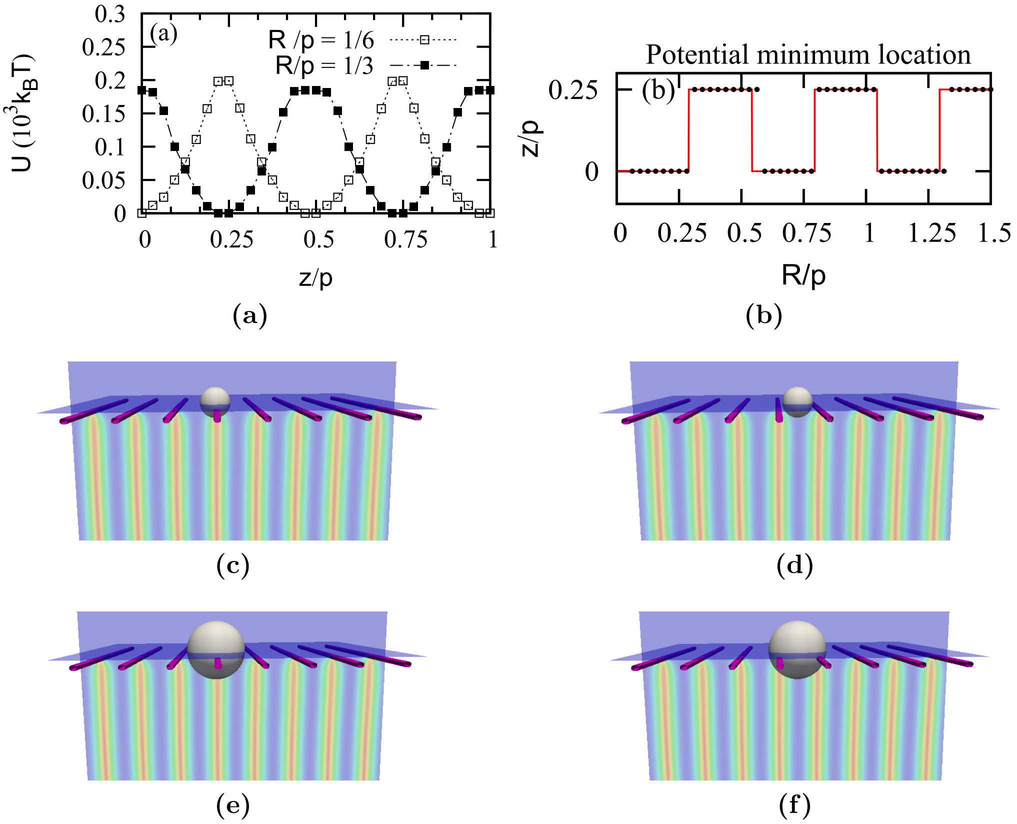

(a) (b) (c) (d) (e) (f)

Figure 4.2 Simulations by J. Lintuvuori. (a) Plot of free energy of the colloidal particle-LC system when the position of the particle is varied on the interface, for a colloidal particle with zero anchoring ($WR/K = 0$). z is the position from the defect core, p is the liquid crystal pitch. As the liquid crystal director field is head-tail symmetric the plot is symmetric both around a distance of 0.5 p and 0.25 p. (b) Plot of the distance from the disclination core of the minimum of the free energy (in units of the pitch length p) as a function of R/p. The solid (red) line is a prediction based on the colloidal particle covering the largest possible length of disclination. (a) and (b) from [58]. (c) A small colloidal particle $R/p = 1/6$ centred on a defect will remove a section of defect, reducing the energy cost. (d) A small colloidal particle between the defects will not remove any defect core. (e) A large colloidal particle $R/p = 1/3$ centred on a defect only removes that defect. (f) A large colloidal particle between defects removes two defect cores

particles with zero anchoring strength (colloidal particles do not influence the alignment of the LC at their boundaries) in figures 4.2(a) and 4.2(b) show that the energy of the system depends on the position of the colloidal particle on the interface. The equilibrium position varies with the particle size to pitch ratio R/p. The equilibrium position of the colloidal particle's centre changes in order that the colloidal particle covers the greatest length of defect.

The length L of N defect lines covered by a half circle perpendicular to the lines

$$L = 2R + 4\sum_{n=2}^{N} \sqrt{R^2 - [(n-1)p/2]^2}, \tag{4.1}$$

Where R is the radius of a circle centred at $z = 0$ and p is the pitch length. For a circle centred at $z = p/4$ the length of defect covered is.

$$L = 4\sum_{n=1}^{N} \sqrt{R^2 - [((2n-1)/2)p/2]^2}, \tag{4.2}$$

These equations were used to produce the red line in figure 4.2(b).

Nano particles at the interface of a cholesteric where $R/p \ll 1$ occupy well defined locations within the well-ordered phase. Mitov et al. [68] find that platinum nanoparticles decorate the fingerprint texture of a long pitch cholesteric. With hybrid boundary conditions and gold nanoparticles Bitar *et al.* find a range of structures templated by the cholesteric texture which vary with film thickness [1]. The case of micron sized particles or a short pitch cholesteric has not been explored. The cases $R/p = 1/6$ and $R/p = 1/3$ are considered in detail in this chapter.

In addition to the distribution of colloidal particles on the interface the distribution of colloidal particles perpendicular to the interface will be discussed. The colloidal particles are initially dispersed in the liquid crystal and can sequester to the interface reducing the shared area between the two fluids as discussed in chapter 2, section 2.3.4. One of the aims of this chapter is to begin to understand how this trapping behaviour at the interface is modified when one of the liquids has liquid crystalline order.

4.2 Materials and Methods

4.2.1 Sample Preparation

colloidal particle-liquid crystal composites were prepared following the methods in chapter 3. The liquid crystal was a mixture of a nematic MDA-00-1444 (n_e=1.684, n_o=1.507) and chiral dopant MDA-00-1445 (n_e=1.67, n_o=1.5), both from Merck. These were mixed in the following ratios (by mass), 80:20 giving a pitch length

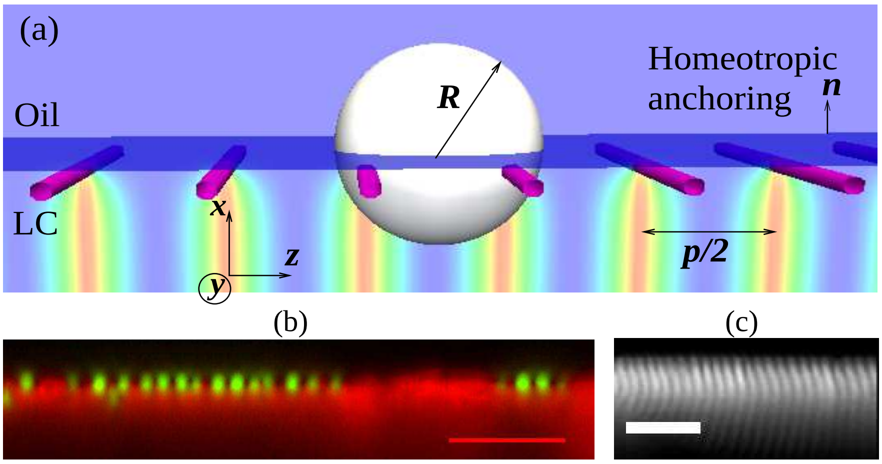

Figure 4.3 The interface viewed in cross section. (a) Schematic of the geometry: one particle of radius R is trapped on the interface between a cholesteric LC and an isotropic fluid (an immiscible oil). In the LC phase, red and blue correspond to director field along y and x, respectively, pink lines are the defects. (b) Fluorescence confocal image of $3\,\mu\mathrm{m}$ particles (green) trapped at the interface between cholesteric (red) and oil (dark) (scale bar $20\,\mu\mathrm{m}$). (c) Fluorescence confocal microscopy image of the cholesteric-oil boundary in the absence of particles, showing that the interface is flat (scale bar $10\,\mu\mathrm{m}$)

of $1.5\,\mu$m and 90:10 giving a pitch length of $3.2\,\mu$m [43]. The pitch was also measured using a Cano wedge and compared with the observed periodicity at the interface (measured using Fourier techniques). The resultant mixtures were labeled with a fluorescent dye Nile Red (Aldrich) in order for confocal microscopy to be used. Low concentrations of dye were used (0.01 % by mass) to ensure that the dye does not disrupt the liquid crystalline order. The colloidal particles were fluorescein isothiocyanate(FITC)-labelled melamine with carboxylate-modified surfaces (Fluka) with a range of diameters ($1\,\mu\mathrm{m}$, $3\,\mu\mathrm{m}$, $6\,\mu\mathrm{m}$, $10\,\mu\mathrm{m}$). These were dried under vacuum at 40°C overnight prior to use, then dispersed into the liquid crystal mixtures via a combination of stirring and sonication as detailed in chapter 3. The colloidal particles have planar surface anchoring with the liquid crystal [43].

All the dispersions of melamine particles in CLC are stable in the bulk with macroscopic sedimentation only observed on a timescale of weeks. Small particles are more difficult to disperse and required a longer duration of sonication. The volume fraction of colloidal particles was 0.1% and the resultant mixtures are stable over the life time of the experiment.

To create a fluid interface with homeotropic anchoring, silicone oil (Aldrich) was spin coated onto a cover slip (Menzel Gläser) to give a uniform layer. Two types of sample were used, open and sealed cells. For the open cells, the oil coated slide was placed on the inverted microscope, a drop of liquid crystal was added followed by more silicone oil. The samples were then left to equilibrate prior to imaging for a minimum of 1 hour; they are quiescent after this time. For sealed cells, mylar spacers (50 μm) were attached to a microscope base slide (SN) using UV curing glue (Norland). Silicone oil was laid down between the spacers, a drop of LC added and a cover slip coated with oil placed on top. The edges of the cell were sealed with epoxy resin (Araldite) along the spacers and silicone vacuum grease (Dow Corning) along the open ends. Sealed cells were used on both upright and inverted microscopes, open cells were only used on inverted microscopes. A schematic of the sealed cells is shown in figure 4.4

The CLC and the silicone oil are slightly miscible at room temperature. This alters the density of the CLC but, has no observable effect upon the pitch. No difference in pitch length is observed between that measured for pure CLC in a Cano wedge and that measured using the fingerprint texture at the interface. The miscibility is temperature dependent; a phase diagram of a similar LC – silicone oil system can be found in [63]. We are well below the cholesteric – isotropic transition (98 °C for our system and observe a stable interface both in the microscopy experiments and pendant drops.

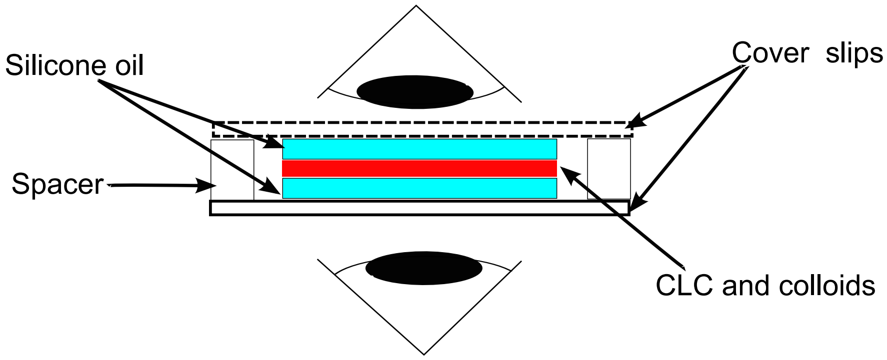

Figure 4.4 A schematic diagram of the experimental set up (not to scale, spacers are 50μm). Samples have been studied from above and below.

4.2.2 Microscopy

The samples were imaged using optical microscopy with an upright Nikon E800 microscope fitted with a QImaging Micropublisher 3.3 colour camera. All images were taken in transmission through crossed polarisers.

Confocal microscopy was performed using a Zeiss Observer.Z1 inverted microscope in conjunction with a Zeiss LSM 700 scanning system and a 63× 1.40 NA oil immersion objective. In order to image the alignment of the liquid crystal in fluorescence the Nile Red doped liquid crystal was excited with a 555 nm diode laser . The FITC labeled colloidal particles were excited using 488 nm diode laser. Transmission signals from both lasers were also recorded. A polarising filter aligned perpendicular to the laser polarisation was placed in the light path for the transmission images to produce an equivalent to standard polarising optical microscopy (see chapter 3 for further details). To increase the signal to noise ratio all images were averaged (4×).

4.2.3 Image Analysis

Particle Tracking

The particle coordinates were found using particle tracking routines developed by E. Weeks and others [9] as described in chapter 3. These were used to find the coordinates of the particle centres in both 2d images and 3d image stacks.

Identification of the fingerprint texture

In order to help identify defect structures, image analysis routines were developed to identify the fingerprint texture in the images. For qualitative analysis the stripes were identified using the following processes implemented using LabVIEW Vision Assistant. The image was (where necessary) converted to grey scale and the contrast enhanced. The image was then thresholded to produce a binary image and eroded to give pixel wide stripes which correspond to the regions in the original image of maximum (minimum) intensity corresponding to regions where the mesogens are parallel (perpendicular) to the interface. The resulting stripes were then overlaid on the original image to aid defect identification.

In order to measure the relative position of colloidal particles and defects a more quantitative measure was required. A series of image processing and measuring steps were applied using idl to extract an equation defining a stripe and to measure the distance from this to the colloidal particle. Each image was processed as follows:

1. A single slice from the Nile Red channel of the confocal was extracted. This was chosen to correspond to the clearest fingerprint texture if an image stack was used.
2. The brightness and contrast were optimised (manually).
3. A threshold was applied to extract the local minima.
4. The binary .tiff array was converted to a text file containing the x y coordinates of the bright pixels (these correspond to the minima).
5. Small regions of interest were defined around each particle and subsequent analysis only performed on regions close to isolated particles.
6. Lines of pixels were identified via ”crawling circle” method. A circle of a user defined radius and start point would record all the pixels within it. It would then move randomly and record the new pixels (move length set by user). If pixels are found in this new region then new pixels would be added to the line. If not, a new direction is tried. Once a direction containing points is found the circle moves along, always moving towards the centre of mass of the new points until the edge of the image is reached. The output from this algorithm was inspected manually to ensure single stripes had been found and that all points had been included.
7. A linear fit was applied to the pixels in each of the extracted lines.
8. The distances from the colloid coordinates to the adjacent lines are calculated.
9. The distances were converted into units of the global pitch which was measured using Fourier techniques (see below).

The periodicity of the fingerprint texture was measured using Fourier techniques in idl. A fast Fourier transform of the image was performed using the inbuilt idl function. A radial average of the transformed image was performed. The peak in this average corresponded to the periodicity of the stripe pattern.

Identification of the LC-oil interface

In order to find the location of the liquid crystal – oil interface, the mean image intensity per slice is plotted as a function of depth (slice number from confocal stack) as shown in figure 4.5.

4.2.4 Surface Tension

In order to quantify the trapping strength of the colloidal particles at the at the liquid crystal-oil interface a value for the surface tension had to be obtained. A pendant drop method was used as discussed in chapter 3.

4.3 Particle Distributions Perpendicular to the Interface

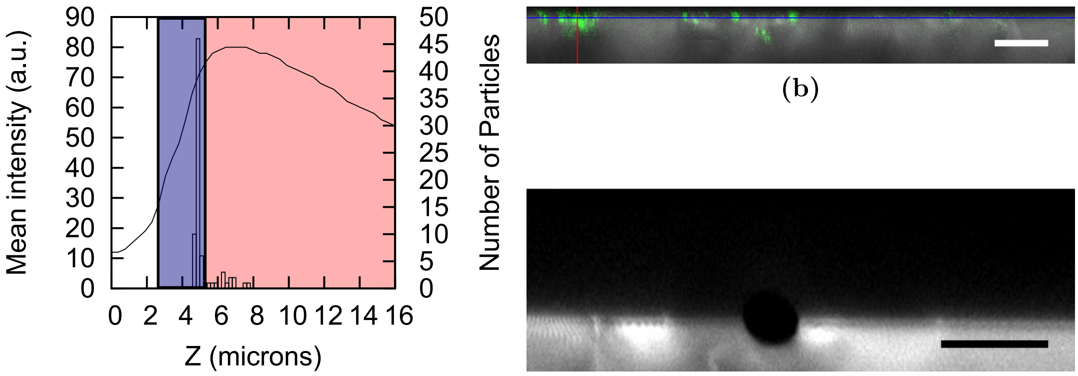

(a) (b) (c)

Figure 4.5 (a) Example graph of image intensity (line) and particle, $R = 3\mu$m, positions (as histogram). Here the white region corresponds to silicone oil and the light (red) to CLC. The dark shaded (blue) region indicates the area where particles were considered to be trapped at the interface (see text for more details). (b) 1 μm particles at the interface (colloidal particles green, liquid crystal grey). (c) A 10 μm particle at the interface of the liquid crystal (grey) colloidal particle is black. Scale bars 20 μm.

Colloidal particles are found to sequester to the interface between the CLC and the oil. colloidal particles trapped at the interface can be seen in figure 4.5(b,c) and figure 4.3(b). As discussed in section 2.4 colloidal particles reduce the shared area between the two media leading, in cases where the Young equation holds (i.e. simple liquids, no complications due to elastic effects), to an energy saving $\Delta G = -\pi R^2 \gamma (1 \pm \mid \cos\theta \mid)^2$ where γ is the interfacial tension, θ is the contact angle of the colloidal particle with the interface and r is the particle radius [10].

For this system the pertinent values are $\gamma \approx 3.8\,\mathrm{mN\,m^{-1}}$, $\theta = 90^\circ$ from observations of large particles as in figure 4.5(c), $R = 1.5\,\mu\mathrm{m}$. The saving for this system is $6.5 \times 10^7\,\mathrm{k_B T}$ indicating that thermal fluctuations will be unable to free the particles from the interface.

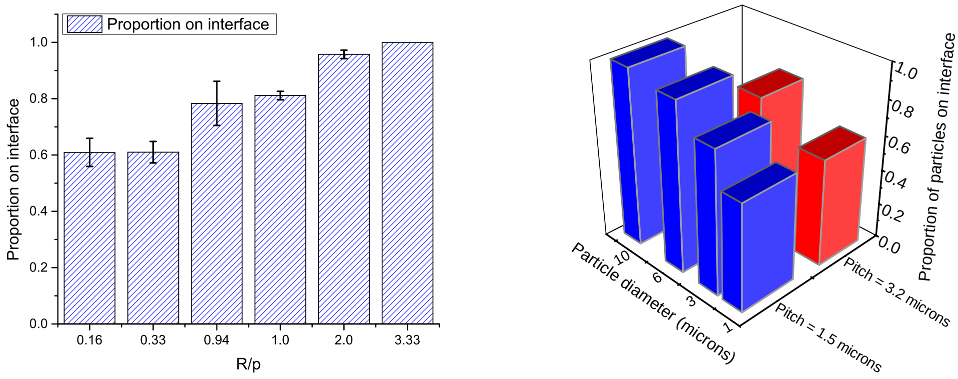

(a) **(b)**

Figure 4.6 (a) Proportion of particles on the interface as a function of radius/pitch length. (Error bars are the error on the mean) (b) Proportion of particles found on the interface as a function of pitch length and particle size.

The position of the particles with respect to the silicone oil – cholesteric interface was determined using fluorescence confocal microscopy. A majority of the particles are found on the interface between the oil and the liquid crystal, colloidal particles (green) can be seen on the interface in figure 4.3(b) and figure 4.5(c). In the case of 1 μm particles figure 4.5(b) particles are also found deep within the bulk liquid crystal.

An example result of the image analysis is shown in figure 4.5(a): the line is the intensity of the fluorescence from the Nile Red dye as a function of depth (confocal slice number). The bars are a histogram of the colloidal particle locations. The interface was taken to be the mid-point of the rise in the fluorescence signal. This was found to correspond well with the point at which the LC texture was first in focus but allowed for automation and comparison between different samples.

The vertical location of the particles with respect to the interface could be found by comparing the colloidal particle coordinates with the interface location. Particles which were within a distance of R + the confocal slice thickness (0.38 μm) were defined as being trapped at the interface (shaded (blue) region in figure 4.5(a)). It is important to note that while particles were found in the bulk of the liquid crystal (light (red) region) they were never found wholly within the silicone oil (white region).

Figures 4.6(a) and (b) show the proportion of the particles found on the interface between the liquid crystal and the silicone oil (as opposed to the bulk of the LC) as a function of particle radius for two different pitch lengths of the cholesteric liquid crystal. The data is the mean proportion at the interface from of all experiments at that pitch length to particle size. Error bars show the standard error on the mean. A greater proportion of large particles ($R > p$) are found on the interface than small ($R < p$) particles. Figure 4.6(a) shows the proportion of particles on the interface as a function of radius/pitch length, more particles are found on the interface as the particle radius increases.

Further, it can be seen in figure 4.6(b) that the particles in $1.5\,\mu$m pitch CLC are preferentially expelled compared to those in $3.2\,\mu$m pitch CLC for the same radius. This effect maybe associated with changes to the liquid crystal elastic properties as a function of the helical pitch. The colloidal particle induces a defect line in the cholesteric with a length that changes inversely with the pitch (see below and [46, 57]; hence the defect is more energetically expensive at shorter pitch lengths.

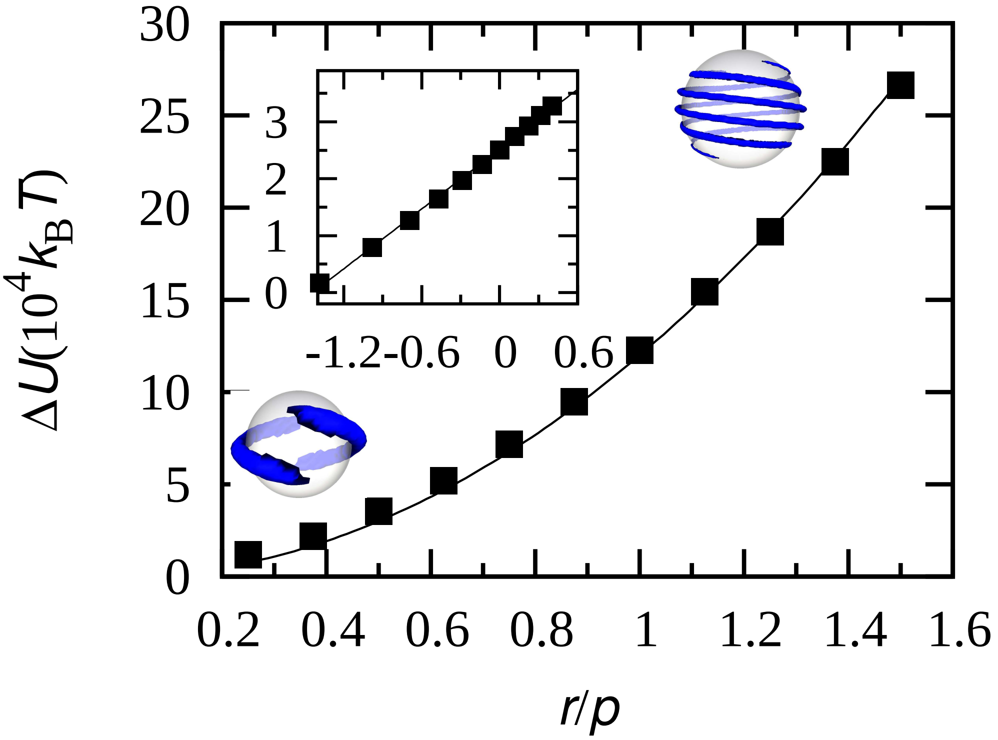

Figure 4.7 Simulation result from J. Lintuvouri, showing the elastic energy cost, ΔU, determined by simulating a colloidal particle, radius r, with planar surface anchoring submerged in a cholesteric liquid crystal, pitch p schematics show the defect structures around particles as discussed in the text. Inset: a log-log plot of the same values. The solid lines are a functional form described in the text.

The preferential expulsion of particles from the cholesteric liquid crystal, as particle size R increases is seen for both of the pitch lengths considered. The fact that not all particles, which were initially mixed into the CLC, are found on the interface, (which is a deep energy minimum in view of the large proportion of the particles sequestered there) indicates that the system reaches a metastable state, with the proportion of particles at the interface unchanged over the lifetime of the experiment (days with closed cells, hours with open ones). This view was confirmed by additional experiments. Particles were mixed initially into the silicone oil. In this case, particles are found in steady state *only* on the interface, and never stuck in the oil phase. It should be stressed that during the initial stages of the experiments (whilst the cholesteric texture is still moving) the colloids are mobile and clusters are seen to break up and reform.

These observations suggest that there is a particle-size dependent force which drives particles to the interface, with larger particles being preferentially expelled. As the particles are found to be expelled to both upper and lower interfaces, with approximately equal probabilities when sandwiched between the silicone oil layers, gravity cannot provide the necessary driving force. In addition, in recent experiments [43] on the bulk system no sedimentation was observed over a time period of a year indicating that any dynamics due to gravity must be extremely slow. Close to the interface, dynamics may be further arrested by the appearance of an elastic barrier which has been predicted for a colloidal particle approaching an aligning surface in a nematic LC [18].

A good candidate to expel the particles to the interface comes from the elastic cost associated with a particle with planar surface anchoring trapped in the bulk of a CLC. The boojum defects seen in the nematic expand to become disclinations in the CLC (shown schematically in Fig. 4.7) [59].

The elastic cost of having a colloidal particle with a finite surface anchoring, W, embedded into bulk cholesteric liquid crystal characterised by a pitch length p and elastic constant K, can be estimated via simulations. These were performed (by J. Lintuvuori) using a Landau-de Gennes free energy model for chiral liquid crystals [8, 35] (details of the simulations can be found in [80]). The elastic penalty can be estimated as the difference ($\Delta U = F - F_{W=0}$) between the minimised free energy of the system where the colloidal particle interacts with the liquid crystal (finite W) written F and the energy of a system with an equivalent non interacting ($W = 0$) colloidal particle $F_{W=0}$ Figure 4.7 shows an estimated ΔU for various colloidal radii R and a constant pitch length p. There is a fit to $\Delta U = a(R/p)^2$, with a a positive constant with the units of energy. The inset shows the same data on a log-log plot. Here the fit is $\ln(\Delta U) \approx n \ln(R/p) + a'$, with $n \approx 1.75 \pm 0.03$. The simulation data are therefore compatible with an energetic cost $\Delta U \sim KR^2/p$.

For a nematic LC the elastic energy cost of having a colloidal particle in the LC scales as $\Delta U \sim KR$. The higher power in R found in the scaling of the free energy cost with respect to the nematic limit can be intuitively explained; larger particles create longer defects which cost additional energy and provide a drive to expel the particles to the interface. This is in contrast to the nematic case where the Boojum defects are independent of the particle radius. Importantly, this elastic cost leads, by dimensional analysis, to an elastic force $\sim KR/p$, which increases with particle size R, this force is not present in the nematic case. This provides a possible explanation for the experimental findings of figure 4.6 that the proportion of colloidal particles at the interface increase when as the particle size increases.

4.4 Particle Distributions on the Interface

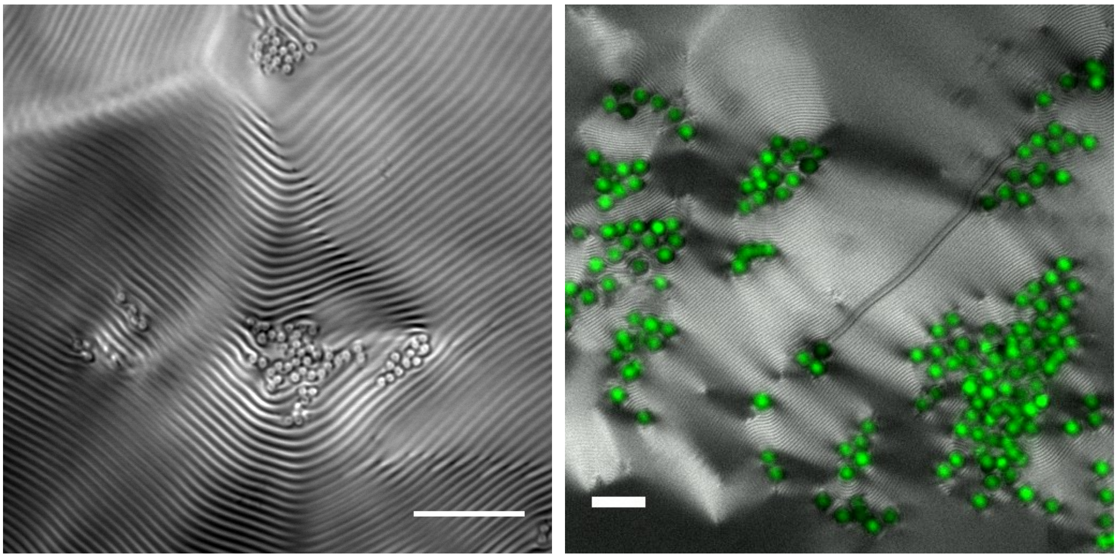
(a) (b)

Figure 4.8 Aggregates of colloidal particles at the interface.(a) A transmission image from the 555 nm laser with crossed polarisers of a 1 μm particles at the interface of a $p = 1.5\,\mu$m CLC. (b) Fluorescent confocal image of a $p = 1.5\,\mu$m CLC, 3 μm colloidal particles are shown in green. Scale bar 10 μm

The arrangements of particles trapped on the interface were studied using confocal microscopy. The direction of the helical axis within the xy plane can vary within the sample. This is in contrast to experiments performed with bulk cholesteric for example those in [43] where the helical axis is forced to lie parallel to the viewing direction. This variation in helical axis direction has an influence on the shapes of the colloidal aggregates. Figure 4.8 shows two examples of the variation in cholesteric texture and the resulting arrangements of particles. Particles are found singly, in chain-like aggregates and in amorphous "clumps". Aggregates form in locations where the helical axis changes direction. This could be due to expulsion of the particles from the ordered cholesteric to zones of high defect density as the system equilibrates.

All the images are taken once the cholesteric texture is static. Once the texture has fully relaxed following sample preparation Brownian motion of the particles is not observed due to the high viscosity of the samples and particle distributions appear to be stationary. The full range of aggregate types is observed for all the particle sizes and pitch lengths. In the following sections the distribution of the $R/p < 1$ colloidal particles with respect to the interfacial defects is discussed prior to the arrangement on the interface of the larger particles.

4.4.1 Templating $R/p < 1$

In addition to colloidal particle clusters which appear to be a universal feature, where $R/p < 1$, particles are seen to form chains along the fingerprint stripes as seen in figures 4.9(c), 4.9(d) and 4.11(c).

In order to test the templating hypothesis discussed above (section 4.1) the position of the particles with respect to the stripe texture was measured using image analysis routines (see section 4.2.3). Histograms of particle position with respect to the defect are plotted in figure 4.9(a) and 4.9(b). This distance is in units of z/p where $z/p = 0$ is the defect. For the particles in the longer pitch cholesteric $R/p = 1/6$ shown in figure 4.9(a) there is evidence of templating. Colloidal particles are found preferentially in the defects. For the particles in the shorter pitch mixture $R/p = 1/3$ no clear templating effect is seen.

The templating of the particles in a longer pitch length LC $R/p = 1/6$ at the interface suggests that the interfacial defects have some effect on the colloidal particle position. However, the lack of a preferred position for the $R/p = 1/3$ samples indicates that the physics is more complicated than the simple model

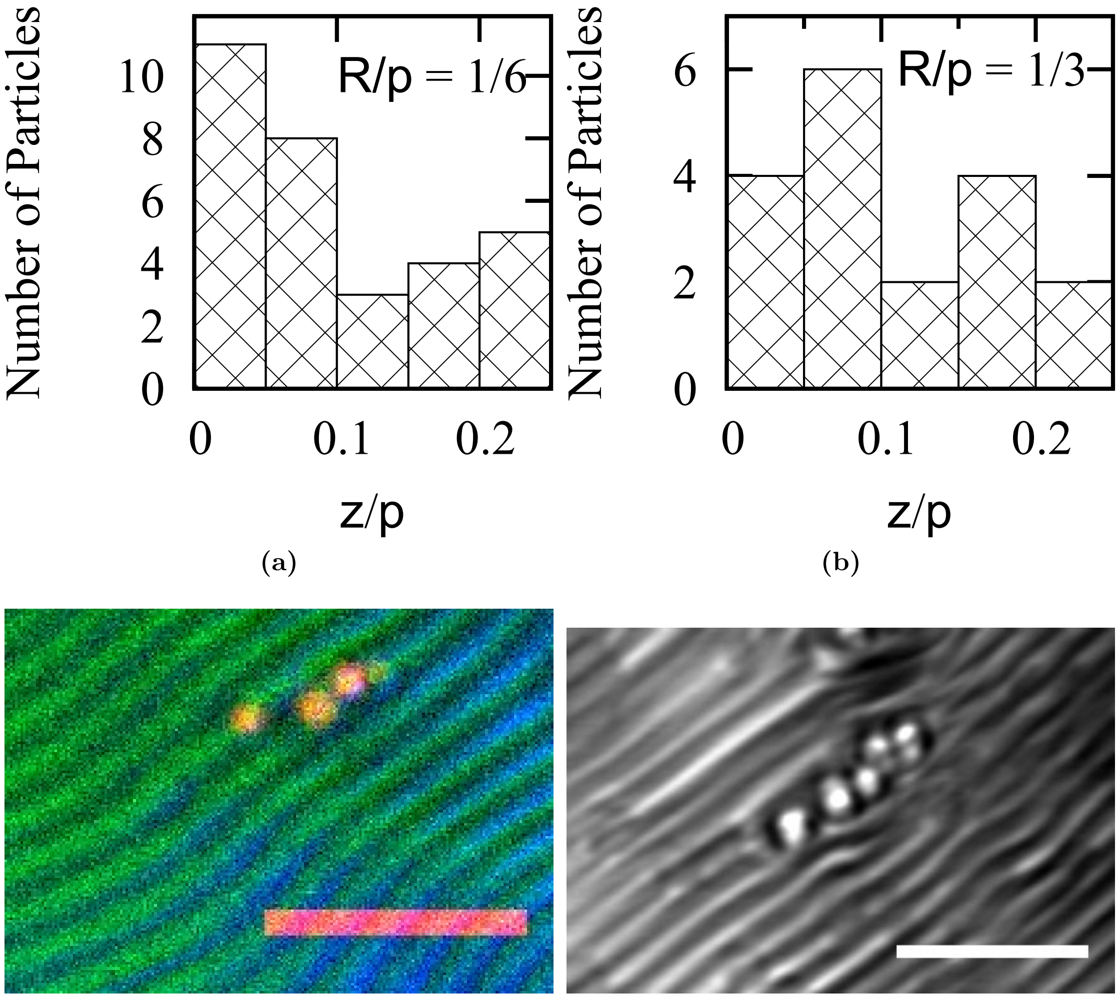

(a) (b)

(c) (d)

Figure 4.9 Experimental histograms of the distribution of isolated particles at the cholesteric-oil interface, for (a) $\frac{R}{p} = \frac{1}{6}$ (R $= 0.5\,\mu\mathrm{m}$ and p $= 3.2\,\mu\mathrm{m}$), and (b) $\frac{R}{p} = \frac{1}{3}$ (R $= 0.5\,\mu\mathrm{m}$ and p $= 1.5\,\mu\mathrm{m}$) (c) Fluorescence microscopy image showing an isolated particle and a dimer, each lying atop disclination lines $\frac{R}{p} = \frac{1}{6}$ (d) Transmission microscopy image of a longer chainlike aggregate $\frac{R}{p} = \frac{1}{3}$; the disclination lattice is partially disrupted in this case.

discussed in section 4.1.2. In the simple model, the anchoring strength W at the colloidal particle was set to zero. The colloidal particles had no effect on the alignment of the liquid crystal.

In the experiments the anchoring strength is unknown but it is unlikely to be zero. Simulations performed (by J. Lintuvuori) at finite anchoring strength reveal that the colloidal particles themselves create defects. These defects can interact with the interfacial defects as seen in figure 4.10(a) to 4.10(d). For $R/p = 1/6$ this

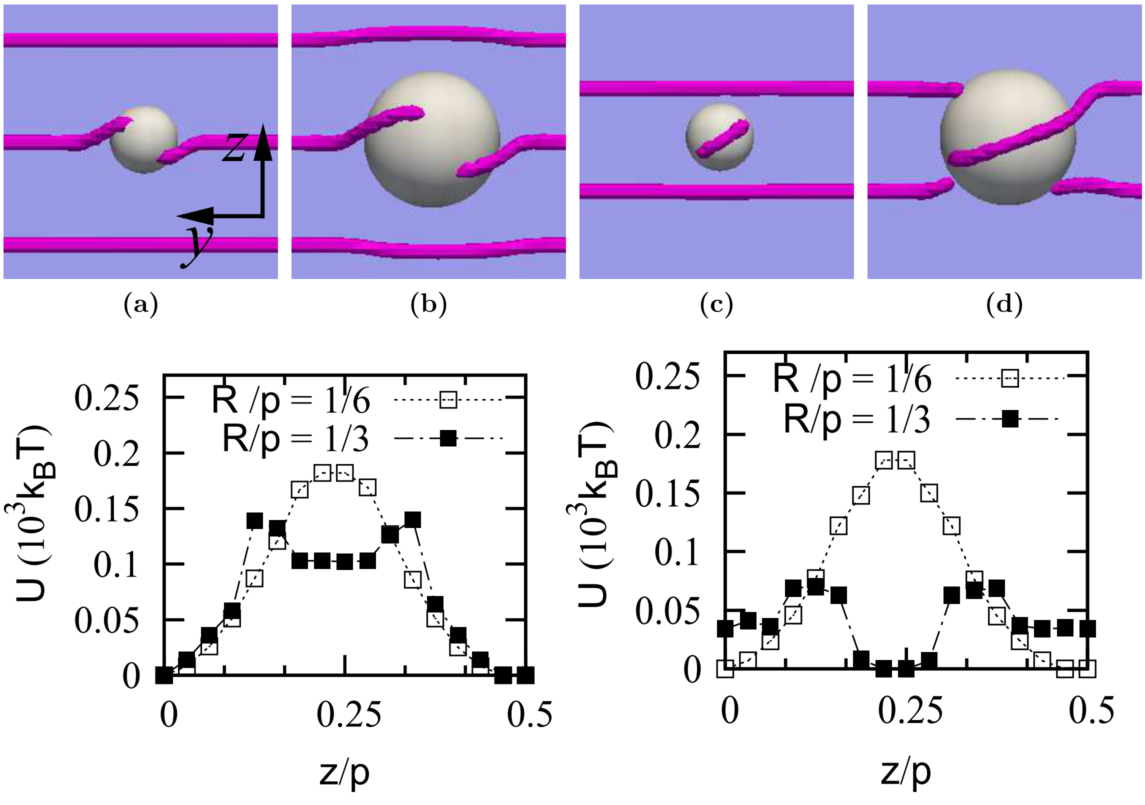

(a) (b) (c) (d)

(e) (f)

Figure 4.10 Simulations by J.Lintuvouri. (a) to (d) Disclination structures found in simulations for a colloidal particle trapped at the cholesteric-oil interface with strong anchoring at the particle surface. Particle size is varied at fixed surface anchoring W, and pitch p. The dimensionless ration $WR/K = 5.3$ (a) and (c), and $WR/K = 10.67$ in (b) and (d). In (a) and (b) the colloidal particle is centered on a disclination, in (c)and (d) midway between disclinations. (e) Plots of the free energy landscapes corresponding to the schematics. (f) At an intermediate anchoring strength $WR/K = 2/7$ the energy landscape becomes more complex and flatter particularly in the case of the "larger" $(R/p = 1/3)$ particles

rewiring of the defects has very little effect on the the shape of the free energy landscape figure 4.10(e) (open symbols). However for $R/p = 1/3$ case the energy landscape has been significantly altered. The position of minimum has moved from its position of $z/p = 0.25$ in the zero anchoring case to $z/p = 0$. This implies that the physics of the system is governed by anchoring strength W as well as the particle size to pitch ratio R/p.

In order to make comparisons a dimensionless ratio $w = WR/K$ which is the strength of the anchoring at the colloidal particle surface relative to bulk elasticity in the liquid crystal is defined. For small w the colloidal particle position depends solely on the ratio R/p and seeks to cover the largest possible length of defect. As w is increased the energy landscape becomes more complex. For intermediate values of w and $R/p = 1/3$ the landscape is fairly flat and rough as seen in figure 4.10(f). This landscape is unlike to be able to act as a good template for colloidal particles. The lack of templating in our experimental system could be accounted for by this complex landscape.

4.4.2 $R/p > 1$

Large particles also form chains as well as amorphous aggregates. The position of particles with respect to the interfacial stripes is no longer easy to study as the helical axis becomes distorted close to the particles, figure 4.1. In between the particles the surface anchoring conditions and the helical axis direction cannot both be satisfied. The direction of the helix becomes distorted to allow the surface anchoring to be maintained. For particles larger than the pitch length the particles do not touch within the chains figures, 4.1(b), 4.11(a), and 4.11(b). The spacing is roughly the period of the stripes, suggesting that there may be cholesteric layers wrapping the particles similar to previous observations of “onions” around colloidal particles held in the oily streak network of a cholesteric [43].

Some deformation of the helical axis is required in order to accommodate the surface anchoring of the liquid crystal at the colloidal particles. The lowest energy configurations could well be the chain-like aggregates, figure 4.11, which involve relatively little perturbation of the direction of the helical axis.

This is in contrast to bulk cholesterics where only plate-like aggregates perpendicular to the helical axis are observed [43]. In that study the anchoring enforce a uniform helical axis direction. It is tempting to say that the chains correspond to the edges of these plates, found perpendicular to the helical axis where the direction of the axis is reasonably uniform. However, the chains are lines along the interface and do not propagate deep into the sample as they would if they represented a slice through a plate.

Single Particles

Figure 4.12 shows the arrangement of the cholesteric layers around single particles. We identify three distinct cases. In the first, figures 4.12(a) and (b), the layer spacing, direction and alignment are relatively unperturbed by the presence of the particle and no obvious defects are seen. This is likely to be the lowest energy state and corresponds to that found in simulations [58]. In the computational studies a defect, in the form of a Boojum expanded into a line, is formed which, for us, could be unresolvably close to the particle surface.

In the second case figures 4.12(c) and (d), the particles are associated with a *Chi* edge defect. This defect separates regions with differing numbers of layers (i.e. additional cholesteric layers are introduced). *Chi* edge defects are postulated to be the structure of the oily streaks found in the Grandjean (planar) texture of the cholesteric [35]. The association of colloidal particles with oily streaks, leading to the stabilisation of the oily streak network has been reported [104] so it is unsurprising that colloidal particles are found in analogous regions here. The formation of defects costs energy due to the formation of a disordered core: in the bulk case it has been postulated that the particle takes out this high energy region pinning the defect in place as discussed in chapter 2 section 2.3.3. A similar mechanism is likely to be in play here leading to the colloidal particles stabilizing the defect.

There are also defects spatially separated from the particles, figure 4.12(e). Here the external defect may represent the topological charge required to balance that of the defect created at the particle. Other more complicated cases are also observed, figure 4.12(f). It is possible that these spatially extended arrangements of defects are metastable in comparison to more compact configurations. We find these defect structures for all particle sizes and pitch lengths. It is possible that the wide variety of defect structures encountered leads to the variety in particle aggregate size and shape.

4.5 Conclusions

We have studied a cholesteric liquid crystal – silicone oil interface decorated with particles. The final distribution of particles perpendicular to the interface, has a significant dependence on their size. Large particles are preferentially expelled to the interface for both cholesteric pitch lengths studied. This particle–size dependent expulsion is not seen for simple fluid–fluid interfaces and has not been reported for experiments on colloids at nematic–isotropic interfaces. Using simulations we establish that the elastic energy penalty of a colloid in the bulk of the CLC scales as KR^2/p, leading to a force $\sim KR/p$ which suggests that this is the cause of large particles being preferentially expelled. To fully exclude all other effects, experiments should be done using a nematic–silicone oil interface and identical particles. This is suggested as an avenue for future work.

The arrangement of particles in the plane of the interface is also size dependent: when the particles are smaller than the pitch connected chains are found. The predicted templating of the colloidal particles by the interfacial defects is observed for $R/p = 1/6$ but is absent for $R/p = 1/3$. This indicates that the templating is extremely sensitive to the particle size and the anchoring strength of the LC at the colloidal particle.

For larger particles the cholesteric layers wrap the particles in a manner suggestive of the “onions” in [43] leading to a separation of particles within chains. These chains form perpendicular to the helical axis (parallel to the cholesteric layers). Disordered aggregates are seen where the direction of the helical axis is not uniform suggesting colloidal particles are expelled to regions of high disorder. The association of single particles with at least three different defect types suggests that the colloidal particles themselves may be responsible for the disorder.

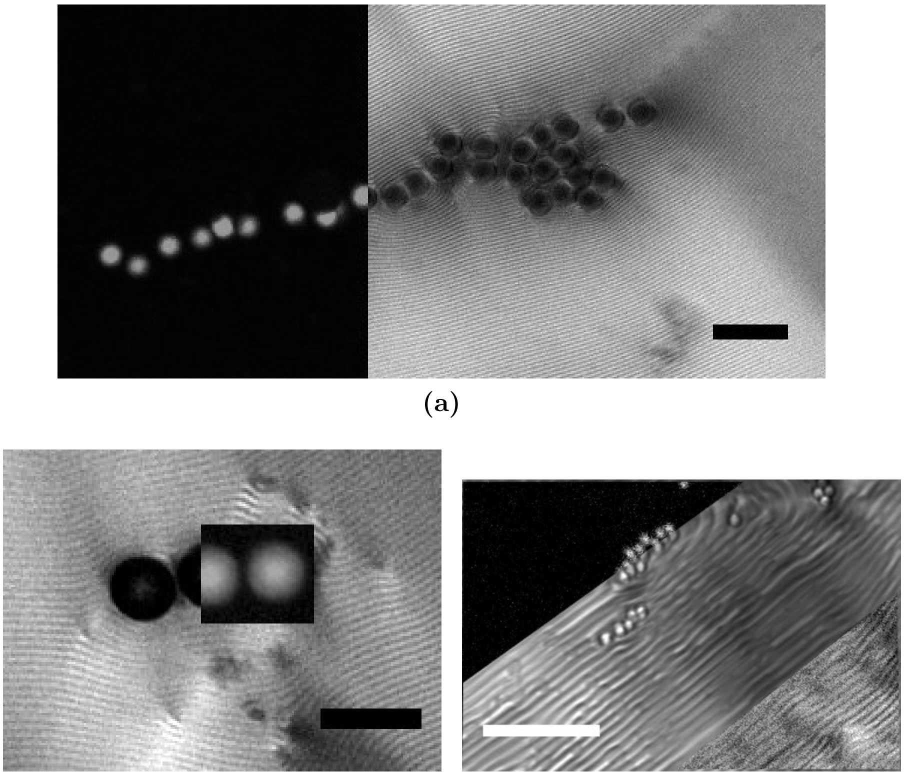

(a)

(b)

(c)

Figure 4.11 Confocal images of particles at the LC interface. Particle centres found using particle tracking routines and distances calculated. (a) $3\,\mu$m particles at the interface of a $1.5\,\mu$m pitch CLC confocal image. The right hand side is the fluorescent signal from the CLC showing the arrangement of the cholesteric layers. The left hand side shows the fluorescent signal from the colloidal particles. Average inter-particle spacing (centre to centre) $3.44\,\mu$m (i.e. $0.44\,\mu$m + diameter) (b) $6\,\mu$m particles at the interface of a $1.5\,\mu$m pitch CLC, fluorescent signal from the CLC showing the arrangement of the cholesteric layers, the overlay shows the confocal fluorescent signal from the colloidal particles. Inter-particle spacing (centre to centre) $6.56\,\mu$m, (i.e. $0.5\,\mu$m + diameter) (c) $1\,\mu$m particles at the interface of a $1.5\,\mu$m pitch length CLC. Confocal image: Top section signal from the colloidal particles, centre section transmission signal, bottom section fluorescent signal from CLC. The particles are touching. Scale bars $10\,\mu$m. All textures observed through the transparent silicone oil layer.

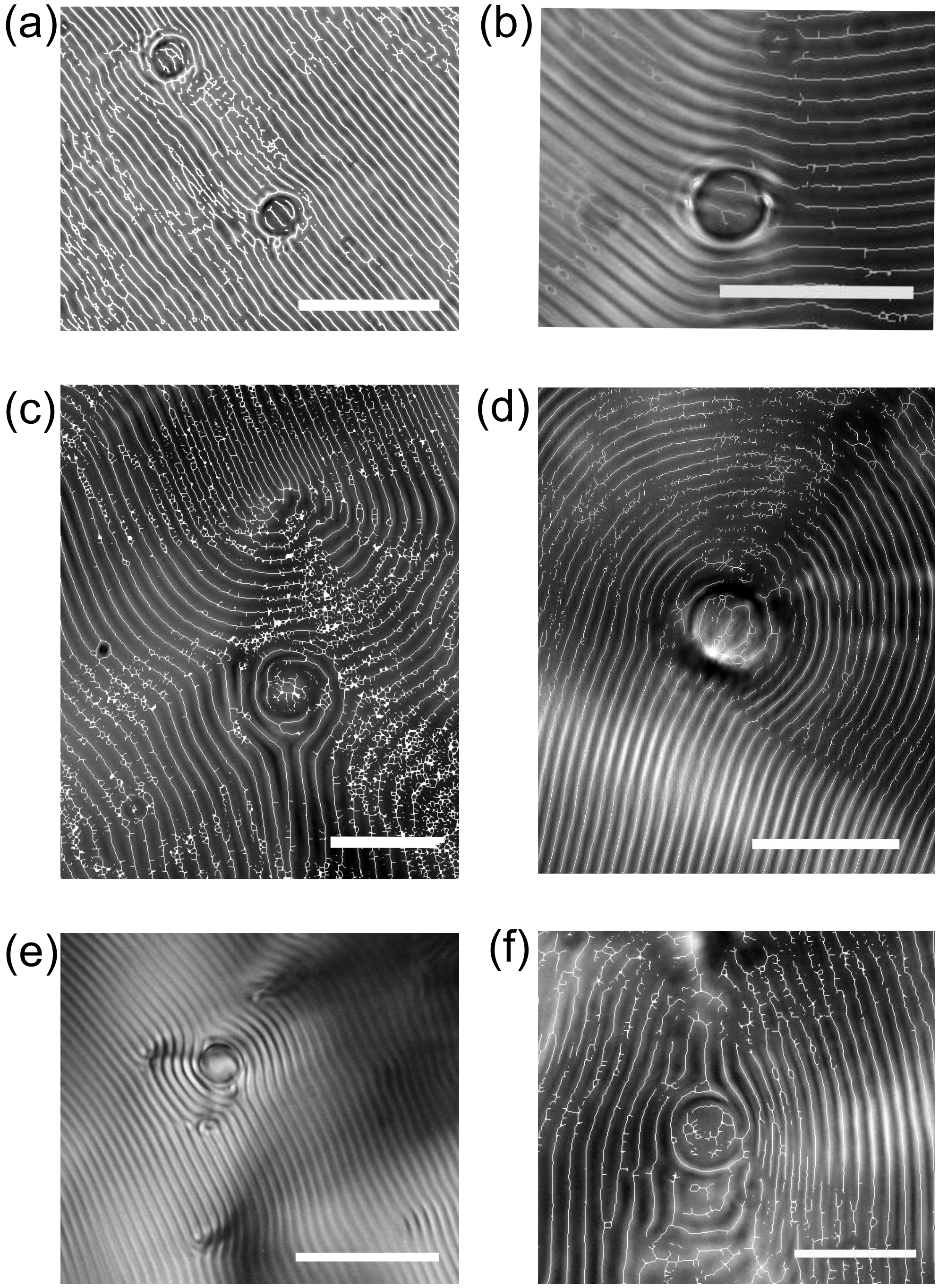

Figure 4.12 Polarising optical microscopy images of single particles showing the influence of particles on the cholesteric layers. Bright lines denoting pixels with local maximum intensity added to guide the eye. Scales bars (a,d,e) 10 μm (b,c,f) 5 μm. (a) 3 μm particles in 1.5 μm pitch CLC; (b) 3 μm particle in 1.5 μm pitch CLC ; (c) 6 μm particle in 1.5 μm pitch CLC; (d) 3 μm particle in 1.5 μm pitch CLC; (e) 3 μm particle in 1.5 μm pitch; (f) 3 μm particle in 1.5 μm pitch CLC.

Chapter 5

Colloidal Particles in Blue Phases

5.1 Introduction

This chapter concerns experiments on samples of colloidal particles dispersed in cholesteric blue phases. Blue phases only exist in a narrow range of temperatures and chiralities due the delicate balance between satisfying an increased degree of twist at the expense of the formation of defects. The thermodynamics of the blue phases are discussed in chapter 2.

In recent years, methods have been developed to increase the stability of blue phases whilst retaining their responsiveness for display applications. These have taken a variety of approaches including: using dispersed polymers [49], bent core molecules [16] and dispersed nanoparticles [20]. The most successful of these have increased the temperature range of blue phases to 50 K. The increased stability of polymer and nanoparticle-dispersed blue phases is attributed to the "core-replacement" mechanism as discussed in section 2.3. Only nanoparticles with a weak particle LC interaction created by careful surface chemistry have been shown to successfully increase stability and these are difficult to resolve optically due to their small size [21]. The increased stability of bent core mixures is ascribed to an increased degree of flexoelectricity [16]. No such bent core molecules are used in this thesis.

Blue phases have also been proposed as a means to assemble photonic crystals [84] from dispersed nanoparticles. Simulation studies [85, 93] indicate that success depends strongly on the size of the colloidal particles and the anchoring strength and type.

Whilst the behaviour of colloidal particles with planar anchoring in nematic [92] and cholesteric [43] is well understood, there have been only limited experiments on micron-sized colloidal particles in blue phases [27]. These studies have focused on the ability of colloidal particle to increase the (temperature) existence range of the blue phase. They show that for micron–sized colloidal particles there is only a negligible increase in blue phase stability. Given the quantitative difference in behaviour between colloidal particles dispersed in nematic and cholesteric LCs [43] it is interesting to explore the behaviour of large colloidal particles dispersed in BPs. There are no published images showing the relationship between the LC and colloidal particles in a blue phase.

This chapter presents studies of micron–sized colloidal particles dispersed in blue phases and their influence on the cholesteric to blue phase transition and blue phase - isotropic coexistence. The behaviour of these colloidal particles in nematic and cholesteric LCs has been extensively charcterised [43]. This chapter extends that work to the behaviour of these particles withing the blue phase. The colloidal particles do not automatically destroy the blue phase but they do radically alter the melting transition.

5.2 Phase Transitions of Blue Phases

Blue phase are found between the cholesteric and isotropic phase in highly chiral LCs. The typical phase sequence in order of increasing temperature is:

Cholesteric →BPI →BPII →BPIII →Isotropic

Which blue phases are seen depends on the chirality of the sample as discussed in chapter 2. The different textures of BPI and BPII are shown in figure 5.1. The blue phases have been extensively studied using scanning calorimetry [95]. The transition from the blue phase to the isotropic phase is strongly first order [95]. However, the phase transitions from the cholesteric to the blue phase and between the three separate blue phases been shown to be weakly first order [95]. There is only a small amount of latent heat associated with the transition and there is a discontinuous jump in the order parameter at the transition temperature. Coexistence of BP domains within both the isotropic and cholesteric phases has been observed [78]. Coexistence of all three blue phases has also been reported [11].

The first order nature of the transitions means that supercooling is a possibility. There is an energy barrier between the meta-stable higher temperature phase and the equilibrium lower temperature phase, this must be overcome in order for the transition to take place. No such barrier exists for second order phase transitions. In pure samples only supercooling of BPI is observed [47]. Supercooling in samples with a BPI – smectic transition has also been observed [26]. Here, Demikhov *et al.* observe a separate blue phase, dubbed BPS is observed which has both BP and smectic characteristics. BPII and BPIII do not readily supercool. Supercooled and superheated examples of "pure" (un-doped with polymers, colloidal particles or bent core molecules) BPII or BPIII have not been reported in the literature.

Adding nanoparticles to the blue phase has been shown to increase the range of stability of the blue phase [20]. The nanoparticles increased the stability of BPIII at the expense of BPII which was no longer observed. The nature of the transitions was also altered. The transitions become broader and "smear out" with increased concentrations of nanoparticles.

Supercooling of BPI is seen in these nanoparticle-doped samples [20]. This supercooling of BPI is also observed in samples stabilised with polymers [49] and with bent core molecules [19]. However, supercooling of BPII has only been observed in a single BP system which uses very specific bent core molecules [79].

5.2.1 Disorder

The addition of colloidal particles to liquid crystal is a means of introducing disorder, which has a significant effect on phase transitions [82]. Disorder is generally subdivided into two types, quenched and annealed disorder. Quenched disorder is the case where the distribution of whatever is responsible for the disorder (impurities, colloidal particles etc.) doesn't change during the transition. In the case discussed in this thesis this would correspond to the colloidal particles being fixed in place during the transition. Annealed disorder is the opposite; here the distribution of impurities alters on the time scale of the transition. In the LC-colloidal particle case this is equivalent to the colloidal particles being expelled from the ordered phase as it forms.

The effect of disorder on phase transitions has been extensively studied. It has been shown that the addition of quenched disorder effectively smooths out a first order phase transition, making it second order above a certain degree of randomness [74]. The theory of disorder in liquid crystals has been applied successfully to the case of aerosils dispersed in nematics and nematics confined within in random pore glasses [22]. An extensive review can be found in [83]. Disorder creates local areas of order within the disordered phase or disorder within an ordered phase. This is equivalent to a local temperature; mesogens close to the source of the disorder e.g. a colloidal particle, will undergo a phase transition at a temperature depending on the coupling between the mesogens and the particle. The local transition temperature will be different to the bulk phase transition temperature.

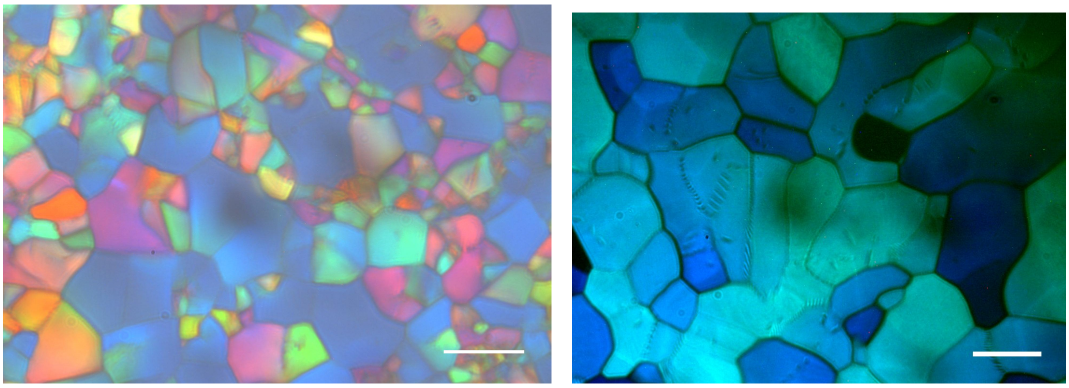
(a) (b)

Figure 5.1 Polycrystalline textures of (a) Blue Phase I and (b) Blue Phase II. Taken in transmission using a polaring optical microscope. These are true colour images. BPII has a larger domain size than BPI for our system. Scale bars 50 µm

.

5.3 Materials and Methods

The liquid crystal used in this chapter is a three-component commercial mixture. It consists of two nematic liquid crystals, 5CB (Aldrich) and a fluorinated nematic mixture, JC1041-XX (Chisso). The composition of the mixture is commercially sensitive but an example of the molecules can be found in [103]. Finally a chiral dopant ZLI-4572 (Merck) is added to create a chiral nematic liquid crystal. Varying the concentration of the chiral dopant varies the pitch of the liquid crystal. The composition and estimated pitch length of the liquid crystals used in these studies can be found in table 5.1 This was calculated using values for the

Mixture	Concentration of chiral dopant	Pitch length
Long pitch	7%	0.40 µm ± 0.01 µm
Short pitch	10%	0.29 µm ± 0.01 µm

Table 5.1 The chiral dopant concentrations used in this study

helical twisting power of ZLI-4572 from [103]. Short pitch mixtures exhibit both BPI and BPII. These can be as seen in figure 5.1. Long pitch mixtures exhibit only BPI. The three components were mixed by stirring until uniform.

Melamine colloidal particles $r = 1.5\,\mu\text{m}$ are used. As their behaviour in cholesterics has been characterised [43] and they are easily resolved in confocal microscopy. These are prepared as discussed in chapter 3. They have planar surface anchoring with the liquid crystal [43]. These colloidal particles have been shown to form flat sheets surrounded by defects in the cholesteric phase [43]. Simulations suggest that such colloidal particles will be tightly wrapped in a spiral defect line within the cholesteric phase [59]. These defect structures have been observed in a long pitch cholesteric [46] but are impossible to resolve optically in the short pitch material used here.

The colloidal particles were added to these liquid crystals via stirring and sonication as described in chapter 3. A range of volume fractions (from $\varphi_{vol} = 0.5\%$ to $\varphi_{vol} = 20\%$) were used but most of the samples were at $\varphi_{vol} = 1\ \%$. Once the colloidal particles were uniformly dispersed samples were loaded into glass capillaries (0.05 x 1 x 500 mm) or hand built sample cells (see chapter 3) via capillary action. The cells were sealed using silicone vacuum grease (Dow Corning) and used immediately.

To create a blue phase the samples have to be heated to the correct temperature. The temperature needs to be carefully controlled as the mixtures used have only a $\sim 1\,°\text{C}$ temperature range. Some preliminary experiments were performed using an Instec Hotstage. This had the advantage that it could be used in conjunction with the confocal microscope to allow the colloidal particles to be imaged in three dimensions. However, despite its stated 0.01 °C stability, it exhibited temperature gradients both across the window and in the z direction. These were found to have a significant effect on the sample. To avoid these temperature gradients and allow a greater control of heating rate a custom heating stage was constructed by Hugh Vass. The stage as shown in figure 5.2 can be used on both upright and inverted microscopes. The temperature is controlled via a Lakeshore 331 temperature controller to ± 0.005 °C.

Blue phases are only prepared by heating from the cholesteric as the colloidal particles rapidly sediment out from the isotropic phase. The lower viscosity of the isotropic phase together with the slow cooling rates required for these studies means that the colloidal particles are annealed away before the blue phase forms on cooling. When blue phases are prepared by heating, the elastic nature of the cholesteric and blue phases prevents the colloidal particles from sedimenting. Bulk samples of colloidal particles in the cholesteric phase are stable to sedimentation for months.

Samples were mounted in the hotstage using heat sink paste (RM) between the sample holder and the stage to ensure good thermal contact. A lid was placed over the sample inside the stage body to increase thermal stability. Once mounted, the sample was heated rapidly ($10\,^{\circ}\mathrm{C\,min^{-1}}$) to within 5 °C of the blue phase transition. The heating rate was then decreased to $1\,^{\circ}\mathrm{C\,min^{-1}}$. For the final stage (within approximately 1 °C of the transition) the heating rate was decreased further to $0.1\,^{\circ}\mathrm{C\,min^{-1}}$. During heating, time lapse images were recorded using the confocal microscope. Once the blue phase transition was observed the temperature was kept constant until the transition was complete. Further heating and cooling of the sample was then performed within the blue phase to study the effect of the colloidal particles. The temperature was recorded digitally via an adapted LabView application provided by Lakeshore.

5.4 Results

5.4.1 Colloidal Particles in the Cholesteric Phase

Colloidal particles mixed into cholesteric liquid crystals have been shown to stabilise the oily streak network forming a colloidal particle stabilised defect gel [104]. Colloidal particles with planar alignment form flat sheets perpendicular to the helical axis [43]. In this study similar behaviour is observed; flat plates of colloidal particles are found surrounded by defects and always at the junction of oily streaks as can be seen in figure 5.3.

On heating towards the blue phase transition the oily streak network undergoes significant rearrangement. This rearrangement of defects also moves the

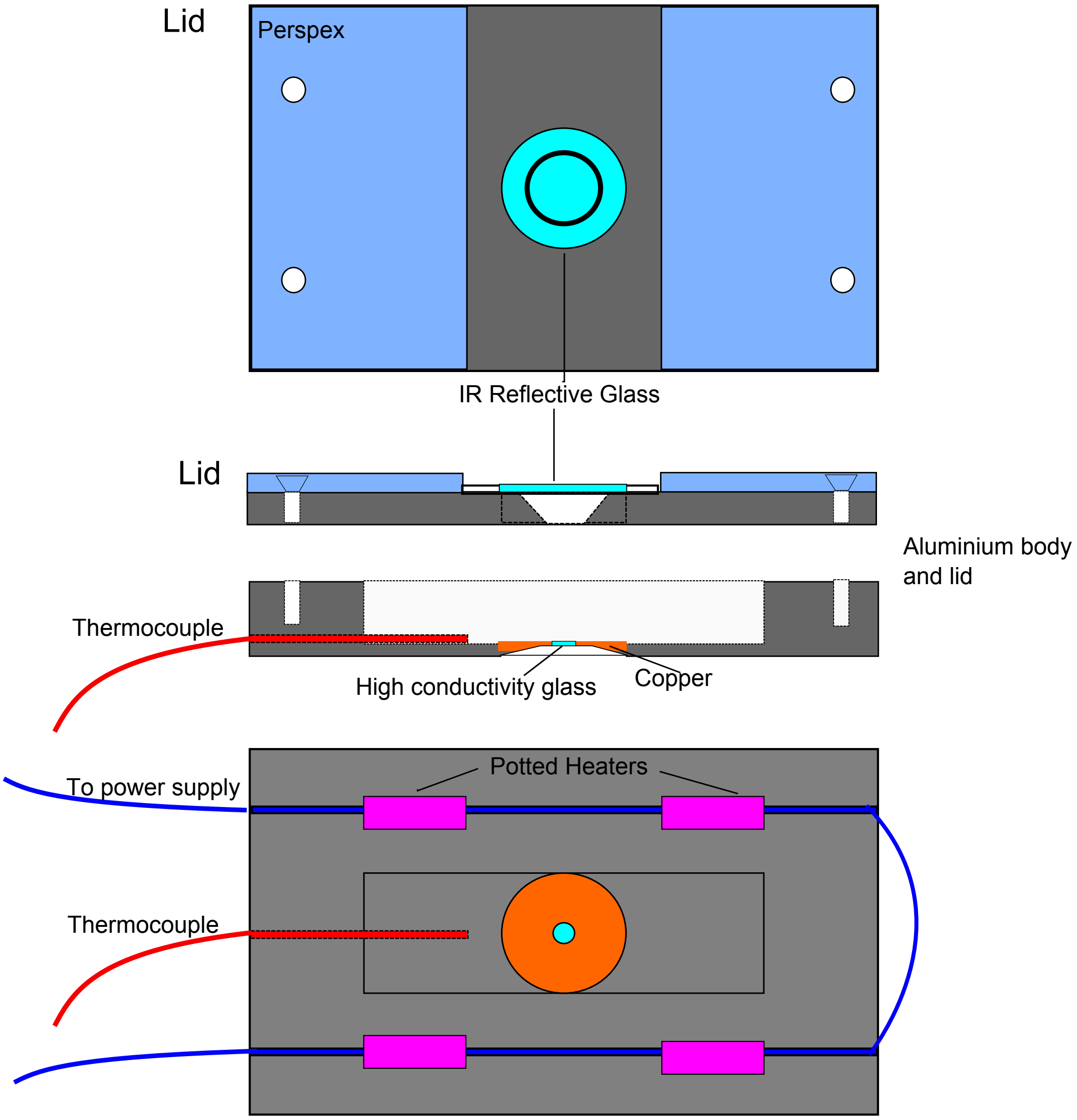

Figure 5.2 A schematic of the hotstage used for blue phase experiments

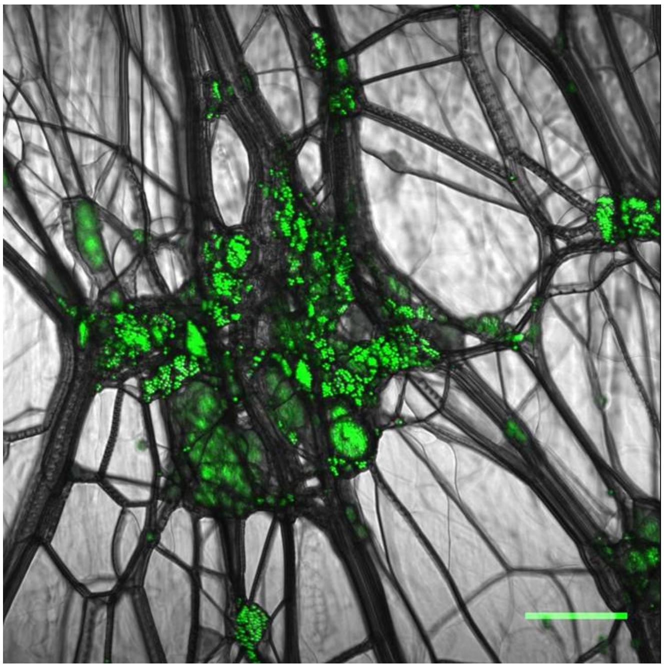

Figure 5.3 A composite confocal microscope image of the fluorescent signal from the colloidal particles (green) held in the oily streak network (grey imaged in transmission with crossed polarisers) of a the cholesteric. Scale bar 50 µm

associated colloidal particles. However, on average the structure of the colloidal particles remains roughly constant. Colloidal particles remains in flat plates dispersed throughout the sample. This was confirmed using confocal microscopy in conjunction with the Instec stage. Using this stage allowed the distribution of colloidal particles throughout the sample volume to be observed. It is important to keep in mind that this is how the colloidal particles are distributed prior to the blue phase studies.

5.4.2 Cholesteric to Blue Phase Transition

The oily streak network and other defects present in the cholesteric act as nucleation sites for the blue phase. In figure 5.4 a sample with a dense oily streak network and no colloidal particles is heated rapidly ($5\,^{\circ}\mathrm{C\,min^{-1}}$ and then $1\,^{\circ}\mathrm{C\,min^{-1}}$) to close to the blue phase transition temperature. The rapid heating ensures that the defect network does not have time to anneal. On heating through the transition the oily streak defects thicken as the blue phase grows from the cores figure 5.4(b). The blue phase grows outwards from the defects with islands of aligned cholesteric texture figure 5.4(d) the last to disappear.

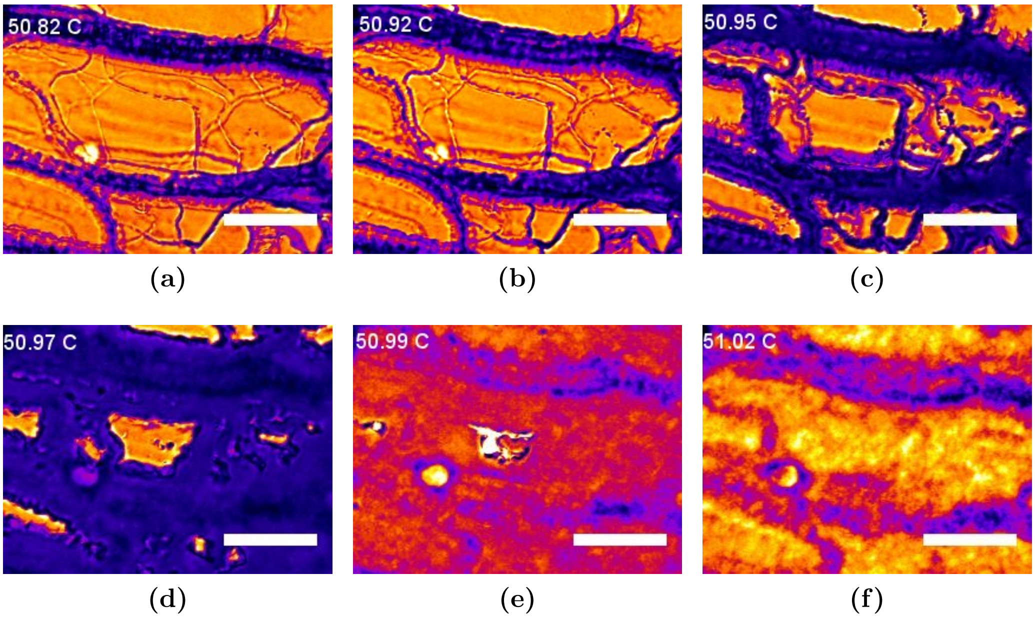

(a) (b) (c) (d) (e) (f)

Figure 5.4 The transition from cholesteric to blue phase in a planar cell. These images are taken using a confocal microscope between crossed polarisers. False colour has been used to enhance contrast. (a) The cell has not been annealed prior to use. Oily streak defects (dark purple) are present in the cholesteric. (b) - (e) The blue phase (purple with a rough texture) grows from the defects leaving islands of (orange and smooth) cholesteric. (f) These eventually disappear leaving the sample with a rough texture. The initially defected regions are still visible as the blue phase grains have different orientations here. Scale bars 50 µm.

The oily streaks are a rather random defect structure. An array of ordered defects can be produced by using a Cano wedge cell. A schematic picture of such as cell is shown in figure 5.5(a). The boundary conditions result in a parallel array of defect lines figure 5.5(b). These defects are created where the number of cholesteric pitches able to fit into the gap between the two plates increases by a half e.g. from 1 to 1.5. A schematic of such as cell can be seen in figure 5.5(a). Details of its construction can be found in chapter 3. On heating through the phase transition the blue phase initially nucleates along these lines figure 5.5(c) and grows outwards before eventually filling the whole sample figure 5.5(c) to 5.5(e).

Colloidal particles stabilise the oily streak network [104] pinning it in place but otherwise do not introduce any new physics in the cholesteric phase. Colloidal particles are themselves surrounded by defects [43] as can be seen in figures 5.3 and 5.6(a). These defects act as nucleation sites for the blue phases. The blue phase can be seen to grow from the colloidal particles and the oily streaks simultaneously

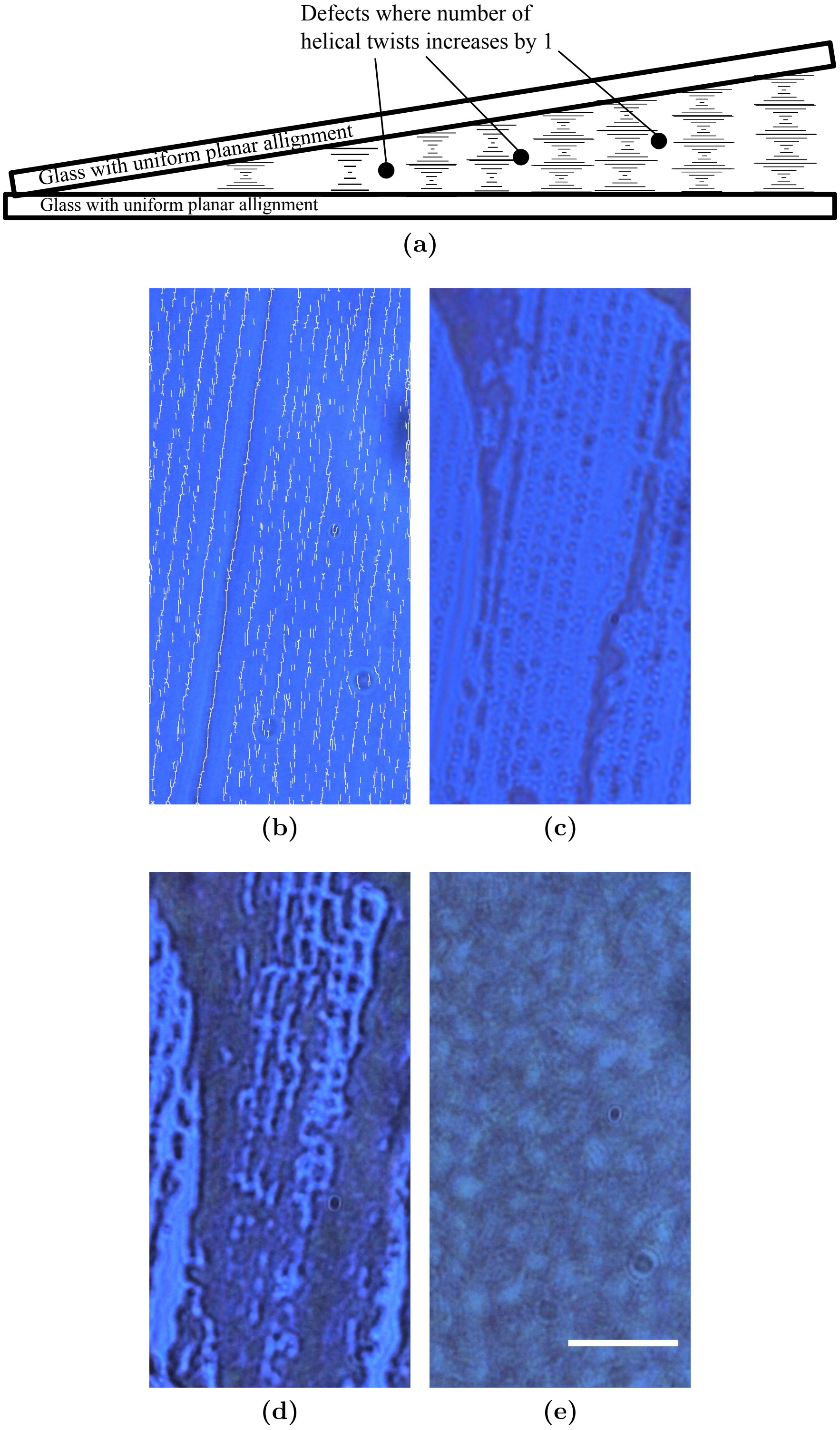

(a)

(b) (c)

(d) (e)

Figure 5.5 (a) Schematic of a Cano wedge. When the number of cholesteric pitches able to fit between the two slides increases by half a defect formed. (b) The defects can be seen as an array of parallel lines (The position of intensity minima are overlaid to guide the eye). (c) to (e) Transition from cholesteric to Blue Phase. The blue phase grows outwards from the defects before filling the entire cell in (e). Images taken using a polarising optical microscope and are true colour. Scale bar $20\,\mu\mathrm{m}$

figure 5.6(b). As in the case with no dispersed colloidal particles, the islands of aligned cholesteric between defects are the last to transition to the blue phase figure 5.6(c).

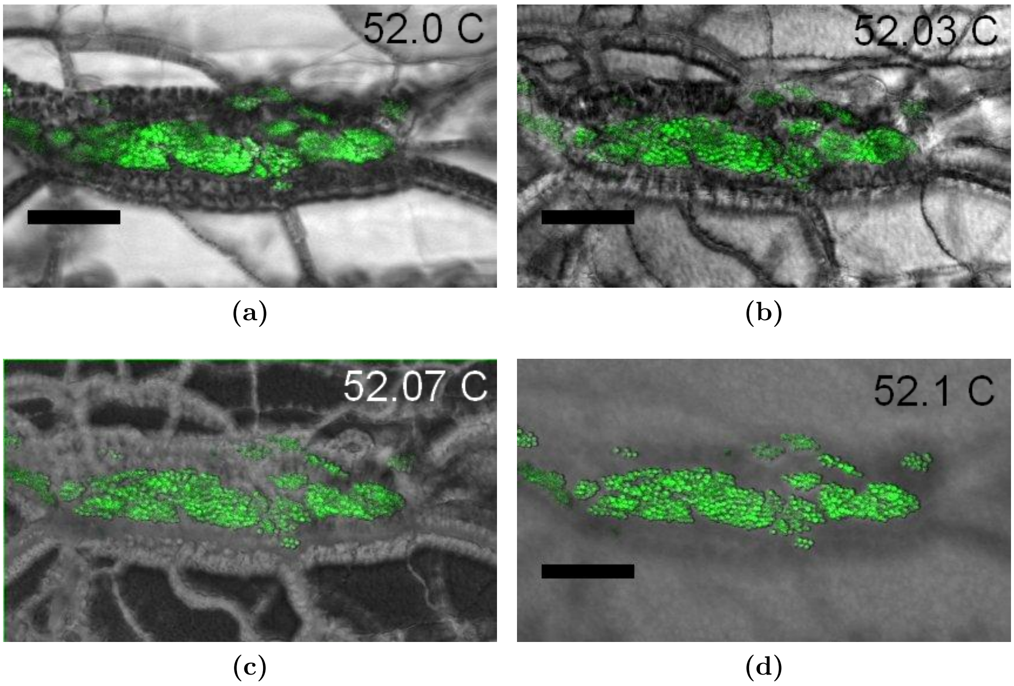

(a) (b) (c) (d)

Figure 5.6 The transition from cholesteric to blue phase in the presence of colloidal particles. (a) Prior to the transition, colloidal particles are held in the oily streak network, the thick dark lines. (b) Blue phase starts to grow from these lines making them thicker. (c) The blue phase (pale) continues to grow from the defects, leaving islands of dark ordered cholesteric phase. These islands gradually shrink. (d) Eventually colloidal particles are left embedded in a blue phase. Darker shading indicates where the principle defects were as the blue phase had a greater choice of alignment in these regions. Scale bars $50\,\mu\mathrm{m}$

5.4.3 Colloidal particles and Coexistence

Evolution of BP - Isotropic Coexistence

New effects due to the colloidal particles occur as the blue phase melts. Adding colloidal particles to a blue phase liquid crystal affects the kinetics of the phase transition between the blue phase and the isotropic. Colloidal particles influence the temperature at which this transition occurs and how the blue phase melts.

As discussed in the previous section, colloidal particles and their associated defects act as nucleation sites for the blue phase. In low chirality samples once the sample is in BPI the colloidal particles are observed surrounded by BPI, figure 5.6(d) and figure 5.8(a). On further heating but at temperatures below the final melting point dark regions are observed around the colloidal particles, figure 5.11. Colloidal particles within these regions move due to Brownian motion indicating that locally the elastic modulus is lower. Very occasionally dark regions without colloidal particles can be observed once the temperature is raised further, figure 5.9. This is rare, typically blue phases melt from the regions around colloidal particles which grow to fill the whole sample. Finally, the whole blue phase melts. The dark regions become completely black. This indicates that the regions are present though the full height of the sample. Colloidal particles within these black regions sediment through the isotropic phase onto the sample boundaries.

In samples with higher chirality the liquid crystal can exhibit both BPI figure 5.1(a) and at slightly higher temperatures BPII figure 5.1(b). The presence of colloidal particles has no discernible effect on the BPI to BPII phase transition, figure 5.8. Unlike the cholesteric to BPI transition there is no evidence of nucleation from the colloidal particles or BPI grain boundaries. Once the sample is heated further in BPII dark regions similar to those seen in lower chirality samples surround the colloidal particles, figure 5.7(d). The transition temperatures of these phenomena with reference to the cholesteric to BPI transition can be found in table 5.2.

The observance of dark regions prior to the blue phase - isotropic transition is also seen in samples without any colloidal particles figure 5.11(b).

5.4.4 The Phase of the Dark Regions

Once the melted regions have appeared colloidal particles are free to move within them. Colloidal particles do not leave the dark regions. If dark regions shrink, due to a temperature fluctuation, clusters of colloidal particles become more compact indicating a phase separation. Particle tracking was used to give more information about the melted regions. Image analysis routines discussed in chapter 3 were used to find the particle centres. Isolated particles were then identified and their motion tracked using particle tracking techniques by E. Weeks and others [9]. Only isolated particles were tracked as a definite radius is required to calculate a diffusion constant (see below). Using isolated particles also ensures the highest

Chirality	Total Range of Blue Phases	Transition to BPII	Temperature above Cholesteric to BP Transition at which Filled Regions Appear	Temperature above Cholesteric to BP Transition at which Empty Regions Appear
Low	0.49 ± 0.01 °C	Not Seen	0.15 ± 0.005 °C	0.26 ± 0.02 °C 3 observations
High	0.66 ± 0.03 °C	0.24 ± 0.01 °C	0.37 ± 0.02 °C	Not seen

Table 5.2 Table of appearance temperatures of the various transitions with reference to the Cholesteric to BPI transition

accuracy in particle position (colloidal particles in dense clumps are harder to identify accurately) and avoids hydrodynamic effects due to interactions between particles. The disadvantage is that there are relatively few isolated particles.

Particles which undergo Brownian motion obey the diffusion equation

$$\langle r^2(t) \rangle = 4Dt = \frac{4k_BT}{6\pi\eta a}t, \tag{5.1}$$

where $\langle r^2(t) \rangle$ is the mean square displacement and D is the diffusion coefficient defined as above. η is the viscosity and a the particle radius. The 4 in the equation is due to the fact that the (3d) movement of the colloidal particles is only imaged in 2d. By plotting the mean square displacement of particles against time, a diffusion coefficient can be calculated and the viscosity of the medium in which the motion is taking place measured, assuming all other parameters are known.

Fitting a straight line through the early section of the graph gives a diffusion constant of $D = 0.12 \pm 0.03$ µm^2 s^{-1}. This gives a viscosity of $\eta = 0.005 \pm 0.002$ Pa s. The viscosity of 5CB at a similar temperature is 0.016 Pa s. The gradient of the graph changes at later times. This is most like an experimental artifact as particles may become arrested (due to e.g. temperature fluctuations, interactions with other particles or the coverslip). Tracking algorithms are also more prone to error at long times and can track particles which have ceased to move reducing the value of $< r^2 >$. No physically meaningful data can be extracted beyond this point.

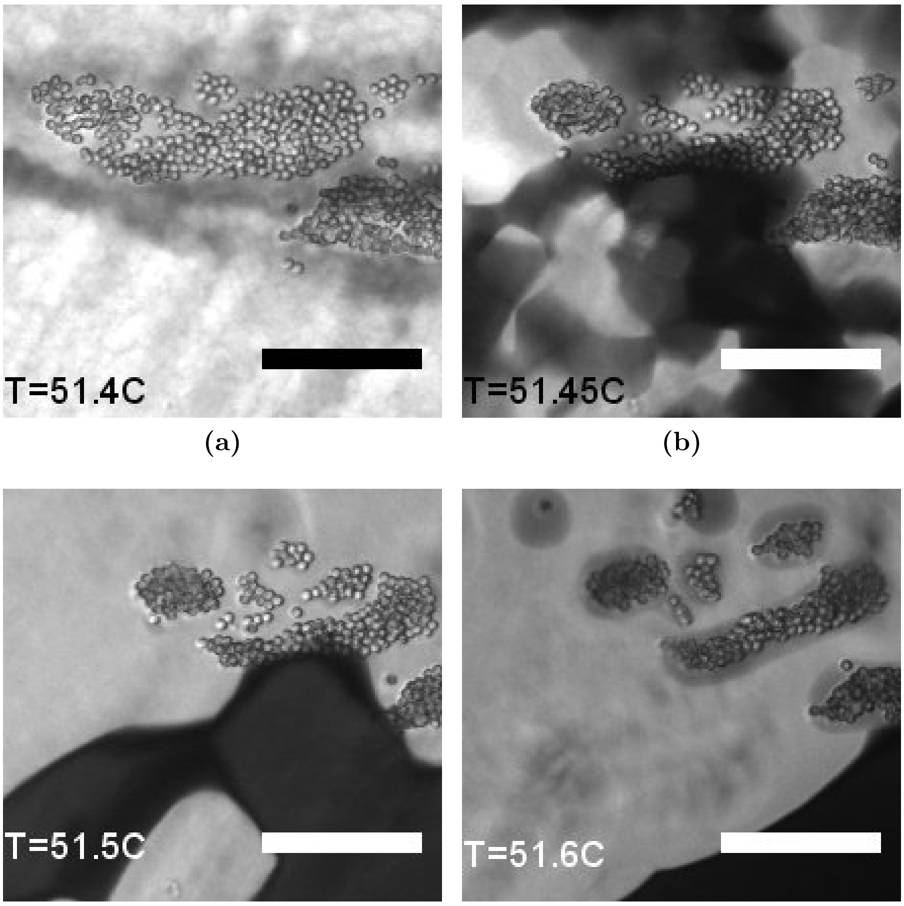

(a) (b) (c) (d)

Figure 5.7 Transmission images taken via confocal with crossed polarisers. (a) Colloidal particles in BPI. (b) Transition from to Blue Phase I to Blue Phase II (c) further heating towards the isotropic in the presence of colloidal particles leads to the BPII coarsening. (d) Melted regions surrounding colloidal particles. Scale bars 50 µm

There are numerous sources of error. As a scanning confocal microscope was used there is a large (1.56 s) time step between images. This will lead to an overestimate of the velocity of the particles and an under-estimate of the viscosity. There is an error of ± 1 °C in the temperature as the dark regions appear at different temperatures in different samples. Finally, the error in the absolute particle position is ± 0.312 µm as defined by the image resolution and the limits of accuracy of the image analysis routines. See [9] and discussions in chapter 3.

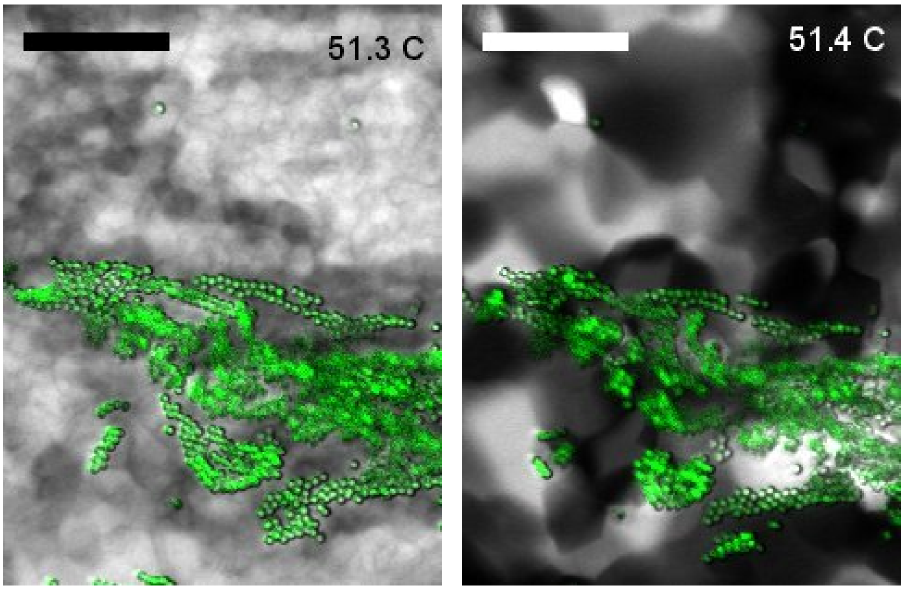

(a) (b)

Figure 5.8 Composite confocal images of colloidal particles (green) in (a) Blue phase I (grey scale) and (b) Blue phase II. Scale bars 50 µm

Facets

The isotropic (dark) regions can exhibit facets as seen in figure 5.12. The facets are most evident in BPII where the blue phase domains are much larger than the melted regions, see figure 5.12(a). In BPI, the domain size is much smaller than the inclusions so the facets are less easy to visualise, figure 5.12(b).

The facets are extremely temperature sensitive. Very small temperature fluctuations (smaller than the stability of the temperature stage) can cause the facets to round off and disappear. Facets can reappear at later times in response to temperature fluctuations.

Melted Regions and Associated Colloidal Particles

The relationship between the area of the melted region and the area of the colloidal particles is not straight forward. The area and shape of the melted regions are extremely temperature sensitive and fluctuate within the temperature stability of the temperature stage. We measure the maximum extent of the melted regions at a temperature below the BP to isotropic transition and compare it to the number of associated colloidal particles.

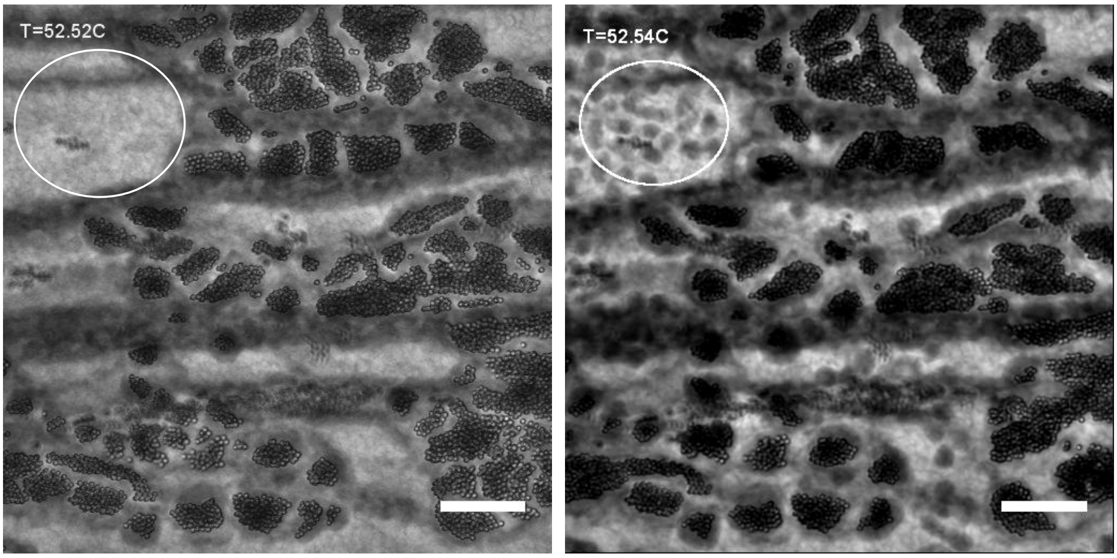

(a) (b)

Figure 5.9 Transmission images of colloidal particle clusters in BPI. (a) Initially melted regions are only observed around colloidal particles. The circled colloidal particle free region is uniform blue phase. (b) At higher temperatures melted regions are also observed separate from the colloidal particles in the circled region. Scale bars 50 µm

Melted regions are selected by hand using imageJ. Various image analysis routines have been developed in an attempt to automate the process but they ultimately require a large amount of human intervention due to the complicated background of the sample. Hand selection was equally reliable. As colloidal particles are clustered, there is insufficient resolution to extract individual colloidal particle coordinates so a coarse-grained approach was adopted. An idl algorithm was developed. The fluorescent signal from the colloidal particles was smoothed, a threshold applied and the clusters of colloidal particles identified as regions of connected pixels using in–built idl routines. The values of the threshold and smoothing as well as minimum region size are set by the user. The area of each colloidal particle region is calculated.

The colloidal particle areas and the areas of the associated melted regions are compared. Specifically, we compare the excess melted region (the area of melted region minus the area of the associated colloidal particles) with the area of the underlying colloidal particles. Colloidal particles are found in essentially flat sheets so the area of the fluorescent signal is a good proxy for the number of colloidal particles. The results can be found in figure 5.13. In the central region (excluding very large and very small number of colloidal particles) the excess area

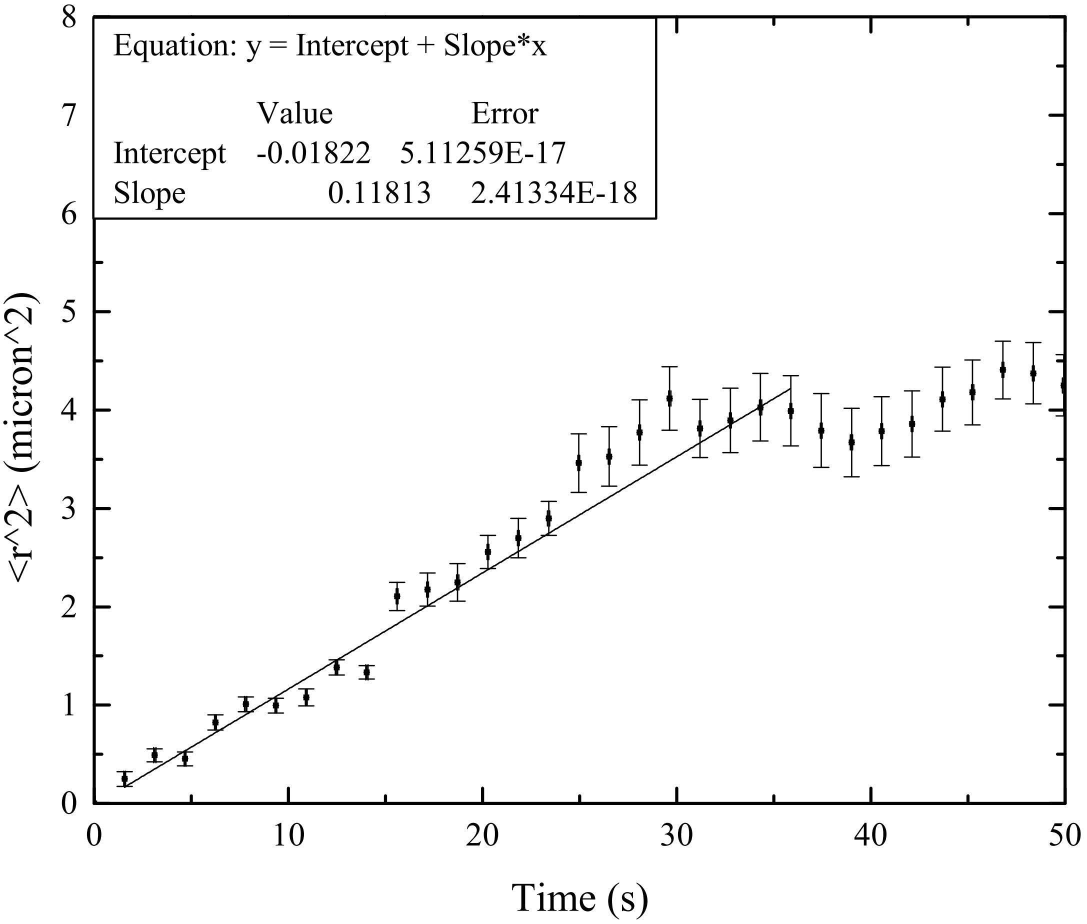

Figure 5.10 Plot of $\langle r^2(t) \rangle$ for single particles. Line is a linear fit through early times prior to $\langle r^2(t) \rangle$ saturating. Beyond this point, particle tracking becomes unreliable.

is inversely proportional to the number of colloidal particles. This indicates that the melted region associated with a colloidal particle cluster is independent of the cluster size and roughly constant.

The size of the melted regions and their associated colloidal clusters are essentially uncorrelated as can be seen in figure 5.14.

5.5 Discussion

Colloidal particles dispersed in a liquid crystal with a blue phase have been shown to influence the cholesteric to blue phase transition in a limited way and the blue phase to isotropic transition quite significantly. The colloidal particles and their associated defects act as nucleation points for the blue phase. Colloidal particles

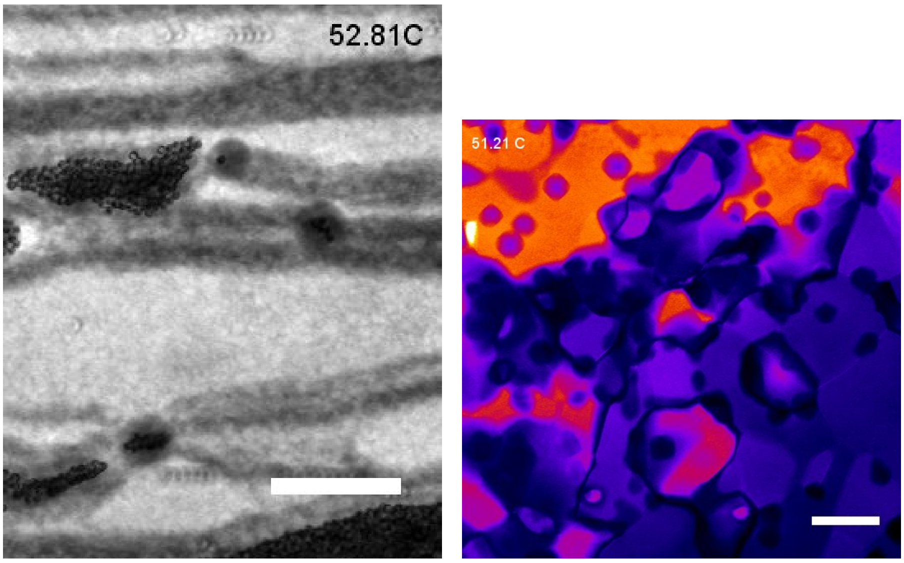

(a) (b)

Figure 5.11 Transmission images taken with a confocal microscope of (a) dark regions around colloidal particles in BPI in a low chirality sample. (b) Dark regions in BPII also form prior to the transition to the isotropic in samples with out colloidal particles This image is false colour to enhance contrast. Scale bars 50 µm

appear to induce localised melting of the BP, at temperatures below the blue phase to isotropic transition. Studying the movement of colloidal particles within these regions suggests that they are composed of the isotropic phase. The excess area of the locally melted regions is essentially constant. These locally melted regions can be faceted. In the following section each of these observations will be discussed in turn.

5.5.1 Nucleation from the Cholesteric

The observation that the blue phase grows preferentially from preexisting defects, either in the form of oily streaks, defects surrounding colloidal particles or defects created using a Cano wedge, is unsurprising. The formation of BPI from a uniformly aligned cholesteric requires the formation of a lattice of defects. As previously discussed (see chapter 2) these defects cost energy. In cases where the cholesteric already possesses defects it is likely that there is a lower cost for defect formation and the blue phase can preferentially grow from the defect regions. The blue phase which grows from these regions exhibits a greater range of colours indicating different alignments of the ordered BPI platelets (grains). This is in contrast to the BPI in regions where the cholesteric had uniform alignment.

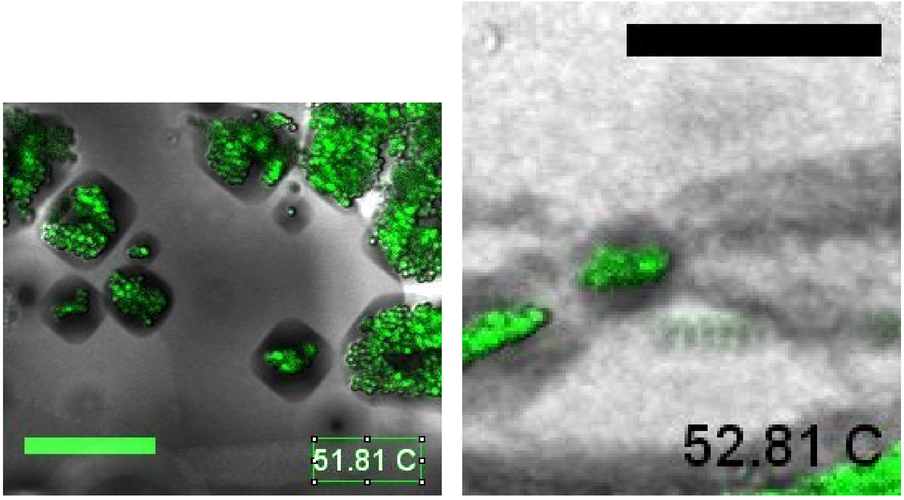

(a) (b)

Figure 5.12 Composite confocal images of colloidal particle (green) surrounded by faceted inclusions in (a) BPII Scale bar $20\,\mu\mathrm{m}$ and (b) BPI. Scale bar $50\,\mu\mathrm{m}$.

In the aligned regions the blue phase has a single colour indicating that the grains have similar alignments.

Simulation studies by Henrich *et al.* [42] show that a blue phase seed allowed to grow in a uniformly aligned cholesteric forms a disordered blue phase lattice similar in nature to BPIII rather than the equilibrium structure of either BPI or BPII. These disordered structures are kinetically stabilised. Such amorphous structures have not been observed in experiments. It is possible that by growing from a defected region of cholesteric these disordered blue phase structures can be avoided as the mesogens have a greater degree of orientational freedom.

The phase transition in a Cano wedge without colloids has previously been a subject of research and essentially we repeat this in order to obtain improved images. Feldman *et al.* [30] report growth from the defects but attribute the behaviour to the phase transition being re-entrant in chiral strain. The chiral strain of the liquid crystal varies across each region of the wedge. We observe qualitatively similar behaviour for our sample (no colloidal particles) in a a Cano wedge.

In the case of flat samples with colloidal particles there is likely to be some variation of chiral strain close to the colloidal particle. However, our observation that the nucleation starts from the centre of the defects and close to the colloidal particle surface suggests that heterogeneous nucleation and growth of the blue

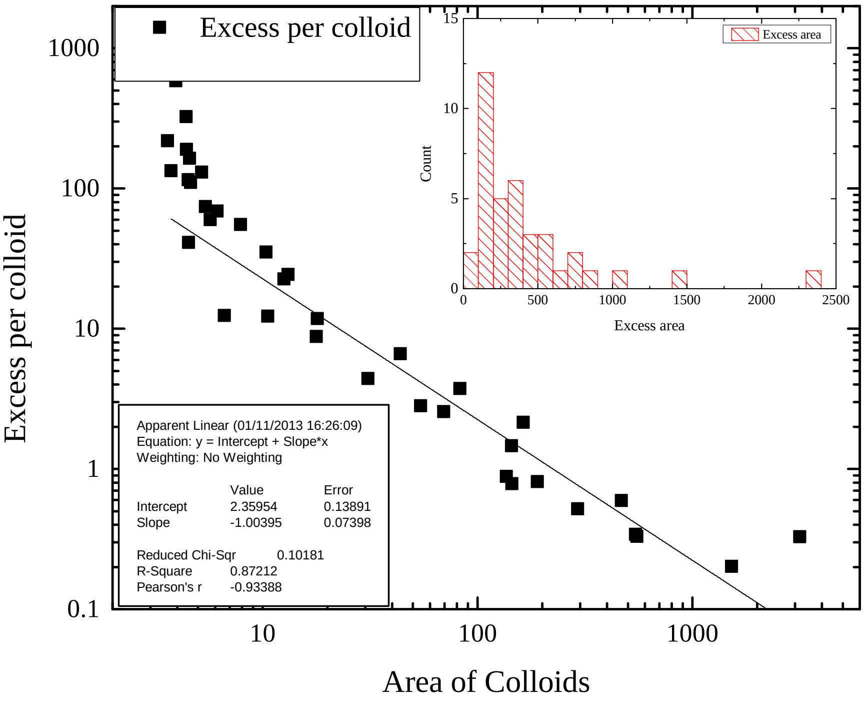

Figure 5.13 The excess area of melted regions per colloidal particle compared to the area of the underlying colloidal particles. The line is a linear fit through the central region. It has a slope of -1. Inset is a histogram of the excess areas.

phase from the isotropic defect core is a more probable mechanism than a re-entrant transition in chiral strain.

5.5.2 Colloidal Particles and Coexistence

Heating the blue phase towards the isotropic results in dark regions forming around the colloidal particles, figure 5.7. The regions are dark due to decreased birefringence. There are two candidate phases which exist at higher temperatures than BPI and BPII which have reduced birefringence. These are BPIII and the isotropic phase.

BPIII is an isotropic disordered lattice of defects [40], is only weakly birefringent and appears as a blue fog in polarising optical images. The materials used in our study do not exhibit BPIII in the absence of colloidal particles. However, given that nanoparticles have been shown to stabilise BPIII [48] and disordered blue

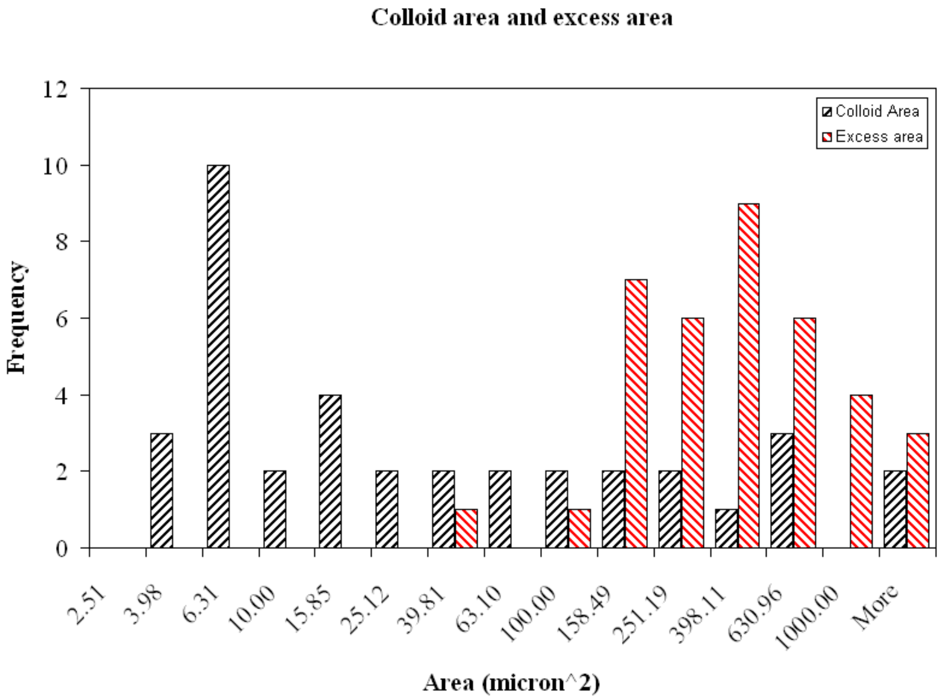

Figure 5.14 Histograms of the excess area of melted regions compared to the area of the underlying colloidal particles. The bins are logarithmic in width

phases have been shown to appear at phase transitions [42] and in the presence of colloidal particles [93], a disordered blue phase cannot immediately be discounted as a candidate for the dark regions.

A more compelling reason to conclude that the dark regions are composed of the isotropic phase is that the colloidal particles move in these regions. BPI and BPII are visco-elastic in character [41, 72]. The cholesteric phase and BPIII are highly viscous and possess a similar viscosity to one another [51]. The isotropic phase is a Newtonian fluid. We measure the diffusion constant of colloidal particles within these dark regions and calculated associated viscosity of the melted regions to be $\eta = 0.005 \pm 0.002$Pa s. This is the same order of magnitude as that of 5CB at the same temperature in the isotropic phase, 0.016 Pa s implying that the dark regions are inclusions of the isotropic phase. The final value for the diffiusion coefficient extracted from the particle tracking results must be used cautiously as the equations used to extract the diffusion coefficient are not applicable in complex fluids. However, the fact that the colloids move at all in these regions and are stationary in both the cholesteric and blue phases is highly suggestive that the region is in the isotropic phase given the difference in viscosity between the LC and isotropic phases.

The presence of the isotropic phase close to the colloidal particles suggests that colloidal particles are acting as nucleation sites for the isotropic phase. There is only limited work on effect of large colloidal particles on an ordered blue phase. Simulations of small colloidal particles with weak or zero surface anchoring dispersed in blue phases find that they are localised at the defect junctions [84] of a cubic blue phase. However, this arrangement is extremely sensitive to the ratio of WR/K. For even moderate values of this ratio the blue phase defect structure becomes disordered [93]. The type of anchoring (planar or homeotropic) also has a profound effect on the colloidal particle positions [38]. Ravnik *et al.* [85] perform simulations on micron size colloidal particles in confinement. They find that for finite anchoring strength at the colloidal particle surface the colloidal particles are surrounded by a cage of defects.

The defects surrounding the colloidal particles are disordered in contrast to those which make up the cubic blue phase lattice. Theories of melting for crystalline solids define melting as the point at which the solid is saturated by glide defects [12]. Surfaces act as nucleation points for those defects [13]. In the blue phase system, is is plausible that the colloidal particles act as nucleation points for the disordered defects required to melt the blue phase.

The colloidal particles create disordered defects which preferentially nucleate the isotropic phase. The flat boundaries of the sample could also act as nucleation points for the isotropic but the blue phase can adapt to the (degenerate planar) boundary conditions imposed by the glass capillary walls without necessarily creating additional defects. There are fewer defects at the surfaces of the sample than at the colloidal particle surface, which further strengthens the case that that the melting is defect mediated.

The fact that colloidal particles only nucleate the isotropic phase and not the higher temperature blue phase (where it is exhibited by the sample) is somewhat puzzling. A tentative explanation is that the region around the colloidal particles will have a higher concentration of defects than the rest of the sample regardless of the nature of blue phase. These defects do not have the structure of either blue phase and so present no advantage for the nucleation of the higher temperature ordered phase.

Studies of disorder in nematic systems have shown that the presence of disorder lowers the nematic - isotropic transition temperature. This appears to be the case here, as the temperature of the cholesteric to blue phase and the blue phase to isotropic transitions are lower close to colloidal particles which act as regions of disorder.

5.5.3 Facets

The faceted nature of the melted regions as shown in figure 5.12 shows that they are constrained by the elastic anisotropy of the embedding blue phase. Faceted regions are larger and more clearly visible in BPII. In BPII the grain size of the blue phase is significantly larger than the faceted regions. Facets within a grain have the same orientation. In BPI the grain size is typically smaller than the melted regions, facets are more irregular and do not have an obvious orientation. There are also more preferential directions for faceting due to the bcc symmetry of BPI.

The interfacial tension between the blue phase and the isotropic phase is anisotropic. This is demonstrated most clearly by the fact that mono-crystals of blue phase grown by slowly cooling from the isotropic phase exhibit clear facets which reflect the underlying symmetry of the blue phase [78]. Careful study of the nature of these facets was used to determine the symmetries of the blue phases. [78].

In the case we study, inclusions of isotropic phase are embedded in a polycrystalline blue phase. At equilibrium the inclusions need to minimise their surface energy for a given volume whilst minimising distortions in the surrounding lattice. In an elastically isotropic medium all inclusions will be spherical, minismising the surface area. In an elastically anisotropic medium facets form, these reflect the symmetry of the surrounding medium. As can be seen from the differing facet symmetry in the two blue phases.

Other systems, principally metal alloys exhibit faceted inclusions embedded in polycrystalline bulk material. Studies of liquid lead inclusions in an aluminium matrix have shown that above a certain inclusion size facets are observed [33]. There is an energy cost associated with deforming the flat facet into a curved interface. This cost is associate with the nucleation of steps on the flat interface and it scales with inclusion radius. The faceted form of the inclusion is shown to be metastable. On heating, facets round off but reform on cooling although with a much more rounded form. The authors suggest that the spherical shape is in fact the equilibrium shape and that faceted inclusions are kinetically arrested. Heating increases atomic mobility and allows the facets to round off.

The faceted inclusions of the isotropic phase in our sample are observed to round on heating. Given the soft nature of the system the degree of heating required to round off a facet is very small, less than the temperature stability of our temperature stage. Faceted regions fluctuate in size and facets appear and disappear in response to very small temperature changes. The fluctuations indicate that the activation energy to create steps in a blue phase interface is very small. This is agreement with the observation that faceted mono-crystals of blue phase can only be grown at very slow cooling rates ($\sim 0.01\,^{\circ}\mathrm{C\,min}^{-1}$).

The effect of inclusion size on facet stability is difficult to measure. Unlike the lead in aluminium experiments the volume of the melted regions is also a function of temperature. Melted regions expand as the sample is heated.

5.5.4 Melted Regions and Associated Colloidal Particles

The presence of the colloidal particles lowers the local transition temperature of the BP - isotropic transition. Regions of isotropic phase can be seen surrounding the colloidal particles. As discussed above it is likely that they are nucleated by the defects associated with the colloidal particles. This is an example of heterogeneous nucleation.

The extent of these melted regions beyond their associated colloidal particles is independent of the number of colloidal particles in the associated aggregate. This observation would seem to contradict the heterogeneous nucleation mechanism. In heterogeneous nucleation the energy balance is between the energy saving of having a volume of lower energy phase balanced by the cost of the surface between the two phases. The presence of an impurity can reduce the second cost by removing a portion of the interface thus reducing the energy barrier to nucleation. If we apply this logic to our system then the larger aggregates with a larger surface area would therefore preferentially nucleate a larger volume of isotropic phase than small aggregates. This, as shown in figure 5.13, is not the case.

A tentative explanation is as follows; the surface tension of the BP - isotropic interface is manifestly anisotropic, as shown by the faceted inclusions discussed in section 5.5.3 and the faceted nature of blue phase crystals grown by cooling from the isotropic. There are different energy costs associated with each of the "crystal" orientations. At the size of melted regions that we can observe this additional anisotropic term appears to dominate over any effects mediated by the colloidal particle surfaces. The elasticity of the surrounding medium is more significant at this length scale than the effects due to the surface area of the inclusions. The elastic anisotropy of the blue phase may influence the extent that a melted region can grow into an ordered blue phase if it is not in a favourable orientation.

5.6 Conclusions

Large colloidal particles dispersed in a BP do not have any appreciable stabilising effect. The behaviour of the colloidal particles in the cholesteric and BPI is not quantitatively different. The colloidal particles do have a profound effect on how the phase transitions between cholesteric, BPs I and II and the isotropic proceed. Colloidal particles added to a blue phase exhibiting liquid crystal perturb the phase transition from the cholesteric to the blue phase and from the blue phases to the isotropic. Colloidal particles and their associated defects act as nucleation sites for the high temperature phase. Colloidal particles do not have an observable influence on the BPI to BPII transition. The symmetry of the defects around the colloidal particles does not reflect the symmetry of either phase and therefore do not present a preferred region of the transition.

Colloidal particles are able to move within locally melted regions of the blue phase. Particle tracking indicates that the viscosity of these regions is similar to that of isotropic 5CB implying that they are composed of the isotropic phase rather than a disordered blue phase. The area of such melted regions surrounding colloidal particles is independent of the number of colloidal particles in a nucleating cluster.

Inclusions of isotropic liquid within the blue phase exhibit facets due to the anisotropy of the BP surface tension. These facets are extremely sensitive to temperature indicating that the energy require to deform these interfaces is low.

5.7 Future Work

The most obvious extension of this work would be to use calorimetry to determine the effect of the colloidal particles on the phase transitions. This would clarify the effect of the colloidal particles and their role in promoting coexistence.

A second avenue would be to vary the ratio WR/K (see chapter 2) by altering the type and size of the particles used. Recent simulations [93] suggest that this ratio has a profound effect on the structures created and whether colloidal particles stabilise or destabilise the uniform cubic blue phase. A limitation of the workpresented was the choice of a particle with what can be assumed to be “strong” anchoring given its role in disupting the BP. A particle with weak planar anchoring which is large enough to be resolved using microscopy techniques should allow the temperature range of the blue phase to be increased and allow particles to be imaged in-situ.

Finally, it would be interesting to study the faceted inclusions in a more systematic manner in order to make explicit the link to melting in metallic alloys.

Chapter 6

Nematic Emulsions With Interfacial Colloidal Particles

6.1 Introduction

In this chapter the effect of colloidal particles on the switching dynamics of liquid crystal emulsion droplets are explored. Droplets of a nematic liquid crystal are dispersed in water, forming an nematic emulsion. These emulsions are extremely sensitive to external stimuli, especially the presence of surface active substances e.g. surfactants or proteins in the continuous phase. Such molecules can alter the alignment at the LC - water interface as discussed in section 2.3.4. The resultant change in the droplet boundary conditions forces a change in defect structure, from two boojums at the poles seen in pure water systems to a hedgehog defect in the droplet centre in systems with surfactant molecules. The presence of colloidal particles perturbs the switching dynamics between the two states. The final state depends on the number and size of colloidal particles present in the liquid crystal.

Dispersions of liquid crystals have a wide range of potential applications from biosensors to micro-lasers [5, 45, 55]. Such dispersions are extremely sensitive to external stimuli. Stimuli include electric fields [29], temperature [54] and impurities added to the continuous phase [7]. The response is a change in defect structure which is easily visible using a polarising optical microscope. The behaviour of simple liquid crystal emulsions is relatively well understood as they have been used as a system to study topological defects for over 40 years [29]. In this chapter the addition of colloidal particles to the dispersed nematic liquid crystal is explored. The particles interact with the defects already present due to the topology of the droplets. Altering the alignment of the liquid crystal at the fluid-fluid interface changes the nature of these defects and hence the interactions between the colloidal particles.

6.2 Background

6.2.1 Previous Studies

Dispersions of LCs in an isotropic matrix have been studied since the early 1970s [29]. Early work in emulsion systems focused on the topological defects present in the droplets [29]. The symmetry of the system and the simple boundary conditions allowed the director field within the droplets to be determined analytically. The process of switching between the two states (planar and homeotropic alignment) was studied by Volovik *et al.* [101].

A practical application of dispersed liquid crystals is Polymer Dispersed Liquid Crystals (PDLC) which were developed in the early 1980s. In these systems droplets of LC are confined in a polymer matrix. The transparency of the polymer film can be controlled by altering the liquid crystal alignment using an electric field. Given that this system had practical applications a greater emphasis was placed on the behaviour of LCs in confined geometries [28].

More recently liquid crystal emulsions have been developed as sensors for certain types of molecules present in the continuous phase. A large number of different substances have been shown to alter the mesogen alignment at the interface. These include surfactants, lipids and proteins [7]. One notable application is a sensor for bacterial endo-toxin developed by Lin *et al.* [55]. The utility as a sensor derives from the easily observed change in defect configuration in response to the target substance. A system which allows a reversible change in alignment controlled via temperature has also been developed [54, 101]. The combination of nanoparticles and surfactants at the interface of a nanodroplet has been shown to exhibit a rich phase behaviour in simulation studies [70]. However, systems of LC emulsions with colloidal particles are only just starting to be explored; a recent work has shown that micron-sized colloidal particles are localised at the boojums of a planar aligned nematic droplet [69].

6.2.2 Theoretical Background

Bare droplets

There is competition between defect formation and surface anchoring at the droplet surface. This leads to a size dependent defect structure.

With pure water, the alignment at the LC water interface is planar. These droplets have two "boojum" defects one at each pole. See figure 6.1(a). Once a surfactant is added the alignment at the interface changes to radial (homeotropic). The change in alignment can be concentration dependent [67, 101]. In the systems discussed in this chapter the concentration is sufficient such that all droplets of all sizes are aligned radially after the addition of surfactant. The lowest-energy defect structure for a radially aligned droplet is a central +1 hedgehog defect.

The presence of defects can be explained by an argument similar in form to that presented for colloidal inclusions within nematics, as discussed in section 2.3 The free energy of a nematic droplet is the sum of bulk and surface terms

$$F = F_V + F_S = \int_V f dV + \int_S \sigma dS, \tag{6.1}$$

The surface term has contributions from the bulk surface tension σ_0 and the anchoring at the interface W_a. The bulk surface tension is typically several orders of magnitude larger than the surface anchoring in thermotropic systems and so droplets are spherical. Typical values for 5CB (no surfactant) $\sigma_0 \approx 30 \times 10^{-3}\,\mathrm{J\,m^{-2}}$ and $W_a \approx 10^{-7}\,\mathrm{J\,m^{-2}}$ (Taken from [54]).

A simple scaling argument predicts a transition between a defect free and a droplet which possesses a defect. Using a single constant approximation the bulk elastic energy scales as KR where K is the elastic constant of the LC i.e. the bulk energy scales linearly with size. The full free energy can be expressed as

$$F = KR + \sigma_0 R^2 + W_a R^2 \tag{6.2}$$

For large R surface energy outweighs the bulk elastic energy. Here, the isotropic part of the surface tension is neglected as it is constant for both alignments.

There is a radius $R \ll K/W_a$ where the LC maintains a uniform alignment at the expense of violating the surface boundary conditions. For larger droplets the surface anchoring conditions are satisfied at the expense of creating defects within the droplet. For typical values of surface anchoring and elastic constants (see above) the characteristic radius at which this should occur is $R \sim 1\,\mu\text{m}$. In reality the situation is more complex and small droplets $R \sim 700\,\text{nm}$ exhibit a radial structure [37]. The precise explanation is unclear but the authors propose that the relative magnitude of the different elastic constants needs to be considered in order to find the correct scaling. In our systems all droplets possess 2 boojums when in pure water (planar aligned) and are therefore larger than this critical size.

The presence of defects is responsible for a stabilisation mechanism unique to LC emulsions. If two droplets each with a central defect attempt to coalesce then in order to conserve topological charge a (-1) defect must nucleate around the neck between the two droplets. This is energetically expensive, there is no net energy saving because the surface area is not significantly reduced at the point when the droplets first come into contact. This leads to the observation in scattering studies that there is a minimum stable droplet size in nematic emulsions equivalent to the critical radius where topological defects are predicted to appear [98].

The use of these systems as sensor depends on the switching behaviour of droplets in response to surfactant molecules. After the addition of a surfactant the interfacial alignment of the droplets changes to homeotropic. However, the droplet cannot switch instantaneously to the hedgehog configuration. Instead switching occurs via intermediate states in the following manner:

1. The surfactant causes the interfacial mesogens to change alignment towards radial. (This is dependent on the concentration of surfactant molecules at the interface).
2. A Saturn ring forms around the centre of the droplet. Figure 6.1(b).
3. Once the alignment is fully radial the Saturn ring shrinks and moves towards one of the poles of the droplet. Figure 6.1(c).
4. The ring becomes a point-like defect at the surface of the droplet. Figure 6.1(d).
5. The defect detaches from the surface and moves into the centre of the droplet. Figure 6.1(e).

6. The hedgehog defect stays in the droplet centre. Figure 6.1(f).

Throughout this process the topological charge of the system is conserved [54, 101].

The realignment of the liquid crystal at the interface is dependent on the surfactant concentration at the droplet interface [60]. If insufficient surfactant is available the system can be arrested in the Saturn ring configuration [101]. In the experiments which follow a concentration of surfactant exceeding that required to realign all the mesogens is used. Miller *et al.* [67] find a size effect for the switching of droplets in response to bacterial endo-toxin. The bipolar configuration is more stable for larger droplets. In contrast to the system discussed in this thesis the switching mechanism of Miller *et al.* does not rely on the complete coverage of the droplet by surfactant.

Droplets with interfacial colloidal particles

The physics of the colloidal particles in the droplets is dominated by interfacial effects. colloidal particles are found at the droplet interface. They are trapped there as they reduce the shared area between the two liquids as discussed in chapter 2. The trapping energy can be approximated using Young's equation:

$$\Delta G = -\pi r^2 \gamma (1 \pm \mid \cos\theta \mid)^2 \tag{6.3}$$

where γ is the interfacial tension, θ is the contact angle of the colloidal particle with the interface and r is the particle radius. This is between 8×10^6 k_BT ($r = 561\,\mathrm{nm}$) and 5×10^4 k_BT ($r = 561\,\mathrm{nm}$) without CTAB and 1×10^6 k_BT ($r = 561\,\mathrm{nm}$) and 9×10^3 k_BT ($r = 561\,\mathrm{nm}$) with CTAB using values for the interfacial tension of 5CB and water with and without CTAB taken from [50] and [34]. colloidal particles are therefore trapped at the liquid crystal water interface and it is practically impossible that they will be removed via thermal effects.

In reality, the surface tension of the liquid crystal has anisotropic components as discussed in chapter 2. They are small compared to the isotropic surface tension and therefore do not significantly alter the strength of the trapping at the interface. However, the anisotropic nature of the liquid crystal can influence the position of the colloidal particle once on the interface. colloidal particles

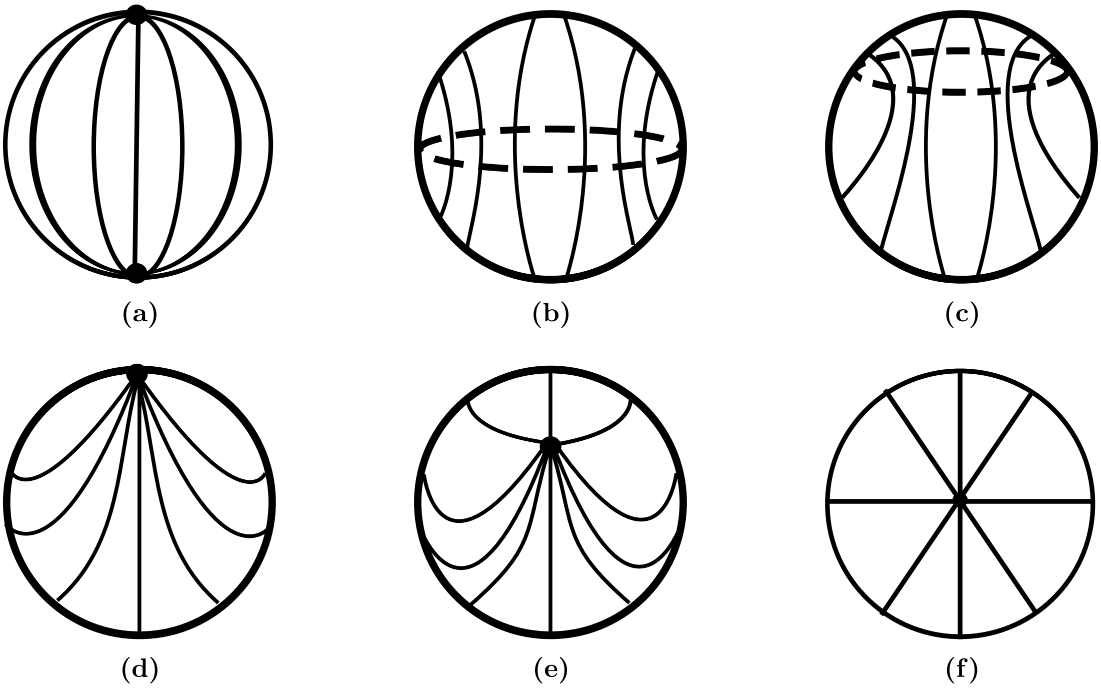

Figure 6.1 Schematic of Switching from Planar to Homeotropic Alignment. (a) Planar alignment, 2 boojums at the poles. (b) A Saturn ring forms at the equator. (c) The ring shrinks towards one of the poles. (d). The ring defect shrinks to a point, an escaped radial configuration. (e) The point defect moves to the droplet centre. (f) The final radial state

interact with interfacial defects in a manner similar to that discussed in chapter 4

Gravity does not play a role in the interfacial effects. As discussed in chapter 2 one can use the Bond number to calculate the relative importance of gravity. For the relevant material parameters taken from [50] the Bond number is $\sim 10^{-11}$ without CTAB and $\sim 10^{-10}$ with CTAB. We can therefore exclude gravitational effects from the interfacial physics. Gravity is responsible for causing the sedimentation of the emulsion droplets over time.

Once trapped on the interface, for planar alignment colloidal particles are localised in the boojums [69].

6.3 Materials and Methods

Preparation of liquid crystal emulsions is fairly straight-forward: droplets are dispersed via mechanical agitation, using a rotor stator, whirly-mixing and/or ultra sound. Droplets are stabilised in the absence of surfactant and/or colloidal particles via elastic effects related to the cost of nucleating new defects as discussed above.

The colloidal particles are poly(methyl methacrylate) (PMMA) with poly(12-hydroxystearic acid)(PHSA) stabiliser. The particles have an average hydrodynamic radius as measured by dynamic light scattering of r =48 nm, 156 nm, 561 nm. The polydispersity of these particles is not available. They do not crystallise so the degree of polydispersity is $> 5\%$.

The particles were dispersed in Nile Red doped 5CB using a combination of ultra sound and whirly mixing as described in chapter 3. The volume fractions used were $\varphi_{PMMA} = 0.25\%$, $\varphi_{PMMA} = 2\%$ for all particle sizes. The dispersion was used once it was uniform. The resultant mixture was dispersed in Millipore H_2O resistivity 18.2 MΩ. The mixture was homogenised using a IKA T-10 Homogenisor fitted with a Tcol S10 N5G head at speed 6 ($\sim$ 30,000 RPM) for 30 seconds followed by whirly mixing for 30 seconds. This was repeated 4 times until a turbid emulsion was created. Early samples were created at $\varphi_{5CB} = 10\%$ these were too turbid to image and so were diluted to $\varphi_{5CB} = 1\%$. Subsequent sample were prepared at $\varphi_{5CB} = 1\%$. No difference in behaviour was observed between the two preparation methods.

At volume fractions of $\geq 5\%$ PMMA colloidal particles in 5CB form a defect mediated gel phase in the bulk [102]. To avoid this behaviour all volume fractions used were ≤ 2 %. This placed a constraint on the number of particles of a fixed radius which could be dispersed in the LC. To increase the number of dispersed particles the size of the colloidal particles was reduced whilst keeping the volume fraction constant. In the bulk the colloidal particles have homeotropic surface anchoring and quadropolar interactions. They are hypothesised to possess a surface ring disclination indicating relatively weak surface anchoring (small W_a) [102].

Solutions of 4 mM hexadecyl-trimethyl-ammonium bromide CTAB and 32 mM Sodium dodecyl sulfate (SDS) were made up using Millipore water. Both these concentrations are equivalent to 4 times the critical micelle concentration (CMC) of the surfactant.

100 µl of the emulsion was deposited on clean cover slips and imaged immediately; alternatively a sample holder consisting of a small vial glued onto a clean cover slip was used. Samples were imaged using a confocal microscope (Zeiss Observer.Z1 inverted microscope in conjunction with a Zeiss LSM 700 scanning system) in

fluorescence confocal and transmission modes. Sequences of the switching process were recorded with a fast camera (Mikrotron MCI362 with a Frame grabber card Mikrotron Inspecta 5) mounted on a Nikon (Ti) inverted microscope with crossed polarisers.

Once the sample was in focus and the planar aligned state had been characterised a known amount of CTAB solution (typically 100 µl)was added using a pipette. The resulting change in orientation was imaged where possible along with the final end point of the system. The emulsion are stable for at least two hours and in bulk for a number of days although they do tend to sediment. On addition of CTAB the emulsions tend to wet the glass slide or the vial walls. Increasing the hydrophilicity of the glass helped to prevent this. To avoid this complication droplets further from the glass slide were imaged as the whole of the glass surface was not affected.

6.4 Results

6.4.1 Switching without Colloidal Particles

Without colloidal particles the nematic droplets have clearly visible boojums figure 6.2(a). On the addition of surfactant they switch to the hedgehog state figure 6.2(b) within 6 seconds. All droplets of all sizes switch to a fully radial configuration confirming that sufficient surfactant has been used to completely realign the surface mesogens. The dynamics of the switching process were observed using a fast camera, figure 6.2(c). The switching followed the sequence of states shown in figure 6.1. The boojums transform into a Saturn ring which shrinks to a point on the droplet surface before moving into the centre of the droplet.

6.4.2 Switching with Colloidal Particles

Adding colloidal particles to the nematic phase perturbs the switching process. Prior to the addition of surfactant the droplets are found in the boojum configuration indicating that the colloidal particles do not significantly affect the anchoring at the droplet surface. After a surfactant is added the colloidal particles

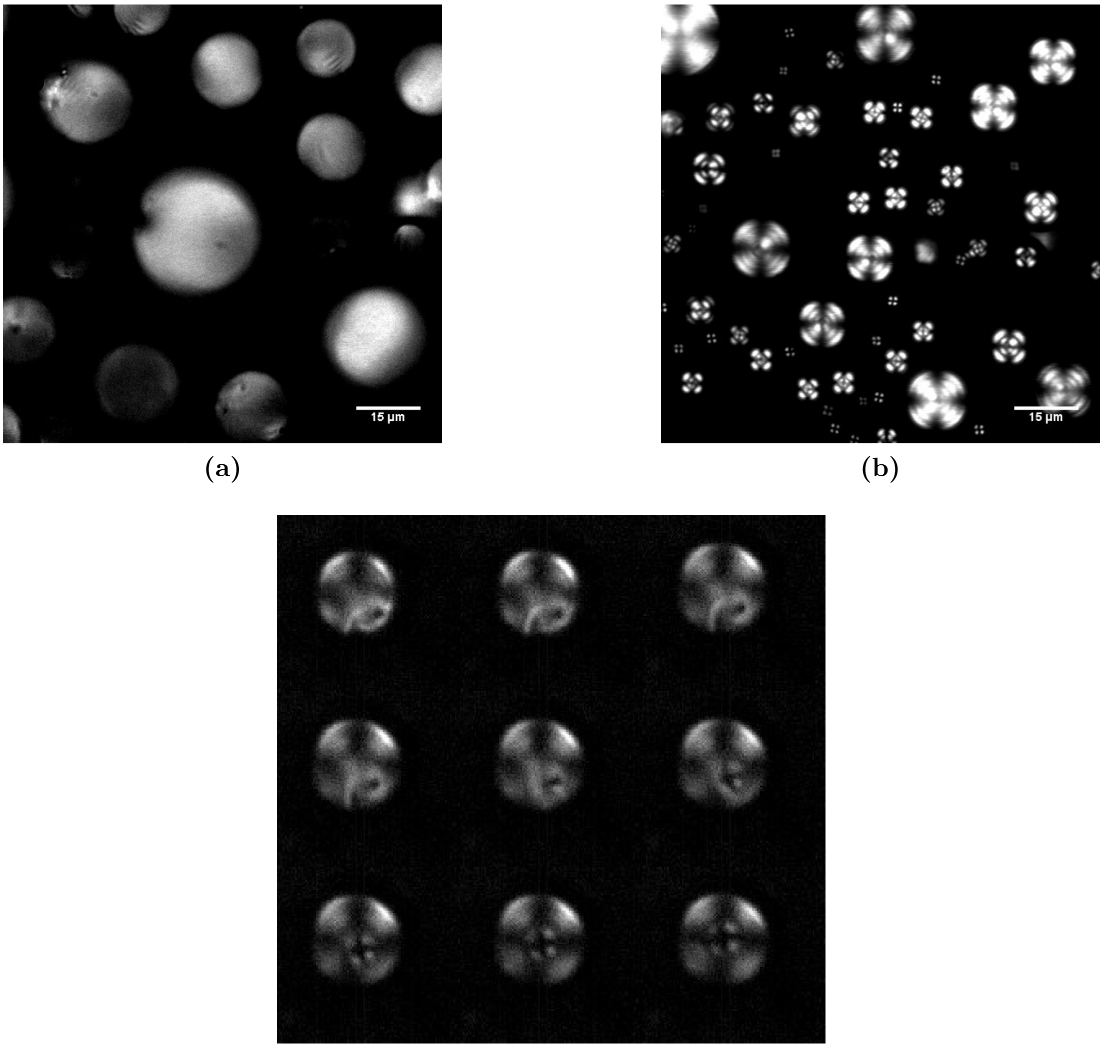

(a) (b)

(c)

Figure 6.2 Nematic droplets without colloidal particles (a) Nematic droplet without colloidal particles prior to the addition of the surfactant. The droplets have planar alignment with boojum defects at the poles. (b) Nematic droplet without colloidal particles after the addition of a surfactant. The droplets have homeotropic alignment and clear central defects. (c) A time series (top left to bottom right) of a droplet switching from planar to homeotropic alignment after a surfactant is added observed via a fast camera between crossed polarisers. The Saturn ring shrinks to a point defect which then moves to the droplet's centre.

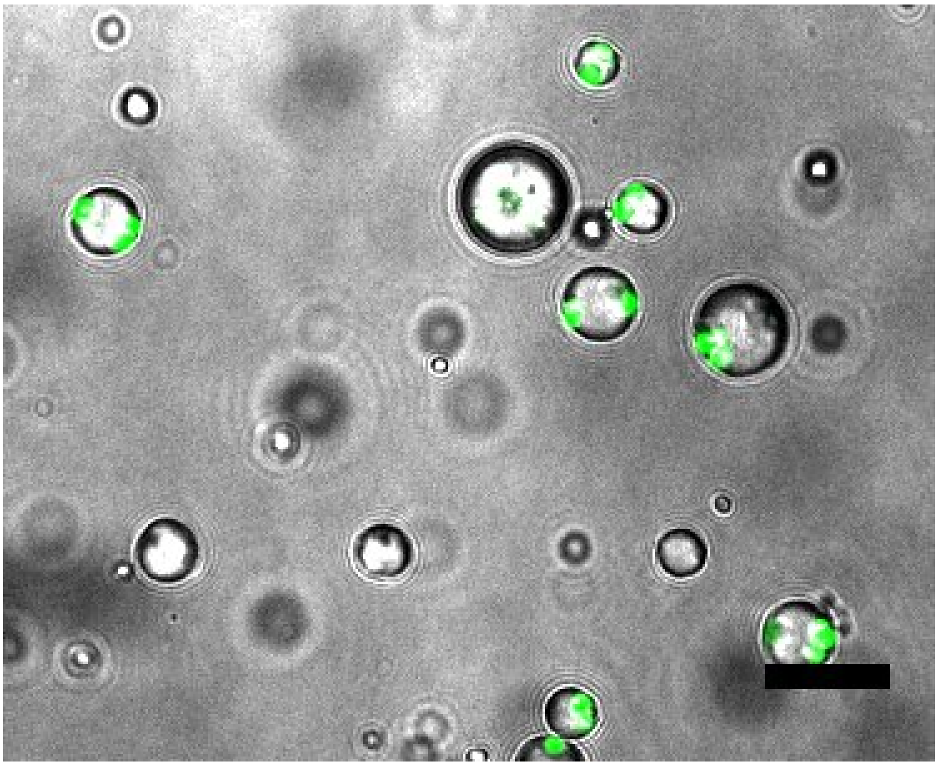

Figure 6.3 Planar aligned droplets imaged in transmission without polarisers. The fluorescence signal from the $561\,\mathrm{nm}$ colloidal particles (green) show they are found at the poles . Scale bar $10\,\mu\mathrm{m}$

cause the switching to be arrested in one of the intermediate defect states and the droplet never achieves the final central hedgehog configuration. The defect structure that is achieved depends on the number of colloidal particles dispersed in the liquid crystal. The behaviour of each of the different colloidal particle sizes and concentrations will be discussed below.

$561\,\mathrm{nm}$ Colloidal Particles

With this size of colloidal particle there are between 1 and ~ 10 colloidal particles per droplet. In pure H_2O the alignment at the interface is planar and colloidal particles are found at the poles of the droplet, associated with the boojum defects as seen in figure 6.3. The presence of the colloidal particles does not have an observable effect on the stability of the emulsions which are stable for the lifetime of the experiment. No coalescence events were observed. The droplets are not fully covered in particles as they are concentrated at the poles. The equator of the droplets is bare liquid crystal. After adding surfactant the alignment at the interface becomes homeotropic. A Saturn ring forms at the equator as for the bare droplets. This shrinks towards one of the poles. Once at the pole it is prevented from moving into the centre of the droplet and the switching is arrested. The final state is shown in figure 6.4(i) Small droplets have a point defect very close to the colloidal particle. For slightly larger drops a clear point defect is observed inside the droplet but off centre (figure 6.5(b)). This defect arrangement is reminiscent of that proposed in [52] for colloidal particles with homeotropic anchoring at flat interfaces with homeotropic alignment.

For droplets with more than one colloidal particle, colloidal particles which are found at both poles when the droplets are in the planar state, will tend to aggregate at one pole. The defect structure is difficult to determine as the colloidal particles interfere with the imaging but is reminiscent of a shrunken Saturn ring, figure 6.5(a). Small droplets seen in figure 6.5(a) are radially aligned but do not have colloidal particles.

156 nm **Colloidal Particles**

Using 156 nm colloidal particles increases the number of colloidal particles per emulsion droplet to $\sim$ 50. With planar alignment at the interface colloidal particles are still concentrated at the poles figure 6.6(b). However, once the boojums are occupied colloidal particles are found distributed around the rest of the surface of the droplet figure 6.6(a).

On switching the colloidal particles become concentrated in a cap at one of the poles. The associated defect structure is reminiscent of the shrunken Saturn ring seen for larger colloidal particles. For emulsion droplets with very few colloidal particles the escaped radial configuration is recovered figure 6.7.

48 nm **Colloidal Particles**

With 48 nm colloidal particles at $\varphi = 2\%$ there are $\sim$ 3000 colloidal particles per droplet (which would cover $\sim$ 30% of the droplet surface). The colloidal particles are also too small to be resolved individually but a diffuse fluorescence throughout the droplet can be observed. Extrapolating from the behaviour of the 156 nm colloidal particles shown in figure 6.6(a) would suggest they are dispersed across the surface of the droplet. Aggregates of particles are very occasionally observed in the boojums of planar aligned droplets. The fact that the droplets

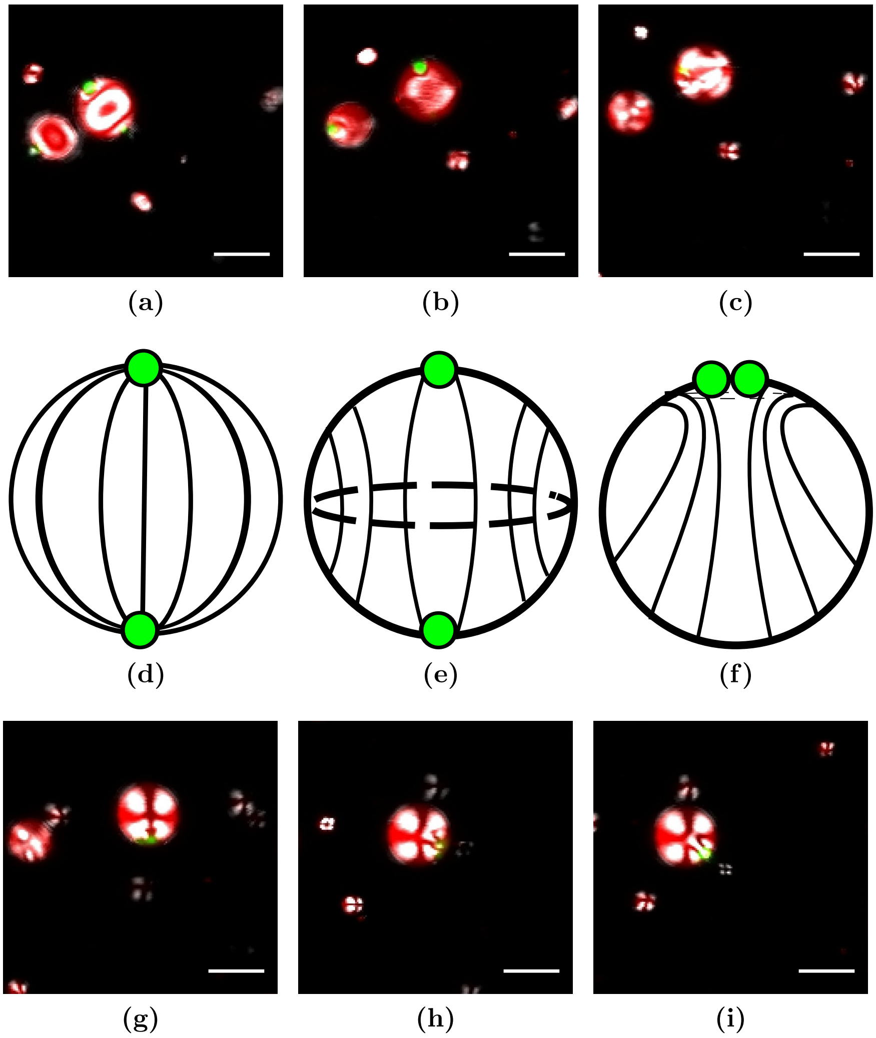

Figure 6.4 A time sequence of switching from planar to homeotropic alignment observed via confocal colloidal particles green, LC red, birefringence grey scale. (a) Prior to switching colloidal particles are found in the boojums. (d) shows a schematic of the director field and colloidal particles in (a). (b) (c) A Saturn ring forms at the droplet equator, spatially separate from the colloidal particles. (e) and (g) to (i) The Saturn ring shrinks to a point which is trapped off centre by the colloidal particle. This final state is shown schematically in (f) Scale bar $5\,\mu\mathrm{m}$

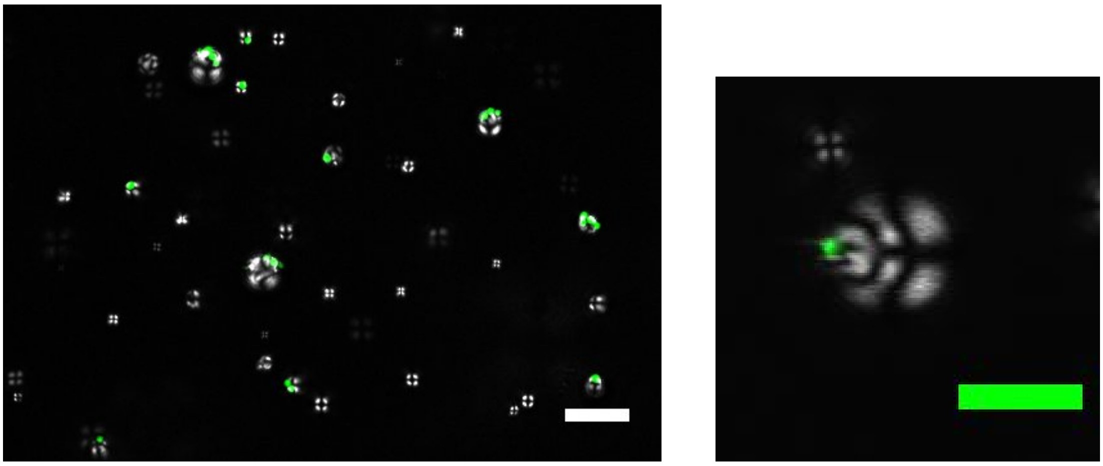

(a) (b)

Figure 6.5 Images of homeotropic aligned droplets with $561\,\mathrm{nm}$ colloidal particles after the addition of surfactant. (a) colloidal particles found aggregated at a single pole. Scale bar $10\,\mathrm{\mu m}$ (b) Homeotropic aligned droplet with clear point defect. Scale bar $5\,\mathrm{\mu m}$

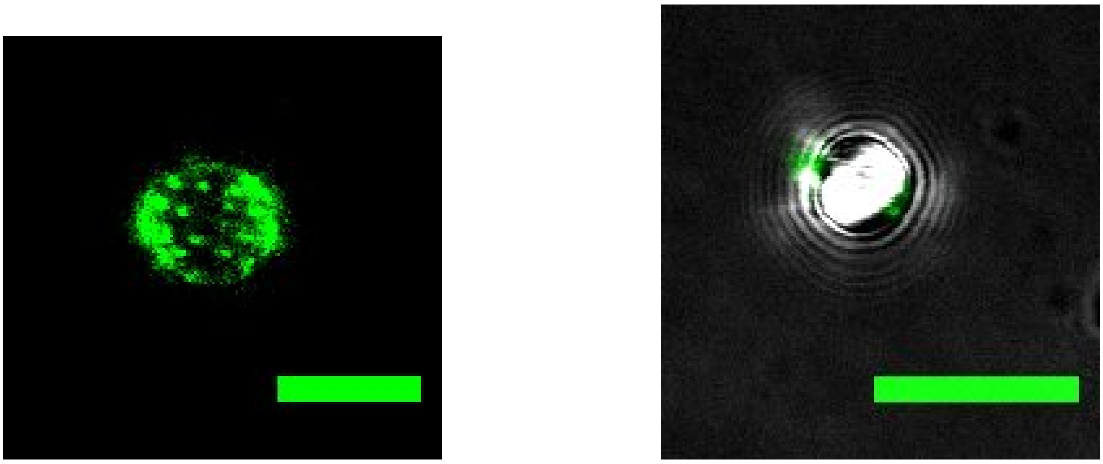

(a) Fluorescent signal from colloidal particles only

(b) Fluorescent and birefringence signal with sparse colloidal particles concentrated in the boojums

Figure 6.6 Confocal images of $156\,\mathrm{nm}$ colloidal particles (fluorescent signal green) on droplets with planar alignment. colloidal particles are concentrated at the poles but can spread out to cover the whole surface. Scale bars $5\,\mathrm{\mu m}$

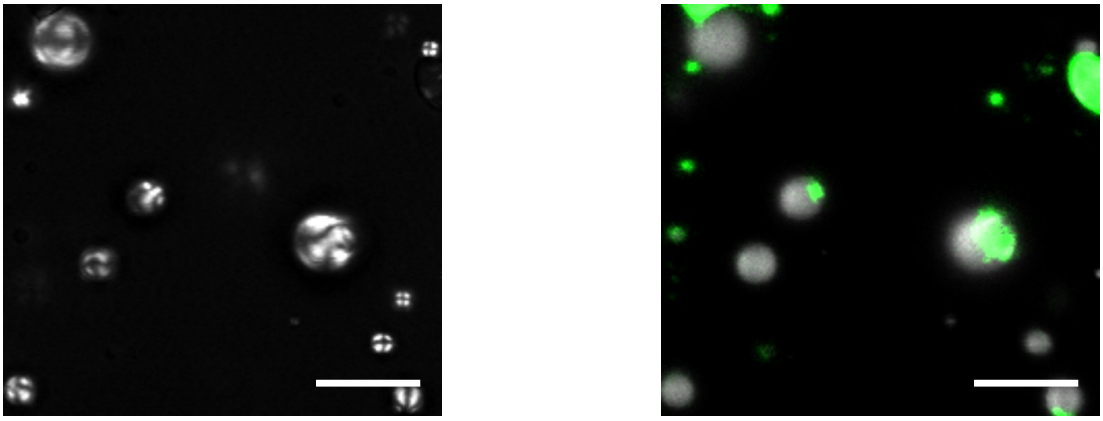

(a) (b)

Figure 6.7 $156\,\mathrm{nm}$ colloidal particles on droplets with homeotropic alignment. (a) Birefringence(transmission) image of a final state droplet. (b) Fluorescent signal from LC (grey) and colloidal particles (green) of the same droplet. Scale bars $10\,\mu\mathrm{m}$

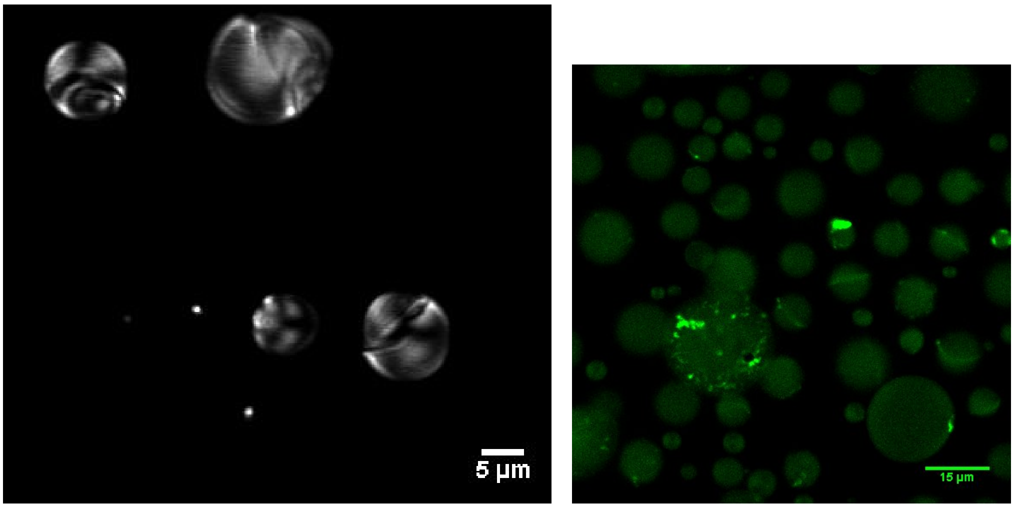

(a) Birefringence of arrested Saturn rings (b) Fluorescence of arrested Saturn rings

Figure 6.8 Arrested Saturn Ring following the addition of surfactant to $\varphi = 2\%$ $48\,\mathrm{nm}$ colloidal particles have boojums prior to the addition of surfactant shows that the nanoparticles do not significantly affect the alignment of the liquid crystal at the interface.

Once a surfactant is added, the droplets begin to switch but a majority become arrested in the Saturn ring configuration. Observations of the nano particle fluorescence shows an increase in brightness within the ring. This indicates an increase in nano particle density. No large aggregates of colloidal particles are observed other than this increased fluorescence in the ring.

The Saturn ring configuration is stable over the lifetime of the emulsion and is present in bulk samples after several days.

Reducing the volume fraction of colloidal particles in the sample from 2% to 0.25% (3% area fraction) or 0.5% (6% area fraction) lead to the majority of the droplets eventually reaching an escaped radial type configuration figures 6.9(c) and 6.9(d)

6.5 Discussion

In the previous section, the behavior of colloidal particles at the interface of nematic droplets dispersed in water has been presented. On droplets with planar anchoring (prior to the addition of surfactant) colloidal particles are associated with the boojum defect. After adding a surfactant, the final configuration of the nematic director in the droplet is dependent on the number of colloidal particles.

The location of the colloidal particles (of all sizes) on droplets with planar anchoring is due to a combination of defect and interfacial effects. With a low density of colloidal particles per droplet the particles are associated with the boojum defects at the pole. Occupying the pre-existing defect removes the isotropic defect core, resulting in an energy saving. In addition occupying the boojum does not lead to further elastic distortions of the LC. Once both boojums are occupied the particles begin to cover the interface.

On the addition of surfactant the alignment of the LC at the droplet interface becomes homeotropic. The lowest energy configuration in the absence of particles is a central hedgehog point defect. A simple scaling argument is sufficient to show why this configuration is not achieved in the presence of even a single colloidal particle. The energy saving produced when a particle occupies the

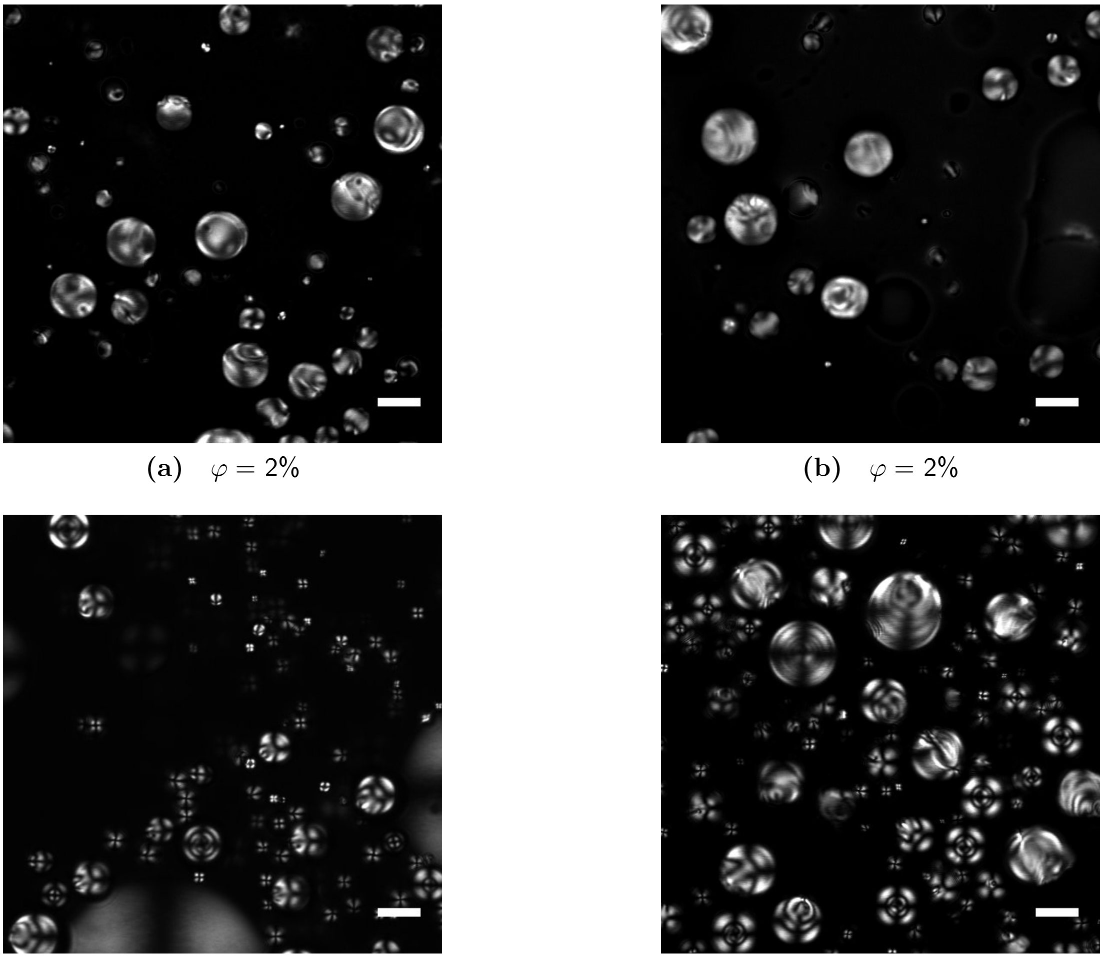

(a) $\varphi = 2\%$ **(b)** $\varphi = 2\%$

(c) $\varphi = 0.25\%$ **(d)** $\varphi = 0.5\%$

Figure 6.9 Final state of $48\,\mathrm{nm}$ colloidal particles with varying volume fractions. Droplets which appear radial are in fact escaped radial this can be verified by their time evolution. Birefringence images, scale bar $10\,\mathrm{\mu m}$

central hedgehog defect is that of removing the isotropic core of the defect. As discussed in section 2.2.6 (in the context of blue phases). Here the energy of the core can be expressed as:

$$E_{core} \sim \frac{4\pi}{3} r_c^3 \varepsilon_c, \tag{6.4}$$

where r_c is the core radius and ε_c is the free energy (per unit volume) associated with melting the nematic to the isotropic phase. r_c in the one constant approximation as previously discussed is $r_c \sim (K/\varepsilon_c)^{0.5}$ Using the appropriate material constants $K \sim 10^{-11}$ N, $\varepsilon_c \sim 10^6$ J m^{-3} [67], $E_{core} \sim 10^{-19}$ J $\sim 3kT$. In contrast the energy saving of having the colloidal particle on the interface is $\sim 10^6$ kT for 561 nm colloidal particles and even for the smallest 48 nm colloidal particles it is $\sim 10^4 kT$. This is four orders of magnitude larger than energy saving from the elastic effects so it is extremely unlikely that the colloidal particle will be removed from the interface. The equilibrium position will therefore have the colloidal particle on the interface and an associated defect in the droplet in order to satisfy the boundary conditions.

When there is more than a single colloidal particle per droplet the situation is more complicated. 561 nm and 156 nm colloidal particles aggregate at one of the poles of the droplet as seen in figures 6.5 and 6.7. The resultant defect is difficult to determine but resembles a shrunken Saturn ring (figure 6.7(a). In the limit of few particles the escaped radial configuration is recovered, figure 6.5(a) This suggests that the larger number of colloidal particles prevents the Saturn ring from shrinking to this state.

The mechanism behind the colloid aggregation is not entirely clear. It is unlikely to be related to additional capillary interactions as even with the change in interfacial tension the Bond number (which relates the interfacial trapping to the force due to gravity) is still $\ll 1$ indication that gravity is unlikely to remove particles from the interface or even deform it. The behaviour is identical for both cationic (CTAB) and anionic (SDS) surfactants which implies that charge effects due to the surfactant are unlikely. There is also the possibility that roughness at the surface of the particle induces capillary interactions [91]. However, these are likely to be of the same order of magnitude for both liquid crystal alignments.

One explanation is that the change in interfacial alignment changes the defect structure at the colloidal particles and hence their elastic interactions. On a flat interface the change in alignment induces repulsive interactions. The change in geometry might alter the interactions. A full exploration of the topology of the system and/or computational modeling would be helpful to clarify this.

The shrinking Saturn ring could also provide an explanation. The ring tends to shrink to a point. Colloidal particles have been shown to pin defects [104] so the ring cannot easily pass any colloidal particles it encounters. However, it can sweep the colloidal particle along eventually forming a cap of close packed colloidal particles. The resultant cap is frequently surrounded by a ring like structure. If the cap formed first there would be nothing to prevent the ring shrinking to the opposite pole and forming an internal point defect.

The stabilisation of the Saturn ring by the 48 nm colloidal particles can be explained via the core replacement mechanism discussed above and in chapter 2. The small colloidal particles can occupy the core of the Saturn ring disclination lowering its energy and stabilising it. The colloidal particles must be able to diffuse into the ring before it shrinks for this mechanism to be effective. Roughly 160 48 nm colloidal particles would be require to completely fill an equatorial Saturn ring. At $\varphi = 2$ % this is only 5% of the colloidal particles contained in the droplet. Reducing the volume fraction of colloidal particles leads to a recovery of the point defect, as there are insufficient colloidal particles to fill the ring. At $\varphi = 0.25$ % around 60 % of the available colloidal particles would be required and the ring can shrink without encountering sufficient colloidal particles. The ring minimises its energy by shrinking towards a point configuration. If it encounters sufficient colloidal particles it can be stabilised at a reduced radius. If not then it forms a point defect pinned to the interface. The stabilisation of a reduced radius ring can be seen with the 156 nm colloidal particles in the form of particle caps. With the 48 nm colloidal particles no particle aggregates are observed and the fluorescent signal from the rest of the droplet (not the ring) remains uniform.

In all cases the ring is not strictly equatorial. This implies that a mechanism whereby the nanoparticles perturb the absorption of surfactant on the surface and inhibit the realignment of the surface mesogens can be discounted. Insufficient absorption of surfactant at the droplet interface would only stabilise an equatorial ring [101].

6.6 Conclusions

The addition of colloidal particles to a nematic liquid crystal emulsion dramatically affects the final defect state on switching from homeotropic to planar alignment at the droplet interface. Sparse colloidal particles pin a point defect at the interface, preventing relaxation to a radial hedgehog. Dense colloidal particles stabilise an interfacial Saturn ring, by pinning it at the interface if the particles are large or by a core replacement mechanism for small particles. Computer simulations would be useful to understand the complex nature of the interactions in the system.

6.7 Future Work

This system presents several promising avenues for future work. It would be interesting to explore whether the anchoring at the particle interface alters the interaction with the defects. Using particles with planar surface anchoring might lead to more complex defect structures. It would also be interesting to discover the minimum and maximum particle size for which a stabilisation of the ring defect is observed. Exploring synergystic particle-surfactant combinations might allow the development of a system which is selectively sensitive to specific molecules in the dispersed phase. Finally, using a cholesteric liquid crystal would add a greater range of defect structures [87]. It could be interesting to see how the particles were influenced by these defects. It might be possible to such link experiments to the flat interface system in chapter 4.

Chapter 7

Conclusions and Future Work

In this thesis three different LC-colloid systems have been explored. The physics of these systems has been shown to be a delicate balance between competing length and energy scales.

In chapter 4 we show that there is a particle size dependent expulsion of colloidal particles to the interface between a cholesteric liquid crystal and an isotropic liquid. We suggest that this is due to the increased elastic cost of submerging large colloidal particles in a chiral LC. This cost is dependent on the ratio of the the particle size to pitch length R/p and is related to the length of the defect which wraps the colloid particle [46, 57]. The phenomenon of particle size expulsion is not seen at simple fluid–fluid interfaces and has not been reported for nematic–isotropic interfaces. Further work, using a nematic–oil interface would allow all other effects to be excluded.

The arrangement of colloidal particles with respect to intrinsic defects on the interface is also dependent on R/p. However, this templating is also strongly influenced by the anchoring strength of the liquid crystal at the colloidal particle interface in relation to the particle size, characterised by WR/K. The defects created by the interaction between the colloidal particle and the LC can cause the intrinsic defects to "rewire" creating a rugged energy landscape which reduces the templating efficiency. Colloidal particles of all sizes are found in aggregates on the interface. These aggregates are associated with regions of disorder, where the helical axis is disrupted. Colloidal self assembly templated by defects has been seen in nematics [2], cholesterics [43, 99] TGB and blue phases [21]. In all these systems the templating success is dependent on the type and strength of the anchoring at the particle–LC interface as well as the particle size.

The clear fingerprint texture at the interface suggests that future experiments could target the effect on the liquid crystal of dragging a colloidal particle along the interface, through the cholesteric “layers”, as simulation results suggest that the viscosity experienced by the particle will be dependent on the direction of motion with respect to the helical axis [59].

The interaction between colloidal particles and an ordered LC underlies the physics of chapter 5. The first images of colloidal particles dispersed in a BP are presented. The arrangement of colloidal particles within the BP is qualitatively similar to their arrangement in the cholesteric phase. This is in contrast to the quantitatively different behaviour between colloidal particles with planar anchoring dispersed in nematic and cholesteric LCs.

The colloidal particles stabilise the cholesteric oily streak defects as in [43, 104] and these defects are shown to be nucleation points for BPI both with and without particles. The colloidal particles also cause localised melting of the blue phase to the isotropic at temperatures below the bulk BP-isotropic transition temperature. Colloidal particles have previously been shown to create defects in ordered chiral phases [46, 57, 59]. It is possible that these defects act as nucleation sites for the higher temperature phases. This colloidal particle induced localised melting suggests an explanation for the failure of large particles with strong planar surface anchoring to stabilise blue phases [27]. Recent simulation work [93], has shown that the ratio WR/K is a critical control parameter in determining the interaction of colloidal particles with BPs. The larger this ratio the greater the disruptive effect of the colloidal particles. This suggests that future work should focus on particles with weak surface anchoring and preferably a lower density than the melamine colloidal particles used in this thesis.

The shapes of the locally melted regions are anisotropic and their sizes are independent of the underlying colloidal particles. This suggests that the anisotropic nature of the blue phase - isotropic surface tension controls the size and shape of the regions. This system has the potential to be used to study melting of composite systems in analogy with hard condensed matter. Similar phenomena e.g. faceted inclusions are seen in metallic systems. In the metallic case the phenomena are often difficult to observe in real time due to the opaque nature of the material and the high temperatures involved. With an even greater degree of temperature control the blue phase system has the potential to be used to study the evolution of these features via optical microscopy at an easily accessible temperature.

Finally, in chapter 6 the response of nematic droplets to the addition of a surfactant was shown to be dependent on the number colloidal particles contained within the droplets. The colloidal particles interact strongly with the defects leading to the arrest of the defect. The final defect configuration depends on the concentration of particles. Whilst the association of colloidal particles with defects in nematic droplets has previously been observed [69] the association of colloidal particles in a Saturn ring has never previously been observed in an emulsion system. This presents a novel way to create rings of colloidal particles, or colloidal particles with equatorial patterning. The observation that the nanoparticles used are never removed from the interface and that a radial configuration is never observed is in contrast to the results of [55, 67] where bacterial endotoxin is shown to move from the boojums to the centre of a radially aligned droplet. However, it is perhaps fortunate that we do not observe this phenomenon as if we did the selectivity of the biosensor system would be called into question.

It would be interesting to explore this system further, potentially in combination with simulations in order to understand the energetics of these pinned states. This system also suggests an extension to the topological stabilisation of bare droplets, a small number of colloidal particles could potentially stabilise a nematic droplet as coalescence would require the nucleation of new defects.

Bibliography

[1] Agez, G., R. Bitar and M. Mitov, "Cholesteric liquid crystal self-organization of gold nanoparticles." *Soft Matter* (2011), **7**, 8198, doi: 10.1039/c1sm05628j.

[2] Agha, H., J.-B. Fleury and Y. Galerne, "Micro-wires self-assembled and 3D-connected with the help of a nematic liquid crystal." *Eur.Phys. J. E* (2012), **35**, 82, doi: 10.1140/epje/i2012-12082-1.

[3] Al-Hamdani, U. J., "Mesomorphic properties of an homologous series of thioalkyl-terminated azomesogens." *Int.J. Mol. Sci.* (2011), **12**, 3182, doi: 10.3390/ijms12053182.

[4] Alexopoulos, A. and E. Franses, "Surface tensions of viscous and anisotropic fluids." *Colloids and surfaces* (1990), **43**, 263.

[5] Aliño, V. J., J. Pang and K.-L. Yang, "Liquid crystal droplets as a hosting and sensing platform for developing immunoassays." *Langmuir* (2011), **27**, 11784, doi: 10.1021/la2022215.

[6] Anderson, V., E. Terentjev, S. Meeker, J. Crain and W. Poon, "Cellular solid behaviour of liquid crystal colloids 1. Phase separation and morphology." *Eur. Phys. J. E* (2001), **4**, 11, doi: 10.1007/PL00013680.

[7] Bai, Y. and N. L. Abbott, "Recent advances in colloidal and interfacial phenomena involving liquid crystals." *Langmuir* (2011), **27**, 5719, doi: 10. 1021/la103301d.

[8] Beris, A. N. and B. J. Edwards, "Thermodynamics of Flowing Systems." Oxford University Press, Oxford (1994).

[9] Besseling, R., L. Isa, E. R. Weeks and W. C. K. Poon, "Quantitative imaging of colloidal flows." *Adv. Coll. and Int. Sci.* (2009), **146**, 1, doi: 10.1016/j.cis.2008.09.008.

[10] Binks, B. and T. S. Horozov, "Colloidal particles at liquid interfaces." Cambridge University Press, Cambridge (2006).

[11] Bouligand, Y., S. T. Lagerwall and B. Stebler, “Blue-phase drops on a glass interface and their decoration at the cholesteric transition.” *Comptes Rendus Chimie* (2008), **11**, 212, doi: 10.1016/j.crci.2007.11.009.

[12] Cahn, R., “Crystal defects and melting.” *Nature* (1978), **273**, 491.

[13] Cahn, R., “Melting and the surface.” *Nature* (1986), **323**, 668.

[14] Carroll, L., “The Hunting of the Snark”,. Macmillan (1876).

[15] Castles, F., F. V. Day, S. M. Morris, D.-H. Ko, D. J. Gardiner, M. M. Qasim, S. Nosheen, P. J. W. Hands, S. S. Choi, R. H. Friend and H. J. Coles, “Blue-phase templated fabrication of three-dimensional nanostructures for photonic applications.” *Nat. Mat.* (2012), **11**, 599, doi: 10.1038/nmat3330.

[16] Castles, F., S. M. Morris, E. M. Terentjev and H. J. Coles, “Thermodynamically Stable Blue Phases.” *Phys. Rev. Lett.* (2010), **104**, 157801, doi: 10.1103/PhysRevLett.104.157801.

[17] Cavallaro, M., L. Botto, E. P. Lewandowski, M. Wang and K. J. Stebe, “Curvature-driven capillary migration and assembly of rod-like particles.” *Proc. Natl. Acad. Sci. U.S.A.* (2011), **108**, 20923, doi: 10.1073/pnas.1116344108.

[18] Cheung, D. and M. Allen, “Liquid-crystal-mediated force between a cylindrical nanoparticle and substrate.” *Phys. Rev. E* (2007), **76**, 041706, doi: 10.1103/PhysRevE.76.041706.

[19] Coles, H. J. and M. N. Pivnenko, “Liquid crystal ’blue phases’ with a wide temperature range.” *Nature* (2005), **436**, 997, doi: 10.1038/nature03932.

[20] Cordoyiannis, G., P. Losada-Pérez, C. S. P. Tripathi, B. Rožič, U. Tkalec, V. Tzitzios, E. Karatairi, G. Nounesis, Z. Kutnjak, I. Muševič, C. Glorieux, S. Kralj and J. Thoen, “Blue phase III widening in CE6-dispersed surface-functionalised CdSe nanoparticles.” *Liq. Cryst.* (2010), **37**, 1419, doi: 10.1080/02678292.2010.519057.

[21] Cordoyiannis, G., V. S. Rao Jampani, S. Kralj, S. Dhara, V. Tzitzios, G. Basina, G. Nounesis, Z. Kutnjak, C. S. Pati Tripathi, P. Losada-Pérez, D. Jesenek, C. Glorieux, I. Muševič, A. Zidanšek, H. Ameinitsch and J. Thoen, “Different modulated structures of topological defects stabilized by adaptive targeting nanoparticles.” *Soft Matter* (2013), **9**, 3956, doi: 10.1039/c3sm27644a.

[22] Crawford, G. and S. Žumer, (Editors) “Liquid Crystals in Complex Geometries.” Taylor and Francis (1996).

[23] Crocker, J. and D. Grier, “Methods of digital video microscopy for colloidal studies.” *Journal of colloid and interface science* (1996), **310**, 298.

[24] Crooker, P. P., "Plenary lecture. The blue phases. A review of experiments." *Liquid Crystals* (1989), **5**, 751.

[25] Danov, K. D. and P. A. Kralchevsky, "Capillary forces between particles at a liquid interface: general theoretical approach and interactions between capillary multipoles." *Adv. Coll. Int. Sci.* (2010), **154**, 91, doi: 10.1016/j.cis.2010.01.010.

[26] Demikhov, E., H. Stegemeyer and V. Tsukruk, "Pretransitional phenomena and pinning in liquid-crystalline blue phases." *Phys. Rev. A* (1992), **46**, 4879.

[27] Dierking, I., W. Blenkhorn, E. Credland, W. Drake, R. Kociuruba, B. Kayser and T. Michael, "Stabilising liquid crystalline Blue Phases." *Soft Matter* (2012), **8**, 4355, doi: 10.1039/c2sm07155j.

[28] Drzaic, P. and P. S. Drzaic, "Putting liquid crystal droplets to work: a short history of polymer dispersed liquid crystals." *Liq. Cryst.* (2006), **33**, 1281, doi: 10.1080/02678290601140563.

[29] Dubois-Violette, E. and O. Parodi, "Emulsions nématiques. effets de champ magnetiques et effects piezoelectrics." *J. Phys. (Paris)* (1969), **30**, 57.

[30] Feldman, A., P. Crooker and L. Goh, "Chiral strain and reentrancy in blue-phase transitions." *Phys. Rev. A* (1987), **35**, 842.

[31] Finkelmann, H., E. Nishikawa, G. Pereira and M. Warner, A new opto-mechanical effect in solids. *Phys. Rev. Lett.* (2001), **87**, doi: {10.1103/PhysRevLett.87.015501}.

[32] Friedel, G., "Les états mésomorphes de la matière." *Ann. Phys.* (1922), **474**, 162.

[33] Gabrisch, H., L. Kjeldgaard, E. Johnson and U. Dahmen, "Equilibrium shape and interface roughening of small liquid Pb inclusions in solid Al." *Acta Mat.* (2001), **49**, 4259, doi: 10.1016/S1359-6454(01)00307-X.

[34] Gannon, M. and T. Faber, "The surface tension of nematic liquid crystals." *Philosophical Magazine A* (1978), **37**, 117.

[35] de Gennes, P. and J. Prost, "The Physics of Liquid Crystals." Oxford Science Pulblications (1993).

[36] Gharbi, M. A., M. Nobili, M. In, G. Prévot, P. Galatola, J.-B. Fournier and C. Blanc, "Behavior of colloidal particles at a nematic liquid crystal interface". *Soft Matter* (2011), **7**, 1467, doi: 10.1039/c0sm00863j.

[37] Gupta, J. K., S. Sivakumar, F. Caruso and N. L. Abbott, "Size-dependent ordering of liquid crystals observed in polymeric capsules with micrometer and smaller diameters." *Angew. Chem.* (2009), **48**, 1652, doi: 10.1002/anie.200804500.

[38] Henrich, Private communication.

[39] Henrich, O., D. Marenduzzo, K. Stratford and M. Cates, "Domain growth in cholesteric blue phases: Hybrid lattice Boltzmann simulations." *Comput. Math. Appl.* (2010), **59**, 2360, doi: 10.1016/j.camwa.2009.08.047.

[40] Henrich, O., K. Stratford, M. Cates and D. Marenduzzo, "Structure of Blue Phase III of Cholesteric Liquid Crystals." *Phys. Rev. Lett.* (2011), **106**, 107801, doi: 10.1103/PhysRevLett.106.107801.

[41] Henrich, O., K. Stratford, P. V. Coveney and E. Cates, Rheology of Cubic Blue Phases. *Soft Matter* (2013), doi: 10.1039/c3sm50228g.

[42] Henrich, O., K. Stratford, D. Marenduzzo and M. E. Cates, "Ordering dynamics of blue phases entails kinetic stabilization of amorphous networks." *Proc. Natl. Acad. Sci. U.S.A.* (2010), **107**, 13212, doi: 10.1073/pnas.1004269107.

[43] Hijnen, N., T. A. Wood, D. Wilson and P. S. Clegg, "Self-organization of particles with planar surface anchoring in a cholesteric liquid crystal." *Langmuir* (2010), **26**, 13502, doi: 10.1021/la101420c.

[44] Horozov, T. S., R. Aveyard, J. H. Clint and B. P. Binks, "Order – Disorder Transition in Monolayers of Modified Monodisperse Silica Particles at the Octane – Water Interface." *Langmuir* (2003), **19**, 2822, doi: 10.1021/la020858x.

[45] Humar, M. and I. Muševič, "Surfactant sensing based on whispering-gallery-mode lasing in liquid-crystal microdroplets." *Opt. Express* (2011), **19**, 19836.

[46] Jampani, V. S., M. Škarabot, M. Ravnik, S. Čopar, S. Žumer and I. Muševič, "Colloidal entanglement in highly twisted chiral nematic colloids: Twisted loops, Hopf links, and trefoil knots". *Phys. Rev. E* (2011), **84**, 031703, doi: 10.1103/PhysRevE.84.031703.

[47] Johnson, D., J. Flack and P. Crooker, "Structure and properties of the cholesteric blue phases." *Phys. Rev. Lett.* (1980), **45**, 641.

[48] Karatairi, E., V. Tzitzios, G. Nounesis, G. Cordoyiannis, J. Thoen, C. Glorieux and S. Kralj, "Nanoparticle-induced widening of the temperature range of liquid-crystalline blue phases." *Phys. Rev. E* (2010), **81**, 041703, doi: 10.1103/PhysRevE.81.041703.

[49] Kikuchi, H., M. Yokota, Y. Hisakado, H. Yang and T. Kajiyama, "Polymer-stabilized liquid crystal blue phases." *Nat. Mat.* (2002), **1**, 64, doi: 10.1038/nmat712.

[50] Kim, J.-W., H. Kim, M. Lee and J. J. Magda, "Interfacial tension of a nematic liquid crystal/water interface with homeotropic surface alignment." *Langmuir* (2004), **20**, 8110, doi: 10.1021/la049843k.

[51] Kleiman, R. N., D. J. Bishop, R. Pindak and P. Taborek, "Shear modulus and specific heat of the liquid-crystal blue phases." *Phys. Rev. Lett.* (1984), **53**, 2137, doi: 10.1103/PhysRevLett.53.2137.

[52] Koenig, G. M., I.-H. Lin and N. L. Abbott, "Chemoresponsive assemblies of microparticles at liquid crystalline interfaces." *Proc. Natl. Acad. Sci. U.S.A.* (2010), **107**, 3998, doi: 10.1073/pnas.0910931107.

[53] Lakowicz, J., "Principles of Fluorescence Spectroscopy." Kulwer Academic, New York, 2nd edition (1999).

[54] Lavrentovich, O. D., "Topological defects in dispersed liquid crystals, or words and worlds around liquid crystal drops." *Liquid Crystals* (1998), **24**, 117.

[55] Lin, I.-H., D. S. Miller, P. J. Bertics, C. J. Murphy, J. J. de Pablo and N. L. Abbott, "Endotoxin-induced structural transformations in liquid crystalline droplets." *Science* (2011), **332**, 1297, doi: 10.1126/science.1195639.

[56] Lintuvuori, J., K. Stratford, M. Cates and D. Marenduzzo, "Self-Assembly and Nonlinear Dynamics of Dimeric Colloidal Rotors in Cholesterics." *Phys. Rev. Lett.* (2011), **107**, 267802, doi: 10.1103/PhysRevLett.107.267802.

[57] Lintuvuori, J. S., D. Marenduzzo, K. Stratford and M. E. Cates, "Colloids in liquid crystals: a lattice Boltzmann study." *J. Mater. Chem.* (2010), **20**, 10547, doi: 10.1039/c0jm01824d.

[58] Lintuvuori, J. S., A. C. Pawsey, K. Stratford, M. E. Cates, P. S. Clegg and D. Marenduzzo, "Colloidal Templating at a Cholesteric-Oil Interface: Assembly Guided by an Array of Disclination Lines." *Phys. Rev. Lett.* (2013), **110**, 187801, doi: 10.1103/PhysRevLett.110.187801.

[59] Lintuvuori, J. S., K. Stratford, M. E. Cates and D. Marenduzzo, "Colloids in Cholesterics : Size-Dependent Defects and Non-Stokesian Microrheology." *Phys. Rev. Lett.* (2010), **105**, 178302, doi: 10.1103/PhysRevLett.105.178302.

[60] Lockwood, N., J. Gupta and N. Abbott, "Self-assembly of amphiphiles, polymers and proteins at interfaces between thermotropic liquid crystals and aqueous phases." *Surf. Sci. Rep.* (2008), **63**, 255, doi: 10.1016/j.surfrep.2008.02.002.

[61] Loudet, J., P. Barois and P. Poulin, "Colloidal ordering from phase separation in a liquid-crystalline continuous phase." *Nature* (2000), **407**, 611, doi: 10.1038/35036539.

[62] Loudet, J., A. Yodh and B. Pouligny, "Wetting and Contact Lines of Micrometer-Sized Ellipsoids." *Phys. Rev. Lett.* (2006), **97**, 018304, doi: 10.1103/PhysRevLett.97.018304.

[63] Loudet, J. C., P. Barois, P. Auroy, P. Keller, H. Richard and P. Poulin, "Colloidal structures from bulk demixing in liquid crystals." *Langmuir* (2004), **20**, 11336, doi: 10.1021/la048737f.

[64] Lubensky, T., "Hydrodynamics of cholesteric liquid crystals." *Phys. Rev. A* (1972), **6**, 452.

[65] Meiboom, S., J. Sethna and P. Anderson, "Theory of the blue phase of cholesteric liquid crystals." *Phys. Rev. Lett.* (1981), **46**, 1216.

[66] Mermin, N., "E Pluribus Boojum: the physicist as neologist." *Physics Today* (1981), 040046.

[67] Miller, D. S. and N. L. Abbott, "Influence of droplet size, pH and ionic strength on endotoxin-triggered ordering transitions in liquid crystalline droplets." *Soft Matter* (2012), 374, doi: 10.1039/c2sm26811f.

[68] Mitov, M., C. Portet, C. Bourgerette, E. Snoeck and M. Verelst, "Long-range structuring of nanoparticles by mimicry of a cholesteric liquid crystal." *Nat. Mat.* (2002), **1**, 229, doi: 10.1038/nmat772.

[69] Mondiot, F., X. Wang, J. J. de Pablo and N. L. Abbott, "Liquid Crystal-Based Emulsions for Synthesis of Spherical and Non-Spherical Particles with Chemical Patches." *J. Am. Chem. Soc.* (2013), 2, doi: 10.1021/ja4022182.

[70] Moreno-Razo, J. a., E. J. Sambriski, N. L. Abbott, J. P. Hernández-Ortiz and J. J. de Pablo, "Liquid-crystal-mediated self-assembly at nanodroplet interfaces." *Nature* (2012), **485**, 86, doi: 10.1038/nature11084.

[71] Muševič, I., M. Skarabot and M. Humar, "Direct and inverted nematic dispersions for soft matter photonics." *J. Phys. Cond. Mat.* (2011), **23**, 284112, doi: 10.1088/0953-8984/23/28/284112.

[72] Negita, K., "Rheological properties in cholesteric and blue phases of cholesteryl isostearyl carbonate: viscosity and effect of electric field on the rheology." *Liquid Crystals* (1998), **24**, 243, doi: 10.1080/026782998207415.

[73] Nehring, J. and A. Saupe, "On the Elastic Theory of Uniaxial Liquid Crystals." *J. Chem. Phys.* (1971), **54**, 337, doi: 10.1063/1.1674612.

[74] Nihat Berker, A., "Critical behavior induced by quenched disorder." *Physica A* (1993), **194**, 72, doi: 10.1016/0378-4371(93)90341-Z.

[75] Nych, A., U. Ognysta, V. Pergamenshchik, B. Lev, V. Nazarenko, I. Muševič, M. Škarabot and O. Lavrentovich, "Coexistence of Two Colloidal Crystals at the Nematic-Liquid-Crystal–Air Interface." *Phys. Rev. Lett.* (2007), **98**, 057801, doi: 10.1103/PhysRevLett.98.057801.

[76] Oettel, M. and S. Dietrich, "Colloidal interactions at fluid interfaces." *Langmuir* (2008), **24**, 1425, doi: 10.1021/la702794d.

[77] Oettel, M., a. Domínguez, M. Tasinkevych and S. Dietrich, “Effective interactions of colloids on nematic films.” *E. Phys. J. E* (2009), **28**, 99, doi: 10.1140/epje/i2008-10360-1.

[78] Oswald, P. and P. Pieranski, “Nematic and Cholesteric Liquid Crystals.” Taylor and Francis (2005).

[79] Park, K.-W., M.-J. Gim, S. Kim, S.-T. Hur and S.-W. Choi, “Liquid-crystalline blue phase II system comprising a bent-core molecule with a wide stable temperature range.” *ACS applied materials & interfaces* (2013), **5**, 8025, doi: 10.1021/am403109q.

[80] Pawsey, A. C., J. S. Lintuvuori, T. A. Wood, J. H. J. Thijssen, D. Marenduzzo and P. S. Clegg, “Colloidal particles at the interface between an isotropic liquid and a chiral liquid crystal.” *Soft Matter* (2012), 8422, doi: 10.1039/c2sm25434d.

[81] Pieranski, P., “Two Dimensional Colloidal Crystals.” *Phys. Rev. Lett.* (1980), **45**, 569, doi: 10.1103/PhysRevLett.45.569.

[82] Plische, M. and B. Bergersen, “Equilibrium Statistical Physics.” World Scientific (1994).

[83] Popa-Nita, V., I. Gerlic and S. Kralj, “The influence of disorder on thermotropic nematic liquid crystals phase behavior.” *Int. J. Mol. Sci.* (2009), **10**, 3971, doi: 10.3390/ijms10093971.

[84] Ravnik, M., G. P. Alexander, J. M. Yeomans and S. Žumer, “Three-dimensional colloidal crystals in liquid crystalline blue phases.” *Proc. Natl. Acad. Sci. U.S.A.* (2011), **108**, 5188, doi: 10.1073/pnas.1015831108.

[85] Ravnik, M., J.-i. Fukuda, J. M. Yeomans and S. Žumer, “Confining blue phase colloids to thin layers”. *Soft Matter* (2011), **7**, 10144, doi: 10.1039/c1sm05707c.

[86] Reinitzer, F., “Contributions to the knowledge of cholesterol.” *Liquid Crystals* (1989), **5**, 7, doi: 10.1080/02678298908026349.

[87] Seč, D., T. Porenta, M. Ravnik and S. Žumer, “Geometrical frustration of chiral ordering in cholesteric droplets.” *Soft Matter* (2013), doi: 10.1039/c2sm27048j.

[88] Smalyukh, I., “Three-dimensional imaging of orientational order by fluorescence confocal polarizing microscopy.” *Chem. Phys. Lett.* (2001), **336**, 88, doi: 10.1016/S0009-2614(00)01471-8.

[89] Smalyukh, I., S. Chernyshuk, B. Lev, A. Nych, U. Ognysta, V. Nazarenko and O. Lavrentovich, “Ordered Droplet Structures at the Liquid Crystal Surface and Elastic-Capillary Colloidal Interactions.” *Phys. Rev. Lett.* (2004), **93**, 117801, doi: 10.1103/PhysRevLett.93.117801.

[90] Smalyukh, I. and O. Lavrentovich, "Three-dimensional director structures of defects in Grandjean-Cano wedges of cholesteric liquid crystals studied by fluorescence confocal polarizing microscopy." *Physical Review E* (2002), **66**, 051703, doi: 10.1103/PhysRevE.66.051703.

[91] Stamou, D., C. Duschl and D. Johannsmann, "Long-range attraction between colloidal spheres at the air-water interface: the consequence of an irregular meniscus." *Phys. Rev. E* (2000), **62**, 5263.

[92] Stark, H., "Physics of colloidal dispersions in nematic liquid crystals." *Phys. Rep.* (2001), **351**, 387.

[93] Stratford, K., O. Henrich and J. S. Lintuvuori, "Self-assembly of colloid-cholesteric composites : A route to switchable optical materials."

[94] Tasinkevych, M. and D. Adrienko, "Colloidal particles in liquid crystal films and at interfaces." *Condensed Matter Physics* (2010), **13**, 33603.

[95] Thoen, J., "Adiabatic scanning calorimetric results for the blues phases of cholesteryl nonanoate." *Phys. Rev. A* (1988), **37**, 1754.

[96] Tintaru, M., R. Moldovan, T. Beica and S. Frunza, "Surface tension of some liquid crystals in the cyanobiphenyl series ." *Liquid Crystals* (2010), **28**, 793.

[97] Tiribocchi, a., G. Gonnella, D. Marenduzzo, E. Orlandini and F. Salvadore, "Bistable Defect Structures In Blue Phase Devices." *Phys. Rev. Lett.* (2011), **107**, 237803, doi: 10.1103/PhysRevLett.107.237803.

[98] Tixier, T., M. Heppenstall-Butler and E. M. Terentjev, "Spontaneous size selection in cholesteric and nematic emulsions." *Langmuir* (2006), **22**, 2365, doi: 10.1021/la0531953.

[99] Tkalec, U., M. Ravnik, S. Copar, S. Zumer and I. Musevic, "Reconfigurable Knots and Links in Chiral Nematic Colloids". *Science* (2011), **333**, 62, doi: 10.1126/science.1205705.

[100] Čopar, S. and S. Žumer, "Nematic Braids: Topological Invariants and Rewiring of Disclinations." *Phys. Rev. Lett.* (2011), **106**, 177801, doi: 10.1103/PhysRevLett.106.177801.

[101] Volovik, G. and O. Lavrentovich, "Topological dynamics of defects: boojums in nematic drops." *Zh Eksp Teor Fiz* (1983), **58**, 1159.

[102] Wood, T. A., J. S. Lintuvuori, A. B. Schofield, D. Marenduzzo and W. C. K. Poon, "A Self-Quenched Defect Glass in a Colloid-Nematic Liquid Crystal Composite." *Science* (2011), **334**, 79, doi: 10.1126/science.1209997.

[103] Yan, J. and S.-T. Wu, "Polymer-stabilized blue phase liquid crystals: a tutorial [Invited]." *Optical Materials Express* (2011), **1**, 1527, doi: 10.1364/OME.1.001527.

[104] Zapotocky, M., L. Ramos, P. Poulin, T. C. Lubensky and D. A. Weitz, "Particle-Stabilized Defect Gel in Cholesteric Liquid Crystals." *Science* (1999), **283**, 209, doi: 10.1126/science.283.5399.209.

Publications

Pawsey, A. C., J. S. Lintuvuori, T. A. Wood, J. H. J. Thijssen, D. Marenduzzo and P. S. Clegg, "Colloidal particles at the interface between an isotropic liquid and a chiral liquid crystal." *Soft Matter* (2012), 8422, doi: 10.1039/c2sm25434d

Lintuvuori, J. S., A. C. Pawsey, K. Stratford, M. E. Cates, P. S. Clegg and D. Marenduzzo, "Colloidal Templating at a Cholesteric-Oil Interface: Assembly Guided by an Array of Disclination Lines." *Phys. Rev. Lett.* (2013), **110**, 187801, doi: 10.1103/PhysRevLett.110.187801